

**BAROREFLEX-BASED PHYSIOLOGICAL CONTROL OF
A LEFT VENTRICULAR ASSIST DEVICE**

by

Shao Hui Chen

BS, Harbin Institute of Technology, 1994

MS, China Academy of Launch Vehicle Technology, 2002

Submitted to the Graduate Faculty of
School of Engineering in partial fulfillment
of the requirements for the degree of
Doctor of Philosophy

University of Pittsburgh

2006

UNIVERSITY OF PITTSBURGH
SCHOOL OF ENGINEERING

This dissertation was presented

by

Shao Hui Chen

It was defended on

June 26, 2006

and approved by

Marwan A. Simaan, Bell of PA/Bell Atlantic Professor, Department of Electrical and
Computer Engineering

J. Robert Boston, Professor, Department of Electrical and Computer Engineering

Luis F. Chaparro, Associate Professor, Department of Electrical and Computer Engineering

Ching-Chung Li, Professor, Department of Electrical and Computer Engineering

James F. Antaki, Professor, Department of Biomedical Engineering, Carnegie Mellon
University

Dissertation Director: Marwan A. Simaan, Bell of PA/Bell Atlantic Professor,
Department of Electrical and Computer Engineering

BAROREFLEX-BASED PHYSIOLOGICAL CONTROL OF A LEFT VENTRICULAR ASSIST DEVICE

Shao Hui Chen, PhD

University of Pittsburgh, 2006

The new generation left ventricular assist devices (LVADs) for treating end-stage heart failure are based upon turbodynamic (rotary) pumps. These devices have demonstrated several advantages over the previous pulsatile generation of LVADs, however they have also proven more difficult to control. Limited availability of observable hemodynamic variables and dynamically changing circulatory parameters impose particular difficulties for the LVAD controller to accommodate the blood flow demands of an active patient. The heart rate (HR) and systemic vascular resistance (SVR) are two important indicators of blood flow requirement of the body; but these variables have not been previously well exploited for LVAD control. In this dissertation, we will exploit these two variables and develop a control algorithm, based upon mathematical models of the cardiovascular system: both healthy and diseased, with built in autoregulatory control (baroreflex). The controller will respond to change in physiological state by adjusting the pump flow based on changes in HR and SVR as dictated by the baroreflex. Specific emphasis will be placed on hemodynamic changes during exercise in which the blood flow requirement increases dramatically to satisfy the increased oxygen consumption. As the first step in the development of the algorithm, we developed a model which will include the autoregulation of the cardiovascular system and the hydraulic power input from the pump. This model provided a more realistic simulation of the interaction between the LVAD and the cardiovascular system regulated by the baroreflex. Then the control algorithm was developed, implemented, and tested on the combined system of the LVAD and the cardiovascular system including the baroreflex. The performance of the proposed control algorithm is examined by comparing it to other control methods in response to varying levels of exercise and adding noises to the hemodynamic variables. The simulation results demonstrate that the controller is able to generate more blood flow through the pump than the constant speed and constant pump head

method, and the heart rate related pump speed method. The simulations with noise show that the controller is fairly robust to the measurement and estimate noises.

TABLE OF CONTENTS

ACKNOWLEDGEMENTS	xiv
1.0 INTRODUCTION.....	1
2.0 BACKGROUND	4
2.1 MODELING OF CARDIOVASCULAR SYSTEM, THE BAROREFLEX AND PUMP.....	4
2.2 PREVIOUS CONTROL FOR LVAD.....	5
2.3 THE PROPOSED INVESTIGATIONS	9
3.0 MODEL OF HEALTHY HEART WITH BAROREFLEX.....	11
3.1 THE CARDIOVASCULAR SYSTEM MODEL	11
3.2 THE BAROREFLEX MODEL	15
3.3 THE COMBINED MODEL OF THE BAROREFLEX AND THE CARDIOVASCULAR SYSTEM	21
3.4 RESPONSE TO SINGLE PARAMETER CHANGE	29
3.4.1 Response to decrease in preload (blood withdrawal)	29
3.4.2 Response to change in afterload (SVR).....	32
3.4.3 Response to change in left ventricular contractility (or Emax).....	36
3.4.4 Response to change in heart rate.....	39
3.5 RESPONSE TO EXERCISE	44
3.5.1 Single level exercise.....	44
3.5.2 Multiple levels of exercise.....	47
3.6 CONCLUSION	51
4.0 FAILING HEART WITH BAROREFLEX	52
4.1 HEART FAILURE AND ASSOCIATED PHYSIOLOGICAL CHANGES	52
4.1.1 Changes in cardiovascular system.....	53

4.1.2	Changes in baroreflex.....	54
4.2	EFFECTS OF CHANGES IN HEART FOR HEART FAILURE MODEL	56
4.2.1	Systolic dysfunction: decrease in E_{max}	57
4.2.2	Diastolic dysfunction: increase in E_{min}	58
4.2.3	Combination of systolic dysfunction and diastolic dysfunction: decrease in E_{max} and increase in E_{min}	58
4.3	DETERMINE THE PARAMETERS OF HEART FAILURE MODEL	59
4.4	SIMULATIONS RESULTS OF HEART FAILURE MODEL.....	61
4.4.1	Simulation result 1 ($V_o = 5$ ml, $V_T = 275$ ml).....	61
4.4.2	Simulation result 2 ($V_o = 35$ ml, $V_T = 300$ ml).....	67
4.4.3	Simulations results of specific clinical heart failure	71
4.5	RESPONSES OF HEART FAILURE TO EXERCISE	75
4.5.1	Hypertrophic heart failure.....	75
4.5.2	Dilated heart failure.....	79
4.6	CONCLUSION	83
5.0	THE COMBINED MODEL OF PUMP AND FAILING HEART.....	84
5.1	THE PUMP MODEL	84
5.2	THE COUPLED MODEL OF THE PUMP AND THE FAILING HEART	87
5.3	CHANGES IN HEMODYNAMICS WITH PUMP IMPLANTED	92
5.4	CONCLUSION	96
6.0	PUMP CONTROL BASED ON HEART RATE AND SYSTEMIC VASCULAR RESISTANCE	97
6.1	PUMP OPERATION.....	98
6.2	PROPOSED PUMP CONTROL BASED ON HR AND SVR.....	100
6.3	COMPARISON OF THE PROPOSED PUMP CONTROL WITH OTHER METHODS.....	113
6.3.1	Constant speed method.....	113
6.3.2	Constant pressure head method	115
6.3.3	Pump speed as a linear function of heart rate.....	116
6.4	PERFORMANCES OF THE PROPOSED CONTROLLER	118
6.4.1	K1 and K2.....	120

6.4.2	LVP	125
6.4.3	SV	128
6.4.4	Noise	131
6.5	CONCLUSION	145
7.0	CONCLUSION AND FUTURE WORK	147
	BIBLIOGRAPHY	150

LIST OF TABLES

Table 3.1. State variables	12
Table 3.2. Parameters and values.....	12
Table 3.3. Phases in a cardiac cycle.....	14
Table 3.4. State variables for baroreflex.....	22
Table 3.5. Values for baroreflex parameters.....	24
Table 3.6. Baseline Hemodynamics.....	28
Table 3.7. Response to change in preload.....	29
Table 3.8. Response to change in afterload	34
Table 3.9. Response to change in left ventricle contractility	37
Table 3.10. Response to change in heart rate.....	41
Table 3.11. Offsets in sympathetic and vagal activity	44
Table 3.12. Hemodynamic changes	46
Table 3.13. Changes in resistances	47
Table 3.14. Multiple exercise levels	47
Table 3.15. Exercise experiment data	50
Table 4.1. Changes in parameters of the heart failure model	55
Table 4.2. Clinical hemodynamics data for heart failure.....	59
Table 4.3. Parameters for the heart failure baroreflex	60
Table 4.4. Heart failure model combinations.....	61
Table 4.5. Simulation results for heart failure (1).....	64
Table 4.6. Simulation results for heart failure (2).....	69
Table 4.7. Hypertrophic heart failure response to exercise	77
Table 4.8. Dilated heart failure response to exercise	81

Table 5.1. State variables	88
Table 5.2. Model parameters	89
Table 5.3. Hemodynamic changes with increasing pump speed	94
Table 5.4. Full and partial pump support.....	95
Table 6.1. Multiple levels of exercise.....	113
Table 6.2. Simulation results for constant speed	114
Table 6.3. Simulation results for constant pump head.....	115
Table 6.4. Simulation results for heart rate related pump speed method.....	116
Table 6.5. Simulation results with $K1=0.005$, $K2=0.005$	124
Table 6.6. Simulation results with $K1=0.003$, $K2=0.003$	124
Table 6.7. Simulation results with $LVP_r = 40$ mmHg.....	127
Table 6.8. Simulation results with $LVP_r = 30$ mmHg.....	127
Table 6.9. Simulation results with smaller SV_r	130
Table 6.10. Simulation results with larger SV_r	130

LIST OF FIGURES

Figure 2.1. In vivo hemodynamics of calf implanted with turbodynamic LVAD.....	6
Figure 2.2. Block diagram of the proposed control scheme.	10
Figure 3.1. Cardiovascular system model.....	11
Figure 3.2. Typical elastance function.....	13
Figure 3.3. Block diagram for the carotid baroreflex.	16
Figure 3.4. Block diagram for the afferent pathway of carotid sinus.	16
Figure 3.5. Characteristic curves for the afferent pathway.....	18
Figure 3.6. Characteristic curve for the efferent sympathetic pathway.	18
Figure 3.7. Characteristic curve for the efferent vagal pathway.....	19
Figure 3.8. Characteristic curve for equation (3.12).....	20
Figure 3.9. Pulsatile heart coupled with baroreflex.	22
Figure 3.10. P-V loops generated by the model and Simbiosys.	27
Figure 3.11. Left ventricular pressure and left ventricular volume.	28
Figure 3.12. Change in P-V loop for 20% blood withdrawal.	31
Figure 3.13. Changes in hemodynamics for loss of blood.....	32
Figure 3.14. Change in P-V loop for -20% in SVR.	33
Figure 3.15. Change in P-V loop for +20% in SVR.	34
Figure 3.16. Changes in hemodynamics for changes in SVR.....	36
Figure 3.17. Change in P-V loop for +40% in E_{max} in the model.	37
Figure 3.18. Changes in hemodynamics for +40 % in E_{max}	38
Figure 3.19. Change in P-V loop for -10% in HR.	40
Figure 3.20. Change in P-V loop for +40% in HR.	41
Figure 3.21. Changes in hemodynamics for change in HR.	43

Figure 3.22. Response to exercise.....	45
Figure 3.23. P-V loops of rest and exercise.....	45
Figure 3.24. Hemodynamic changes from rest to exercise.....	49
Figure 3.25. Changes in hemodynamics for multiple exercise levels.....	50
Figure 4.1. Systolic dysfunction and diastolic dysfunction (Adopted from [56]).	54
Figure 4.2. Changes in baroreflex.....	56
Figure 4.3. Left ventricle pressure volume loop (adopted from [55]).	57
Figure 4.4. Systolic dysfunction (adopted from [55]).....	57
Figure 4.5. Diastolic dysfunction (adopted from [55]).....	58
Figure 4.6. Combination of systolic dysfunction and diastolic dysfunction (adopted from [55]).	59
Figure 4.7. P-V loops for healthy heart and systolic dysfunction heart.....	62
Figure 4.8. P-V loops for healthy heart and diastolic dysfunction heart.	63
Figure 4.9. P-V loops for healthy and the combination of both failure cases.....	64
Figure 4.10. Comparison of simulation results with baroreflex and without baroreflex.....	66
Figure 4.11. Systolic dysfunction P-V loops. ($V_{T0} = 240$ ml).....	67
Figure 4.12. Diastolic dysfunction P-V loops. ($V_{T0} = 250$ ml)	68
Figure 4.13. P-V loops of combination of systolic and diastolic dysfunctions. ($V_{T0} = 205$ ml) ...	68
Figure 4.14. Comparison of simulation results with baroreflex and without baroreflex.....	71
Figure 4.15. P-V loops of failing heart responses to changes in preload (adopted from [71]).	72
Figure 4.16. Model reproduced clinical baseline failing heart P-V loops.	73
Figure 4.17. Simulation results of failing heart response to changes in preload.	74
Figure 4.18. Response to exercise for hypertrophic heart failure.....	76
Figure 4.19. P-V loops of rest (dotted line) and exercise (solid line).....	76
Figure 4.20. Hemodynamic changes from rest to exercise.....	78
Figure 4.21. Changes in hemodynamics for multiple exercise levels.....	79
Figure 4.22. Response to exercise for dilated heart failure.....	80
Figure 4.23. P-V loops of rest (dotted line) and exercise (solid line).....	80
Figure 4.24. Hemodynamic changes from rest to exercise.....	82
Figure 4.25. Changes in hemodynamics for multiple exercise levels.....	82
Figure 5.1. DC motor circuit.....	84

Figure 5.2. Rotary pump characteristic curves [72].....	87
Figure 5.3. The coupled model of pump and failing heart.....	88
Figure 5.4. Pump augmented failing heart with baroreflex	92
Figure 5.5. P-V loops changes with changing pump speed	93
Figure 5.6. Changes in hemodynamics (ratio of partial to full).....	95
Figure 6.1. Static pump characteristic curves and operating point.	98
Figure 6.2. Same SVR and different operating points.	99
Figure 6.3. Change in operating points from rest (1) to exercise (2).....	99
Figure 6.4. Block diagram for the closed-loop control based on HR and SVR.....	100
Figure 6.5. Simplified version of the combined model (aortic valve is taken out).....	101
Figure 6.6. Reduced circuit diagram in mean sense.	101
Figure 6.7. Block diagram for the controller based on the HR and SVR.	103
Figure 6.8. Controller responses to exercise level 2.	105
Figure 6.9. Control errors for H and Q from rest to exercise level 2.....	106
Figure 6.10. Operating point trajectory from rest to exercise.....	106
Figure 6.11. LVP and LVPr.....	107
Figure 6.12. AOP and LVP.....	107
Figure 6.13. Illustration of the operating point and steady errors.....	108
Figure 6.14. $K_2 = 0$ (only H branch is applied).....	109
Figure 6.15. $K_1 = 0$ (only CO branch is applied)	110
Figure 6.16. Steady errors for exercise level 1 and level 3.....	111
Figure 6.17. Operating point for exercise level 3	112
Figure 6.18. Multiple levels of exercise.....	112
Figure 6.19. Constant speed method response to exercise level 2. At 15s, exercise starts.....	114
Figure 6.20. Constant pump head method response to exercise level 2. At 15s, exercise starts. 115	
Figure 6.21. Heart rate related pump speed method response to exercise level 2.	117
Figure 6.22. Response to the exercise for different control methods	118
Figure 6.23. Simulation from rest to exercise.....	119
Figure 6.24. $K_1=0.007$, $K_2=0.007$, $LVPr=50$ mmHg.....	120
Figure 6.25. $K_1=0.002$, $K_2=0.002$, $LVPr=50$ mmHg.....	121
Figure 6.26. $K_1 < 0.004$, $K_2 > 0.004$, noise free (rest to exercise 2)	122

Figure 6.27. $K_1 > 0.004$, $K_2 < 0.004$. noise free (rest to exercise 2)	123
Figure 6.28. Simulation results with different K_1 and K_2	125
Figure 6.29. $LVP_r < 50$ mmHg.....	126
Figure 6.30. Simulation results with different LVP_r . $K_1 = 0.004$, $K_2 = 0.004$	128
Figure 6.31. Smaller SV_r	129
Figure 6.32. Simulation results with different SV_r	131
Figure 6.33. Noise features	132
Figure 6.34. Low level of noises for HR, SVR, H and CO	133
Figure 6.35. High level of noise for H only	134
Figure 6.36. High level of noise for CO only	135
Figure 6.37. High level noise for SVR only	136
Figure 6.38. High level of noise for HR only	137
Figure 6.39. High level of noise for HR, SVR, H and CO	138
Figure 6.40. Noise for H only	140
Figure 6.41. Noise for CO only	142
Figure 6.42. Noise for SVR only	143
Figure 6.43. Noise for HR only	144
Figure 6.44. Noise for all variables.....	145

ACKNOWLEDGEMENTS

I would like to thank my advisor, Dr. Marwan A. Simaan, for his support and guidance throughout the research. I would also like to thank Dr. James F. Antaki and Dr. J. Robert Boston for the physiology education and insightful advices in the weekly meetings. I thank Dr. Ching-Chung Li and Dr. Luis F. Chaparro for taking time and effort to serve on my committee. Special thanks to Antonio Ferreira, for the discussions and making an enjoyable environment. I would also like to thank my family, my wife Jie Li and my daughter Tianyi Chen for their love and support.

This research was supported by National Science Foundation (NSF) under contract ECS-0300097 and in part by National Institutes of Health / National Heart, Lung, and Blood Institute (NIH/NHLBI) under contract 1R43HL66656-01. I would like to express my gratitude to them for their financial support.

1.0 INTRODUCTION

Congestive heart failure is estimated to affect five million people in the US [1], which is characterized by impaired ventricular performance, exercise intolerance, and shortened life expectancy. Although drug therapy has had significant impact on quality of life and survival for moderate heart failure, mortality remains unacceptably high. Heart transplantation is the only accepted method to treat severe cases of the disease. Unfortunately, heart transplantation is limited by the number of donor organs, less than 3000 per year. The left ventricular assist device (LVAD) is therefore an alternative for many cases of end-stage heart failure [2, 3].

The first generation of LVADs was based on positive displacement (pulsatile) pumps. Recently, turbodynamic pumps have received growing acceptance on account of small size and high efficiency [4-8]. The rotary part of this type of pump, which is driven by a motor, generates a pressure difference across the pump in resistance of the arterial pressure. In a typical bypass application, where the inlet and outlet of the pump connect the apex of the left ventricle and the aorta respectively, the pump helps unload the failing left ventricle by reducing its work requirement and assuming the role of providing pressure and flow to the systemic circulation. However, the control of the LVAD emerges as a challenge for the rotary pump application. Because the pump actively draws blood from the left ventricle, the flow should be adjusted according to the available blood returning to the left ventricle.

For a normal heart, the cardiac output (CO) is determined by two factors: stroke volume (SV) and heart rate (HR),

$$CO = SV * HR$$

Larger stroke volume and higher heart rate imply larger CO. Stroke volume increase is the result of a complex physiological process: increasing preload, increasing contractility and decreasing afterload. Preload is the amount of the venous blood returning to the heart. The contractility of the heart is an index of its strength of contraction. The afterload refers to the systemic vascular

resistance (SVR), the output load of the left ventricle. More generally, the physiological status of the patient may demonstrate a wide range of variation, due to exercise intensity and emotional changes. For a patient with heart failure, one or more of these functions may be damaged or attenuated therefore heart transplantation or the augment of the LVAD is needed. As learned with total artificial hearts, the inability of the device to respond to the blood flow demand of the body can dramatically impact the quality of life for these patients [9]. Thus a controller that can detect and adapt to the real time physiological changes of the body is crucial for the LVAD recipients leaving hospital, returning to normal lifestyle and improving the quality of life.

Furthermore, two detrimental situations, backflow and suction, may occur for the pump operation if the pump speed is not suitably set [4, 5]. If the rotational speed (or pump flow) is too low, the blood will regurgitate from the aorta to the left ventricle through the pump (i.e. backflow). For this case, the cardiac output is not augmented but decreased. If the rotational speed is too high, the pump may attempt to draw more blood than available in the left ventricle. The latter will cause kinking at the connection of the left ventricle and cannula (suction) or the collapse of the left ventricle, which may result in damage to the heart muscle, blood, and/or vasculature.

Since the LVAD is applied to unload the failing left ventricle, the basic control objective is to mimic the native heart function [4, 5]. From above we know that the native heart adjusts to the physiological cardiac output requirement by a combination of preload, contractility, afterload and heart rate. However, not all this information is readily available to the LVAD controller, especially for an ambulatory patient. Thus the main objective for the LVAD control outside the hospital settings is to incorporate varied and sometimes limited control inputs and to adapt the pump speed to the physiological state of the patient.

This dissertation discusses a controller which will incorporate multiple hemodynamic variables (measured and/or estimated) and will respond to the physiological changes of the body. The specific inputs for the controller considered here are the heart rate and the systemic vascular resistance which are under the control of the baroreflex. In real life, the heart rate can be estimated from the electrical current to the drive motor of the LVAD and the systemic vascular resistance can also be estimated by using blood pressure and blood flow [10]. These will be used to estimate the physiological state changes and drive the pump speed toward the desired operating point.

This dissertation is organized as follows. First, in chapter 2, the LVAD control and the modeling of the cardiovascular system, the baroreflex and the pump are reviewed, and the proposed investigations and technical approaches are described.

In chapter 3, the models of the cardiovascular system and the baroreflex are presented and coupled. The parameters for the healthy cardiovascular model are determined to simulate the normal hemodynamics. The responses to single parameter change are examined by using physiological simulation software as reference. The response to exercise is compared to the exercise experiment data in the literature.

In chapter 4, model parameters are determined for the VAD patient with failing heart. Because of the progressive deterioration of the failing heart and the related cardiovascular system, there are some substantial changes in the cardiovascular system and the baroreflex. The changes in the cardiovascular system and the baroreflex are found out by surveying the literature and mapped to the heart failure model.

In chapter 5, the failing heart model is coupled to the pump model and its behavior is examined. The simulation results are compared to the data available in the literature.

In chapter 6, a physiological controller is developed which incorporates multiple inputs (heart rate and systemic vascular resistance). The heart rate and systemic vascular resistance are two important indicators of the physiological state of the body. Including this information will improve the pump control. The physiological controller is implemented and tested with the baroreflex + failing heart + pump model. The response to exercise of the control method is examined. The performance of this controller is compared to that of other available pump control methods such as constant pump speed, constant pump head and heart rate related pump speed method.

In chapter 7, the progress to date is concluded and future work is discussed.

2.0 BACKGROUND

Basically, there are three ways of investigating the interactions between the native circulation and the implanted pump: simulation on model, mock circulatory system, and animal experiment. The mathematic model consists of abstraction of the basic circulation elements, such as the heart and the arterial network. The mock loop is the counterpart of a certain model by using some devices instead of abstraction. The animal experiment is the preclinical feasibility test of a certain pump or pump controller. This research is focused on the model and simulation.

2.1 MODELING OF CARDIOVASCULAR SYSTEM, THE BAROREFLEX AND PUMP

The cardiovascular system is usually modeled by using electrical network with the voltage representing pressure, the current representing flow and charge representing volume. The ventricular function and the arterial network are the two main foci of the modeling efforts. Generally the left ventricle is model as a time varying capacitor (or elastance) which may take form of exponential [11], sinusoidal [12] or double hill function [13]. There are two ways of modeling the arterial network: lumped and distributed system. The windkessel models are typical lumped system modeling of the arterial network. A variety of windkessel models have been developed which are basically RLC networks [14, 15]. The transmission line is a typical distributed system modeling of the arterial network which simulates the pressure wave as a function of time and location [16-18]. It is noteworthy that the parameters of the models are fixed.

Besides the modeling of the heart and the arterial network, there are also efforts on modeling the baroreflex, the cardiovascular regulation system. The baroreflex is a built in

feedback system which stabilize the arterial pressure by varying the cardiac output and the systemic resistance. There are some pressure sensors located at the aortic arch and carotid sinus, which convert the pressure into nervous signal. This inbound nervous signal is then transmitted to the central nervous system and translated into outbound nervous signal. The outbound nervous signal stimulates the end organs such as the heart, the vasculature and renal system to keep the blood pressure equal or close to an intrinsically established setpoint.

Models of the baroreflex can be found in [19-21]. The baroreflex in [19] is modeled as a static mapping between the arterial pressure and the heart rate (or the systemic vascular resistance). The baroreflex models in both [20] and [21] consist of the baroreceptor (pressure sensor), the afferent pathway, the efferent pathways, and end organs effectors. With the baroreflex model coupled to the cardiovascular system, the parameters of the cardiovascular system such as the heart rate and the systemic vascular resistance are not fixed any more but become pressure-dependent.

The rotary pump model is effectively a current (blood flow) source connecting the ventricle to the systemic arterial system. The input of the model is the rotational speed and/or the electrical current. The variables that define the interface of the pump with the cardiovascular system are the inlet and outlet pressure, and pump flow [4, 22]. With this interface, the pump model can be coupled to the cardiovascular system model and used to simulate the interaction between the pump and the cardiovascular system and examine the performance of a control method.

2.2 PREVIOUS CONTROL FOR LVAD

The principal goal of the blood pump controller is to respond to and meet the body demand for cardiac output. The inputs of the controller are available hemodynamic variables of the patient and the output of the controller is the pump speed or electrical signals such as voltage and current. Figure 2.1 shows the animal experiment data with a rotary pump implanted where the pump speed is a ramped from 7.8 to 14.5 krpm over 150 seconds. The task of the controller is to provide a speed in the range of optimal zone or safe zone while avoiding suction zone or under pumping zone.

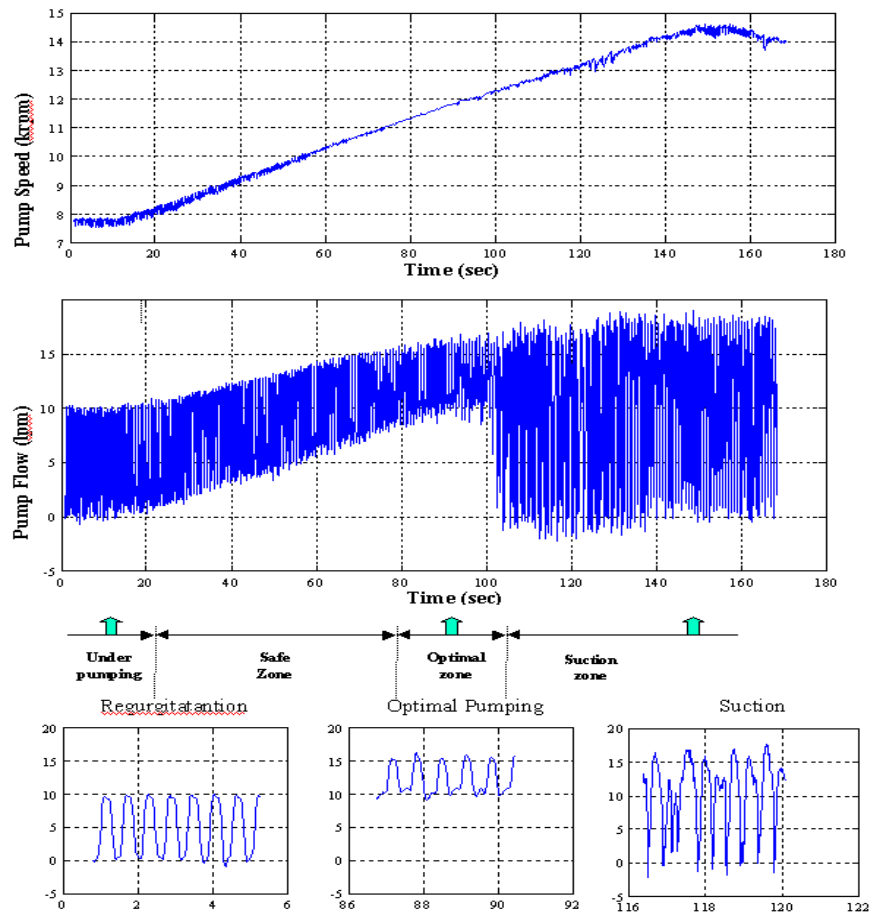


Figure 2.1. In vivo hemodynamics of calf implanted with turbodynamic LVAD
(University of Pittsburgh, unpublished data).

The pump speed is a ramp from 7.8 to 14.5 krpm. From left to right, the operating zones: back flow, safe, optimal and suction. The bottom shows traces of waveforms of pump flow for low speed, optimal speed and high speed.

However, the controller development is handicapped by the limited availability of physiological information of the body. Early solution for the control problem was to set a constant speed for the LVAD and recipients were supervised in the hospital [5]. While this open-loop method is easy to implement, the disadvantage is that once the physiological condition of the patient changes, the patient would be at risk of adverse phenomena such as back flow and suction.

Because of the limited available information for the controller, some sensor-less methods for LVAD control were developed by using the pump variables such as current, voltage and

speed [23-26]. This technique is based on the observation that pressure across, and flow through, a rotary VAD can be inferred or estimated from the electrical current and frequency of the pump's motor. Several other investigators have adopted a similar "sensor-less" approach to estimate pressure and flow [27-32]. However, these estimations and controllers are reliable only in a relatively narrow range of pump variables. When the pump is operating in a wide range of the patient's physiological situations, these controllers may mislead the pump to hazards for the recipients.

As to control strategy, one simple idea for the controller is to maximize the flow while avoiding suction (optimal zone in Figure 2.1). Some suction indices are based on time domain characteristics and frequency domain extraction from waveform of the pump flow. The harmonic spectral index is one of them [26]. This method is based on the observation that high frequency components in pump flow or pump current increase in suction zone compared to the fundamental frequency component. Another method is using the pulsatility of the flow as control input [4]. A method reducing the uncertainty of the suction detection was also developed [33]. More generally, keeping hemodynamic variables such as the atrial pressure, the aortic pressure and cardiac output close to nominal values may lead to multiple objectives optimization [6]. Hierarchical control for LVAD, an intelligent structure based on multiple objectives optimization and expert system, is further discussed in [34, 35]. The main challenge for this class of methods is the adaptability of the suction detector if SVR changes. To further exploit the fact that the minimum pump flow achieves the extremum at the point of suction event (around 100s in Figure 2.1), a controller was developed which tracks the extremum even as SVR changes [36]. The disadvantage of this class of methods is that the pump speed is close to the upper bound of the optimal zone and thus is precariously close to suction.

Controllers to keep the average pressure across the pump (or between the aorta and the left ventricle) constant have been developed in [31, 38-40]. This class of controllers can provide a pump speed in the safe zone or optimal zone for a certain SVR. However, the operating pump speed may move into the under pumping zone or suction zone if the SVR varies due to change in physiological state of the patient. The disadvantage for this class of methods is that these controllers require pressure sensors mounted at the inlet and outlet of the pump. If the use of pressure sensors is not practical, then the pressure difference may be estimated from the

rotational speed and/or the motor current by using sensor-less methods [31]. This would be limited by the applicable physiological range.

An investigation using oxygen saturation of the blood for control purpose has also been reported [41]. In an animal experiment a proportional control law was implemented that increased the flow of a total artificial heart in proportion to changes in the mixed venous oxygen saturation (MVO₂) which is acquired by an indwelling sensor. The addition of a MVO₂ sensor would benefit the overall robustness of the controller; however changes in MVO₂ are relatively slow, as compared to the rapid changes in vascular resistance, for example. A controller based on MVO₂ alone would not be able to respond to the rapid physiological changes and to avoid suction.

Other control approaches such as using the heart rate as a controller input have been reported [42]. As one part of the circulation regulatory system, the heart rate is an indicator of blood flow demand of the body. In the animal experiment, the controller adjusted the pump speed in response to increasing or decreasing heart rate in a linear relationship. The HR in this study was calculated from the pump current. In-vivo results demonstrated a positive response of this control scheme to treadmill exercises. However, this method does not take the change in SVR into account. From rest to exercise, there is a dramatic decrease in SVR accompanying the increase in heart rate. For the case of heart failure where the heart is not pumping effectively, change in SVR is a major mechanism to generate the desired cardiac output. The controller based on the HR alone may fail to provide the appropriate cardiac output for the physiologically changing body.

This dissertation will discuss an improved controller that incorporates the heart rate and the systemic vascular resistance and respond to the physiological changes of the body instantaneously based on the baroreflex, the built in cardiovascular regulation system. The heart rate can be inferred from pump current and the systemic vascular resistance can be estimated from blood flow and blood pressure. By incorporating the information of the heart rate and the systemic vascular resistance, the controller can vary the pump speed in response to the change in physiological state of the body, even for the challenging case of exercise.

2.3 THE PROPOSED INVESTIGATIONS

The main goal of this work is to improve the LVAD support for patients with heart failure. A physiological control algorithm will be developed, based on the models of implanted LVAD, the heart, circulation and regulatory system. The underlying principle of demand based control is the baroreflex, the autoregulatory system of the circulation, which manages the blood pressure and cardiac output. For a healthy person, the baroreflex regulates the blood pressure and cardiac output according to different physiological states of the body by changing heart rate, heart contractility, systemic vascular resistance and total blood volume. For a patient with heart failure, the baroreflex is preserved fairly well even though some end organs functions are attenuated or damaged. The proposed controller will use the estimated heart rate and estimated systemic vascular resistance as control inputs to generate the optimal pump speed for a specific physiological state.

The investigations will be based on a combination of existing theory and new models. The specific aims and associated technical approaches are:

- (1) To improve the combined model of the cardiovascular system and the LVAD. The coupled model of a LVAD and a cardiovascular system with a built in baroreflex will be established for simulating the interaction between the LVAD and the cardiovascular system and testing a physiological controller. This model will include the autoregulation of the cardiovascular system and the hydraulic power input from the pump. This model will be more realistic to simulate the interactions between the LVAD and the circulatory system regulated by the baroreflex.
- (2) To develop a physiological control algorithm for the LVAD that can incorporate various sensors inputs and/or estimations. A physiological controller for the LVAD will be developed which incorporates the information of heart rate and systemic resistance. This controller will behave like a part of the autoregulation of the cardiovascular system and thus will be responsive to changes in hemodynamic parameters and variables for different physiological states.
- (3) To implement and validate this control algorithm on the combined model of the LVAD and the cardiovascular system, and examine the performances of the proposed control algorithm by comparing to constant pump speed, constant pump head, and heart rate

related pump speed method. The resistance of the controller to noise will also be examined.

These are illustrated in Figure 2.2.

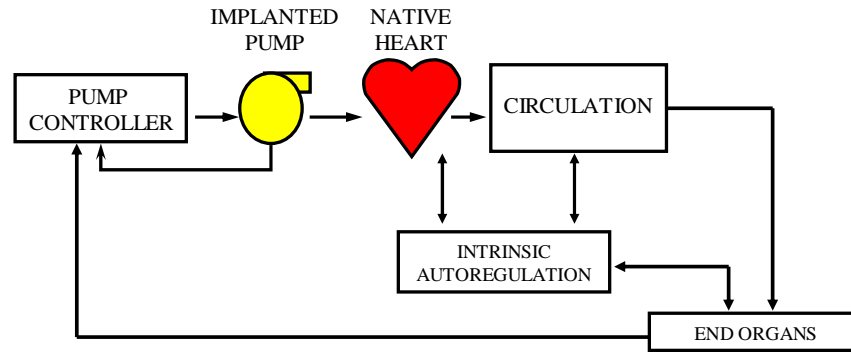


Figure 2.2. Block diagram of the proposed control scheme.

The following chapters will present the up-to-date progress of the investigation, including the healthy and failing cardiovascular models with built in baroreflex, the combined model of the pump and the cardiovascular system with baroreflex, and the proposed pump controller using the heart rate and the systemic vascular resistance as inputs.

3.0 MODEL OF HEALTHY HEART WITH BAROREFLEX

In this chapter, the pulsatile heart model is introduced in section 3.1 first and the baroreflex model in 3.2. Then the two models are coupled to simulate the interaction between them. The parameters of the coupled model are tuned in section 3.3 by using physiological simulation software Simbiosys as a reference. Then the response of the coupled model to single parameter change in preload, afterload, left ventricular contractility and heart rate is compared to that of Simbiosys in section 3.3. The response of the model to exercise is also examined in section 3.4.

3.1 THE CARDIOVASCULAR SYSTEM MODEL

The cardiovascular system model employed here is from [43-46] which is represented by the lumped parameter circuit shown in Figure 3.1. Table 3.1 lists the state variables, and Table 3.2 lists the system parameters and their associated values.

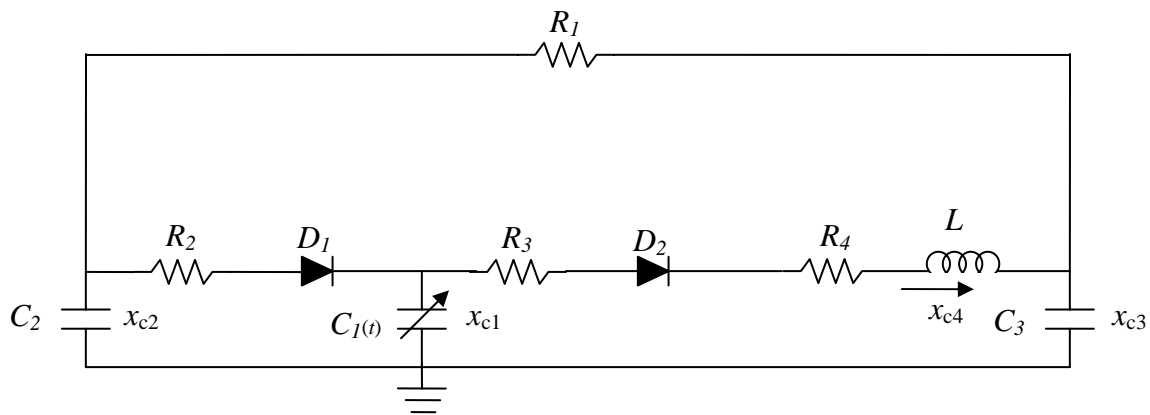


Figure 3.1. Cardiovascular system model.

Table 3.1. State variables

Variables	Physiological meaning (units)
x_{c1}	Left ventricular volume (ml)
x_{c2}	Left atrial pressure (mmHg)
x_{c3}	Arterial pressure (mmHg)
x_{c4}	Aortic Flow (ml/s)

Table 3.2. Parameters and values

Parameters	Physiological Meaning	Value	Units
Resistances			mmHg/ml/s
R_1	Systemic Resistance		
R_2	Mitral valve	0.005	
R_3	Aortic valve	0.001	
R_4	Characteristic resistance	0.0398	
Compliances			ml/mmHg
$C_1(t)$	Left ventricular compliance	Time-varying	
C_2	Left atrial compliance	4.4	
C_3	Systemic compliance	1.33	
Inertances			mmHg.s ² /ml
L	Inertance of blood in Aorta	0.0005	
Valves			
D_1	Mitral valve		
D_2	Aortic valve		

In this lumped parameter circuit, the left ventricle is described as a time-varying capacitor. One way to model its behavior is by means of the elastance function, which is the reciprocal of the compliance. It determines the change in pressure for a given change in volume within a chamber and was defined in [47] as following:

$$E(t) = \frac{LVP(t)}{LVV(t) - V_0} = 1/C_1(t) \quad (3.1)$$

Where $E(t)$ is the time varying elastance (mmHg/ml), $LVP(t) = x_1(t)$ is the left ventricular pressure (mmHg), $LVV(t)$ is the left ventricular volume (ml) and V_0 is a reference volume ($V_0 = 5$ ml for a normal heart), the theoretical volume in the ventricle at zero pressure.

The elastance function

$$E(t) = (E_{\max} - E_{\min})E_n(t_n) + E_{\min} \quad (3.2)$$

Where constants E_{\max} and E_{\min} are related to the end systolic pressure volume relationship (ESPVR) and the end diastolic pressure volume relationship (EDPVR), respectively. $E_n(t_n)$ is the normalized time-varying elastance, so called “double hill” function from [13], $t_n = t/T_{\max}$, $T_{\max} = 0.2 + 0.15t_c$ and t_c is the cardiac cycle.

$$E_n(t_n) = 1.55 * \left[\frac{\left(\frac{t_n}{0.7}\right)^{1.9}}{1 + \left(\frac{t_n}{0.7}\right)^{1.9}} \right] * \left[\frac{1}{1 + \left(\frac{t_n}{1.17}\right)^{21.9}} \right] \quad (3.3)$$

Notice that $E(t)$ is a re-scaled version of $E_n(t_n)$. Figure 3.2 shows the elastance function for $E_{\max} = 2.0$, $E_{\min} = 0.06$, and heart rate 60 bpm.

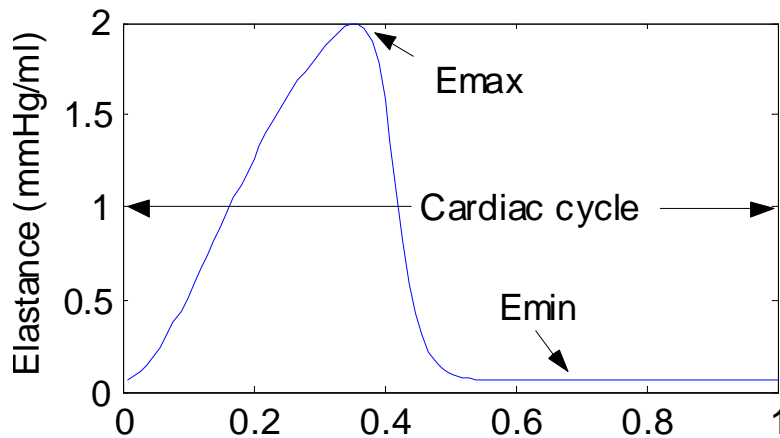


Figure 3.2. Typical elastance function
 $E_{\max} = 2.0$, $E_{\min} = 0.06$, and normalized cardiac cycle.

Since this model includes two diodes, the following phases will occur, over four different time intervals in a normal cardiac cycle, as illustrated in Table 3.3.

Table 3.3. Phases in a cardiac cycle

Modes	Valves		Phases
	D ₁	D ₂	
1	Closed	Closed	Isovolumic contraction
2	Closed	Open	Ejection
1	Closed	Closed	Isovolumic relaxation
3	Open	Closed	Filling
-	Open	Open	Not feasible

For each phase of the cardiac cycle, the state equation can be written into the form of

$$\frac{dx}{dt} = A(t)x \quad (3.4)$$

with different matrix $A(t)$ for each phase, $x = [x_{c1} \ x_{c2} \ x_{c3} \ x_{c4}]^T$.

1) *Isovolumic phase*: In this phase of the cardiac cycle, the aortic and mitral valves are closed. Since the aortic valve is closed, the aortic flow is zero, i.e., $x_{c4} = 0$. In this phase, we have:

$$A(t) = \begin{bmatrix} 0 & 0 & 0 & 0 \\ 0 & -\frac{1}{R_1 C_2} & \frac{1}{R_1 C_2} & 0 \\ 0 & \frac{1}{R_1 C_3} & -\frac{1}{R_1 C_3} & 0 \\ 0 & 0 & 0 & 0 \end{bmatrix} \quad (3.5)$$

2) *Ejection phase*: In this phase, the aortic valve is open, and the mitral valve is closed. In this phase the left ventricle is pumping blood into the circulatory system, where

$$A(t) = \begin{bmatrix} 0 & 0 & 0 & -1 \\ 0 & -\frac{1}{R_1 C_2} & \frac{1}{R_1 C_2} & 0 \\ 0 & \frac{1}{R_1 C_3} & -\frac{1}{R_1 C_3} & \frac{1}{C_3} \\ \frac{E(t)}{L} & 0 & -\frac{1}{L} & -\frac{(R_3 + R_4)}{L} \end{bmatrix} \quad (3.6)$$

3) *Filling phase*: When the heart is filling, blood from the left atrium goes into the left ventricle. The mitral valve is open, and the aortic valve is closed which again implies $x_{c4} = 0$. For this phase,

$$A(t) = \begin{bmatrix} -\frac{E(t)}{R_2} & \frac{E(t)}{R_2} & 0 & 0 \\ \frac{E(t)}{R_2 C_2} & -\frac{(R_1 + R_2)}{R_1 R_2 C_2} & \frac{1}{R_1 C_2} & 0 \\ 0 & \frac{1}{R_1 C_3} & -\frac{1}{R_1 C_3} & 0 \\ 0 & 0 & 0 & 0 \end{bmatrix} \quad (3.7)$$

The case with both valves open does not occur for a normal heart and thus is not included in this model. For a sequence of these phases in a normal cardiac cycle, for example, filling-contraction-ejection-relaxation, the end states of the last phase are initial conditions for the next phase.

3.2 THE BAROREFLEX MODEL

The baroreflex model employed here is from [48-50] with some parameters tuned to simulate the human dynamics. In this model, the baroreflex consists of the baroreceptor, the afferent pathway, the efferent pathways and the regulation effectors. The baroreceptor is a pressure sensor located in the carotid sinus or aorta which converts pressure into afferent firing frequency. Then the afferent firing frequency is translated into efferent signals by the nervous system: sympathetic

firing frequency and vagal firing frequency. These efferent signals are the inputs of the regulation effectors. The regulation effects include changes in vessels resistances and heart rate (or cardiac cycle). For example, if the pressure is lower than the set point, the systemic resistance and heart rate will increase to reduce the error between the current pressure and the set point pressure. The closed loop baroreflex of the block diagram in Figure 3.3 is applied on the cardiovascular model in Figure 3.1. The different parts of the baroreflex are described as follows.

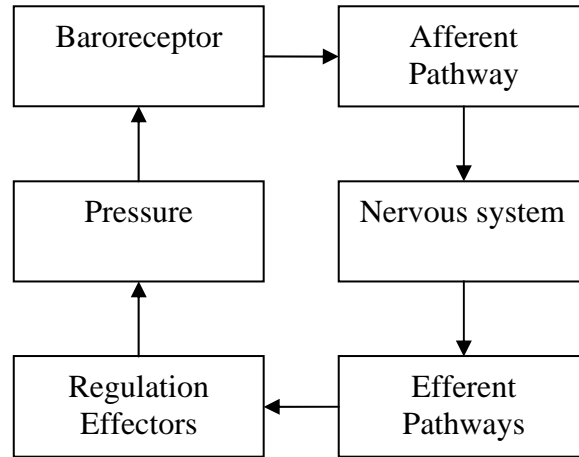


Figure 3.3. Block diagram for the carotid baroreflex.

The baroreflex consists of baroreceptor, afferent pathway, efferent pathway and regulation effectors.

Afferent pathway. In [48] the afferent baroreflex pathway is described as the series arrangement of a linear derivative first-order dynamic block and a sigmoidal function as shown in Figure 3.4.

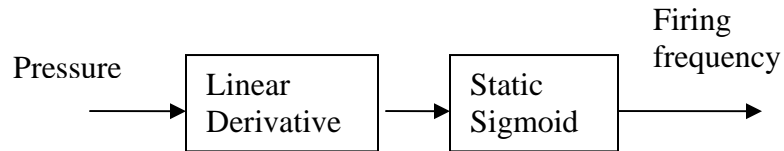


Figure 3.4. Block diagram for the afferent pathway of carotid sinus.

The linear derivative block in Figure 3.4

$$\tau_p \frac{dp}{dt} = p_{in} + \tau_z \frac{dP_{in}}{dt} - p \quad (3.8)$$

Where τ_p and τ_z are the time constants for the real pole and the real zero in the linear dynamic block (usually with $\tau_z/\tau_p > 1$), p_{in} is the carotid sinus pressure, p is the output variable of the linear derivative dynamic block (with dimension of pressure).

The static sigmoidal function in Figure 3.4 is

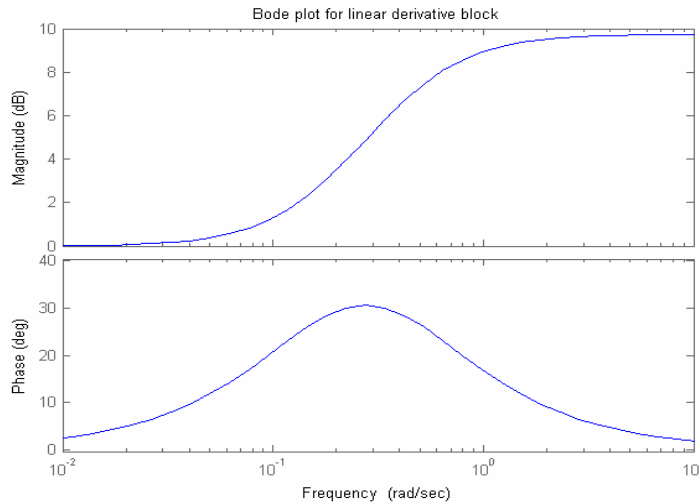
$$f_{as}(P) = \frac{f_{\min} + f_{\max} e^{\left(\frac{P-P_o}{K_a}\right)}}{1 + e^{\left(\frac{P-P_o}{K_a}\right)}} \quad (3.9)$$

where f_{as} is the frequency of spikes in the afferent fibers, f_{\max} and f_{\min} are the upper and lower saturation of the frequency discharge, P_o is the value of the intrasinus pressure at the central point of the sigmoidal functional, K_a is a parameter with the dimension of pressure, related to the slope of the static sigmoidal function at the central point. The characteristic curves for the linear derivative and static sigmoid functions are shown in Figure 3.5.

Efferent sympathetic pathway. The monotonically decreasing function that relates the activity in the afferent and efferent neural pathways is described by an exponential shaped function [48].

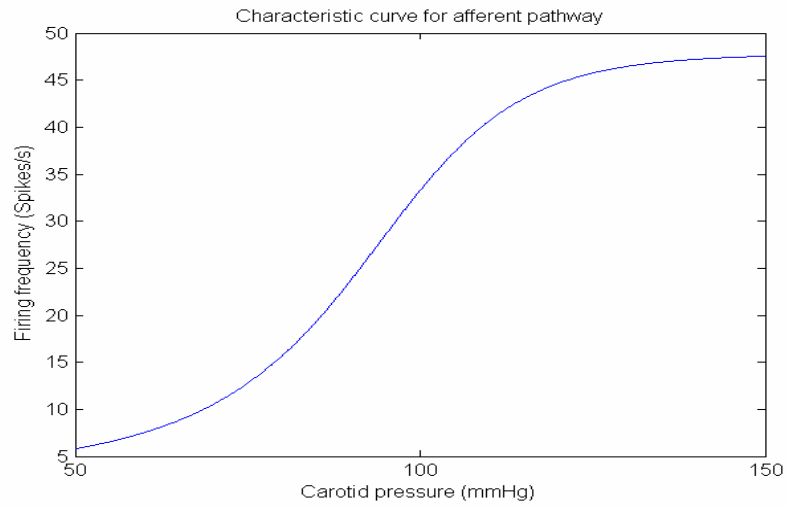
$$f_{es}(f_{as}) = f_{es\infty} + (f_{es0} - f_{es\infty})e^{-K_{es}f_{as}} \quad (3.10)$$

Where f_{es} is the frequency of spikes in the efferent sympathetic nerves, K_{es} , f_{es0} and $f_{es\infty}$ are constants (with $f_{es0} > f_{es\infty}$), f_{as} is the output in (3.9). The characteristic curve is shown in Figure 3.6.



a. Characteristic curve (frequency domain) for afferent pathway (linear derivative).

$$\tau_z = 6.37 \text{ s}; \tau_p = 2.076 \text{ s};$$



b. Characteristic curve for afferent pathway (static sigmoid).

$$P_o = 80 \text{ mmHg}; K_a = 11.758 \text{ mmHg}; f_{\min} = 2.52 \text{ spikes/s}; f_{\max} = 47.78 \text{ spikes/s}.$$

Figure 3.5. Characteristic curves for the afferent pathway.

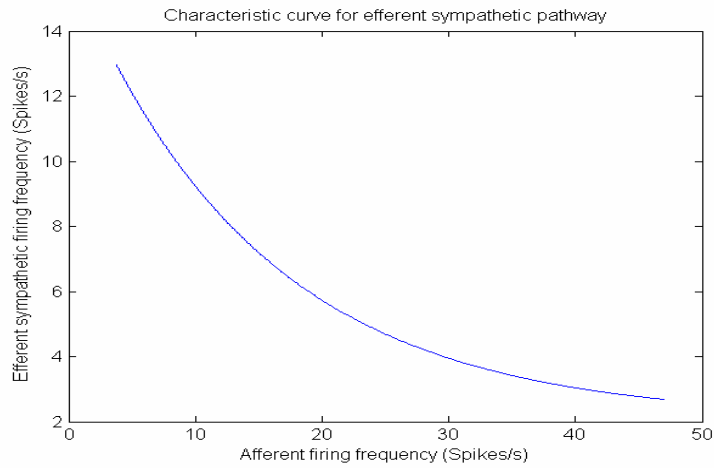


Figure 3.6. Characteristic curve for the efferent sympathetic pathway.

$$f_{es\infty} = 2.1 \text{ spikes/s}; f_{es0} = 16.11 \text{ spikes/s}; K_{es} = 0.0675 \text{ s/spikes}.$$

Efferent vagal pathway. The efferent vagal activity is a monotonically increasing function of the activity in the sinus nerve with an upper saturation. The sigmoidal equation similar to (3.11) is used [48]

$$f_{ev}(f_{as}) = \frac{f_{ev0} + f_{ev\infty} e^{\frac{(f_{as}-f_{aso})}{K_{ev}}}}{1 + e^{\frac{(f_{as}-f_{aso})}{K_{ev}}}} \quad (3.11)$$

Where f_{ev} is the frequency of spikes in the efferent vagal fibers, K_{ev} , f_{ev0} and $f_{ev\infty}$ are constant parameters (with $f_{ev\infty} > f_{ev0}$), f_{aso} is the central value in the characteristic curve in (3.9) and f_{as} is the output in (3.9). The characteristic curve is shown in Figure 3.7.

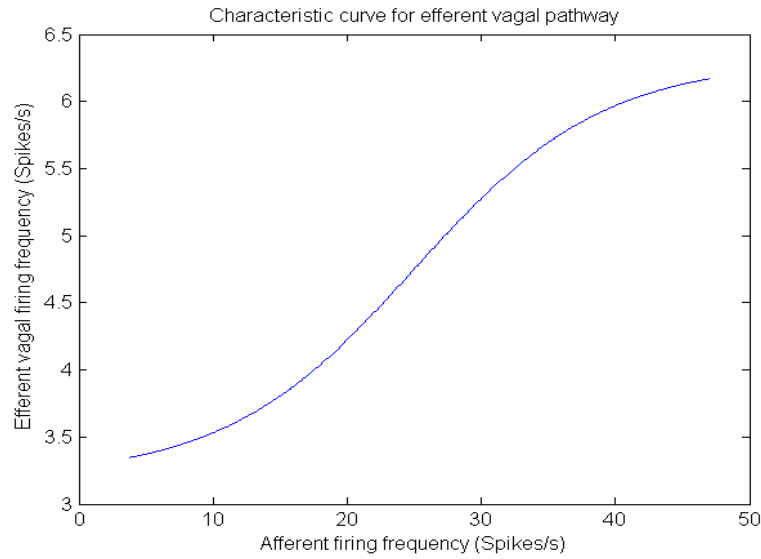


Figure 3.7. Characteristic curve for the efferent vagal pathway.

$$f_{ev0} = 3.2 \text{ spikes/s}; f_{ev\infty} = 6.3 \text{ spikes/s}; f_{aso} = 25 \text{ spikes/s}; K_{ev} = 7.06 \text{ spikes/s}.$$

Regulation effectors

A. Sympathetic effectors on resistances

To simulate the blood flow distribution among the different parts of the body, the systemic vascular resistance is divided into three parts: R_1 , R_2 , R_3 . R_1 is the splanchnic resistance; R_2 is the resistance other than active muscle and splanchnic resistance; R_3 is the active muscle resistance.

The response of the resistances to the sympathetic drive includes a delay, a logarithmic static function, and a low-pass first-order dynamics [48].

$$e_{R_i}(t) = \begin{cases} G_{R_i} \ln[f_{es|_{(t-D_i)}} - f_{es\min} + 1] & f_{es} \geq f_{es\min} \\ 0 & f_{es} < f_{es\min} \end{cases} \quad (3.12)$$

$$\frac{d\Delta R_i(t)}{dt} = \frac{1}{\tau_{R_i}} (-\Delta R_i(t)) + e_{R_i}(t) \quad (3.13)$$

$$R_i(t) = \Delta R_i(t) + R_{i0} \quad (3.14)$$

Where R_i is the resistances with $i = 1, 2, 3$, e_{R_i} is the output of the static logarithmic characteristic function, $f_{es|_{(t-D_i)}}$ is the value of f_{es} evaluated at $(t - D_i)$, τ_{R_i} and D_i are the time constants and delay of the mechanism, $f_{es\min}$ is the minimum sympathetic stimulation, and $\Delta R_i(t)$ is the resistance change with respect to R_{i0} caused by sympathetic stimulation and G_{R_i} is a constant gain factor.

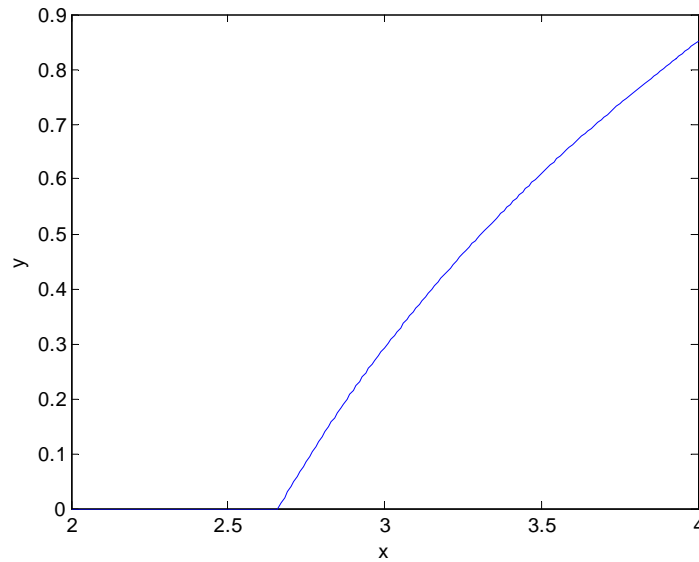


Figure 3.8. Characteristic curve for equation (3.12).

$$y = \begin{cases} \ln[x - f_{es\min} + 1] & f_{es} \geq f_{es\min} \\ 0 & f_{es} < f_{es\min} \end{cases}$$

$$f_{es\min} = 2.66$$

B. Heart rate effectors

The response of the cardiac cycle is a result of both the vagal and sympathetic activities. The cardiac cycle changes induced by sympathetic stimulation are achieved through equations similar to (3.12) and (3.13) [48].

$$e_{Ts}(t) = \begin{cases} G_{Ts} \ln[f_{es}(t-D_{Ts}) - f_{es\min} + 1] & f_{es} \geq f_{es\min} \\ 0 & f_{es} < f_{es\min} \end{cases} \quad (3.15)$$

$$\frac{d\Delta Ts(t)}{dt} = \frac{1}{\tau_{Ts}} (-\Delta Ts(t)) + e_{Ts}(t) \quad (3.16)$$

The cardiac cycle change induced by vagal activity differs from the sympathetic case because cardiac cycle increases linearly with the efferent vagal excitation [48].

$$e_{Tv}(t) = G_{Tv} f_{ev}(t - D_{Tv}) \quad (3.17)$$

$$\frac{d\Delta Tv(t)}{dt} = \frac{1}{\tau_{Tv}} (-\Delta Tv(t)) + e_{Tv}(t) \quad (3.18)$$

Where the meanings of the symbols are similar to that of (3.12) and (3.13).

The cardiac cycle is calculated by assuming a linear interaction between the sympathetic and vagal caused changes [48].

$$T(t) = \Delta Ts(t) + \Delta Tv(t) + T_0 \quad (3.19)$$

Where $T(t)$ is the overall altered cardiac cycle due to sympathetic and vagal stimulation, $\Delta Ts(t)$ is the change due to sympathetic stimulation, $\Delta Tv(t)$ is the change due to vagal stimulation, T_0 is the constant cardiac cycle without any nervous excitation.

3.3 THE COMBINED MODEL OF THE BAROREFLEX AND THE CARDIOVASCULAR SYSTEM

Based on the cardiovascular model in section 3.1, the baroreflex model is coupled to it. In the combined model of Figure 3.9, RI in the cardiovascular circuit model is the SVR which is divided into 3 parallel parts to simulate the blood flow distribution among different parts of the

body. The left ventricle contractility (E_{max}) and total blood volume (V_T , summation of the charge in capacitors and inductors) are results of sympathetic excitation in the model. The arterial pressure is the input for the baroreflex. The SVR , HR , E_{max} and V_T are under the control of the baroreflex. Specifically, the SVR , E_{max} and V_T vary instantaneously; the HR (60/ cardiac cycle) varies cycle by cycle, in other words, the HR remains constant in a cardiac cycle.

The hemodynamic variables generated by Simbiosys (Critical Concepts, Inc) [51] are used as reference for tuning the parameters for this coupled model. Simbiosys is a physiology simulation software which uses mathematical models to simulate the function of the heart and the autonomic control of a human.

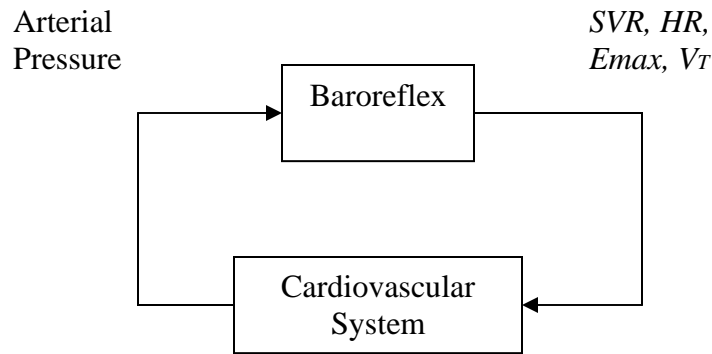


Figure 3.9. Pulsatile heart coupled with baroreflex.

The arterial pressure is the input of the baroreflex, SVR , HR , E_{max} , V_T are under the control of the baroreflex.

Table 3.4 shows the state variables for the baroreflex block and Table 3.5 parameters (most from [48-51]) and values for tuning the baroreflex to generate normal hemodynamics. The resulting steady total blood volume is about 250 ml. The SVR (R_1 in the circuit) in this model is still divided into three parallel parts: R_{11} , R_{12} , R_{13} .

Table 3.4. State variables for baroreflex

x_{b1}	the change in splanchnic resistance due to sympathetic stimulation
x_{b2}	the change in the resistance other than active muscle and splanchnic resistance due to sympathetic stimulation

Table 3.4. (continued)

x_{b3}	the change in active muscle resistance due to sympathetic stimulation
x_{b4}	the change in cardiac cycle due to sympathetic stimulation
x_{b5}	the change in cardiac cycle due to vagal stimulation
x_{b6}	the change in heart contractility due to sympathetic stimulation
x_{b7}	the change in total blood volume due to sympathetic stimulation

State equations:

$$\frac{dx_{bi}}{dt} = -\frac{1}{\tau_i} x_{bi} + u_i(x_{c3}) \quad \text{for } i = 1, 2, 3, 4, 5, 6, 7 \quad (3.20)$$

Where x_{c3} is the arterial pressure in section 3.1.

$$u_i(x_{c3}) = \begin{cases} g_i \ln[f_{es} |_{(t-d_i)} - f_{es\min} + 1] & f_{es} |_{(t-d_i)} \geq f_{es\min} \\ 0 & f_{es} |_{(t-d_i)} < f_{es\min} \end{cases} \quad i = 1, 2, 3, 4, 6, 7 \quad (3.21)$$

$$u_5(x_{c3}) = g_5 f_{ev} |_{(t-d_5)} \quad (3.22)$$

Where $f_{es} |_{(t-d_i)}$ is f_{es} evaluated at $t - d_i$, $f_{ev} |_{(t-d_5)}$ is f_{ev} evaluated at $t - d_5$.

$$f_{es} = f_{es0} + offset_{es} + (f_{es0} - f_{es0}) * \exp\left\{ \frac{-K_{es} * [f_{\min} + f_{\max} * \exp(\frac{x_{c3}-P_0}{K_u})]}{[1 + \exp(\frac{x_{c3}-P_0}{K_u})]} \right\} \quad (3.23)$$

$$f_{ev} = offset_{ev} + \frac{f_{ev0} + f_{ev0} * \exp\left\{ [\exp(\frac{x_{c3}-P_0}{K_u}) - f_{aso}] / K_{ev} \right\}}{1 + \exp\left\{ [\exp(\frac{x_{c3}-P_0}{K_u}) - f_{aso}] / K_{ev} \right\}} \quad (3.24)$$

$$R_{11} = R_{10} + x_{b1} \quad (3.25)$$

$$R_{12} = R_{20} + x_{b2} \quad (3.26)$$

$$R_{13} = R_{30} + x_{b3} \quad (3.27)$$

$$T = T_0 + x_{b4} + x_{b5} \quad (3.28)$$

$$E_{\max} = E_{\max 0} + x_{b6} \quad (3.29)$$

$$V_T = V_{T0} + x_{b7} \quad (3.30)$$

Where $\tau_i, g_i, d_i, f_{es\min}, f_{es\infty}, f_{es0}, K_{es}, offset_{es}, f_{ev0}, f_{ev\infty}, K_{ev}, offset_{ev}, f_{aso}, f_{\min}, f_{\max}, K_a, P_o, SV, R_{10}, R_{20}, R_{30}, T_0, f_{es\min}, E_{\max0}, V_{T0}$ are constants, f_{es} is the sympathetic activity, f_{ev} is the vagal activity.

Table 3.5. Values for baroreflex parameters

Parameter	Value	Physiological meaning
τ_1	10 s	Time constant for resistance
τ_2	10 s	Time constant for resistance
τ_3	10 s	Time constant for resistance
τ_4	4 s	Time constant for sympathetic stimulated cardiac cycle change
τ_5	1.5 s	Time constant for vagal stimulated cardiac cycle change
τ_6	10 s	Time constant for sympathetic stimulated heart contractility change
τ_7	20 s	Time constant for sympathetic stimulated total blood volume change
g_1	0.695	Gain for splanchnic resistance change
g_2	0.53	Gain for other resistance change
g_3	2.81	Gain for muscle resistance
g_4	-0.6	Gain for sympathetic stimulated cardiac cycle change
g_5	0.1	Gain for vagal stimulated cardiac cycle change
g_6	0.475	Gain for sympathetic stimulated heart contractility change
g_7	20	Gain for sympathetic stimulated total blood volume change

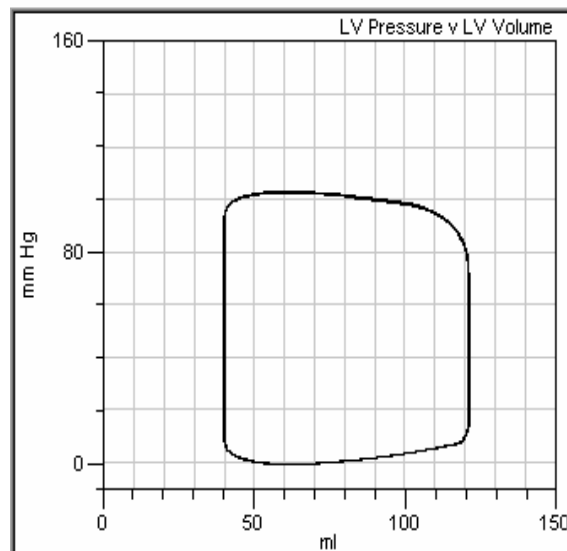
Table 3.5. (continued)

d_1	2 s	Time delay for sympathetic stimulated resistance change
d_2	2 s	Time delay for sympathetic stimulated resistance change
d_3	2 s	Time delay for sympathetic stimulated resistance change
d_4	2 s	Time constant for sympathetic stimulated cardiac cycle change
d_5	0.2 s	Time constant for vagal stimulated cardiac cycle change
d_6	2 s	Time delay for sympathetic stimulated heart contractility change
d_7	5 s	Time delay for sympathetic stimulated total blood volume change
τ_z	6.37 s	Constant
τ_p	2.076 s	Constant
$f_{es\min}$	2.66 spikes/s	Threshold value for sympathetic excitation
$f_{es\infty}$	2.1 spikes/s	Constant
f_{es0}	16.11 spikes/s	Constant
K_{es}	0.0675 s/spikes	Constant
<i>offset_es</i>	0 spikes/s	Offset in sympathetic activity
f_{ev0}	3.2 spikes/s	Constant
$f_{ev\infty}$	6.3 spikes/s	Constant
K_{ev}	7.06 spikes/s	Constant
<i>offset_ev</i>	0 spikes/s	Offset in vagal activity
f_{aso}	25 spikes/s	Constant

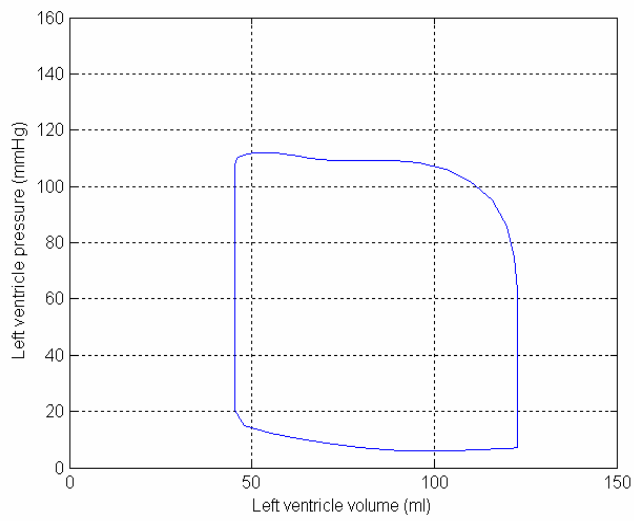
Table 3.5. (continued)

f_{\min}	2.52 spikes/s	Constant
f_{\max}	47.78 spikes/s	Constant
K_a	11.758 mmHg	Constant
P_o	92 mmHg	Constant
R_{10}	2.49 mmHg/ml/s	Constant
R_{20}	0.96 mmHg/ml/s	Constant
R_{30}	4.13 mmHg/ml/s	Constant
T_0	0.2 s	Constant
$E \max_0$	2.2 mmHg/ml	Constant
V_{T0}	205 ml	Constant

The baseline P-V loops for Simbiosys and the model are shown in Figure 3.10 and the waveforms of left ventricular pressure and left ventricular volume are shown in Figure 3.11. Table 3.6 lists the baseline hemodynamics for both the model and Simbiosys. It can be seen that the model reproduces fairly well the baseline hemodynamics generated by Simbiosys.

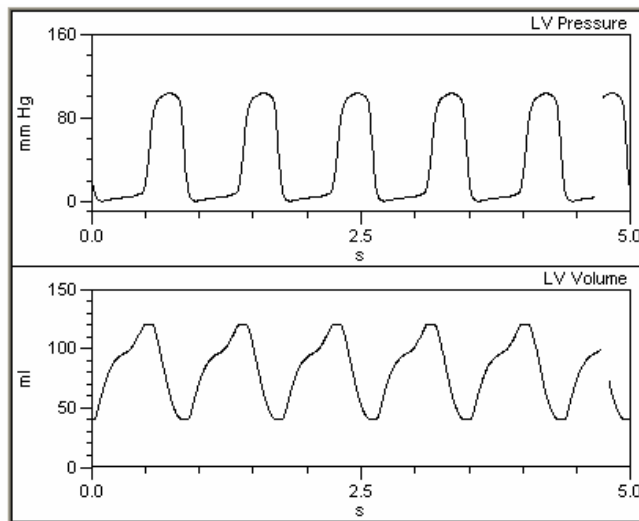


a. Baseline P-V loop from Simbiosys.

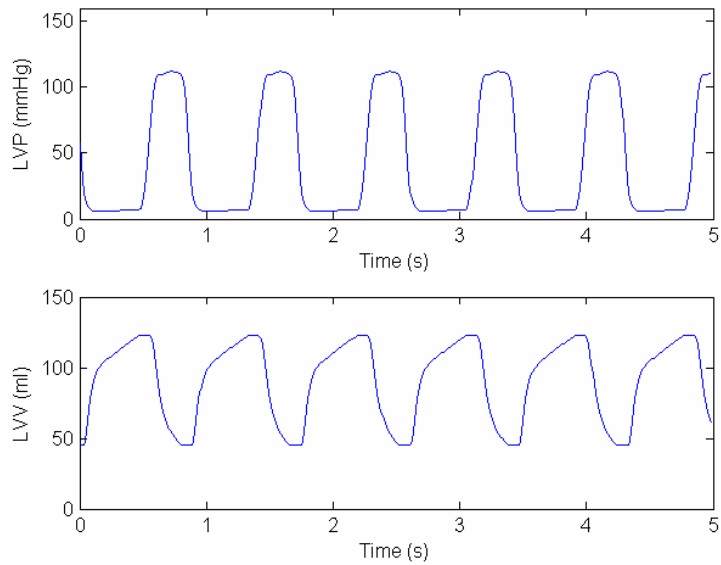


b. P-V loop generated by the model.

Figure 3.10. P-V loops generated by the model and Simbiosys.



a. Left ventricular pressure and left ventricular volume from Simbiosys.



b. Left ventricular pressure and left ventricular volume generated by the model.

Figure 3.11. Left ventricular pressure and left ventricular volume.

Table 3.6. Baseline Hemodynamics

Simbiosys		Model	
LVEDP (mmHg)	7	LVEDP (mmHg)	7
LVESP (mmHg)	90	LVESP (mmHg)	89
EDV (ml)	118	EDV (ml)	121
ESV (ml)	40	ESV (ml)	44
MAP (mmHg)	88	MAP (mmHg)	89
SV (ml)	78	SV (ml)	77
HR (bpm)	68	HR (bpm)	69
CO (l/min)	5.3	CO (l/min)	5.3
LV contractility	1.03	Emax (mmHg/ml)	2.7
Arterial contractility	1.16	SVR (mmHg/ml/s)	0.91
Sympathetic tone	0.137	Sympathetic activity	2.78
Parasympathetic tone	0.360	Parasympathetic activity	6.11

LVEDP: left ventricular end diastolic pressure; LVESP: left ventricular end systolic pressure; EDV: end diastolic volume; ESV: end systolic volume; MAP: mean arterial pressure; SV: stroke volume; HR: heart rate; CO: cardiac

output; Emax: peak left ventricular contractility; SVR: systemic arterial resistance. Sympathetic activity and parasympathetic activity are in mean value (spikes/s). LVESP for Simbiosys is read directly from the panel; LVESP for the model is hard to read thus assumed the same as MAP. The values for LV contractility, arterial contractility are dimensionless relative parameters (needed to be multiplied by a constant contractility); sympathetic tone and parasympathetic tone are dimensionless parameters range from 0 (no tone) to 1 (maximum tone).

3.4 RESPONSE TO SINGLE PARAMETER CHANGE

The behaviors of the model and Simbiosys are compared by examining the response of the both to single parameter change in preload, afterload, left ventricular contractility and heart rate.

3.4.1 Response to decrease in preload (blood withdrawal)

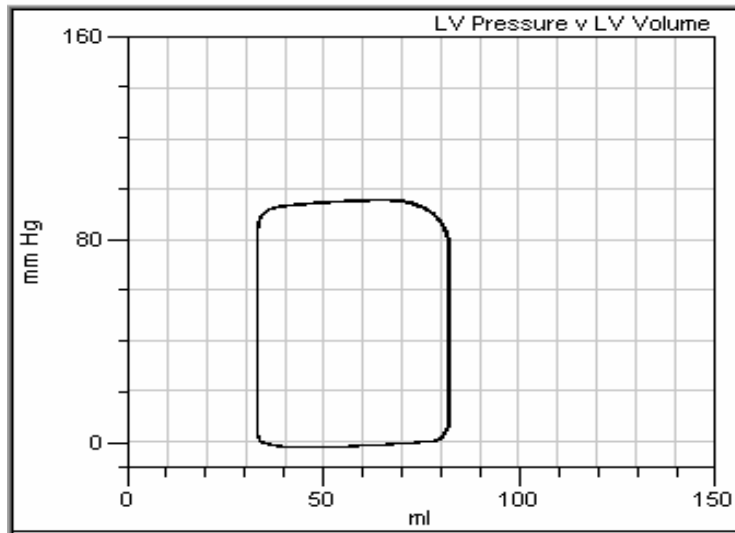
This subsection will examine the response of the model to forced change in preload by using blood withdrawal. The percentage of blood loss is set the same for Simbiosys and the model. For example, for the normal value of total blood volume 5000 ml, -500 ml implies 10 % loss of blood in Simbiosys. Similarly, for the model with total blood volume of 250 ml, -25 ml implies 10% loss of blood. The maximum available withdrawal rate 10000 ml/hr (or 2.78 ml/s) in Simbiosys is used to avoid fluid compensation from the renal system. For the model, the rate of bleeding is the same by decreasing the left ventricular volume. The steady state values are recorded in Table 3.7 after the desired loss of blood is finished. P-V loops are shown in Figure 3.12 for 20% loss of blood. Figure 3.13 shows the changes in hemodynamic variables compared with corresponding baseline values.

Table 3.7. Response to change in preload

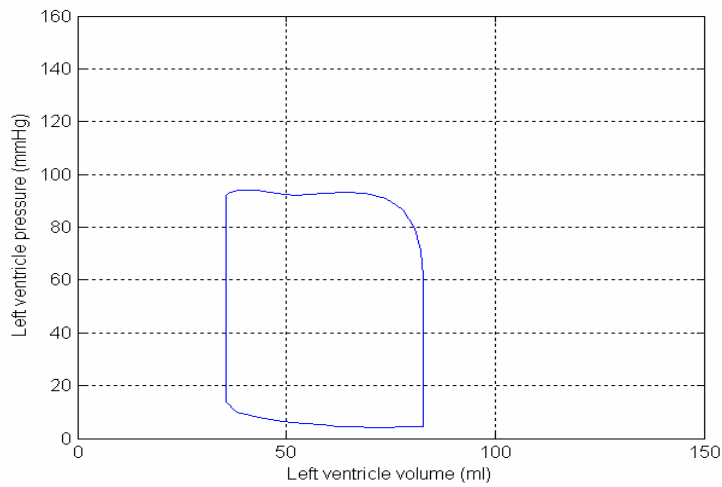
	Hemodynamics	Baseline	10% loss of blood	20% loss of blood	Tendency
	LVEDP (mmHg)	7	4	0	Down
	LVESP (mmHg)	90	87	82	Down

Table 3.7. (continued)

Symbiosys	EDV (ml)	118	104	78	Down
	ESV (ml)	40	37	33	Down
	MAP (mmHg)	88	86	85	Down
	SV (ml)	78	67	45	Down
	HR (bpm)	68	74	98	Up
	CO (l/min)	5.3	5.0	4.4	Down
	LV contractility	1.03	1.05	1.06	Up
	Arterial contractility	1.16	1.22	1.31	Up
	Sympathetic tone	0.137	0.185	0.256	Up
	Parasympathetic tone	0.360	0.360	0.268	Down
Model	LVEDP (mmHg)	7	6	5	Down
	LVESP (mmHg)	89	85	81	Down
	EDV (ml)	121	102	83	Down
	ESV (ml)	44	40	35	Down
	MAP (mmHg)	89	85	81	Down
	SV (ml)	77	62	48	Down
	HR (bpm)	69	76	86	Up
	CO (l/min)	5.3	4.7	4.1	Down
	E _{max} (mmHg/ml)	2.7	2.8	3.0	Up
	SVR (mmHg/ml/s)	0.91	0.98	1.1	Up
	Sympathetic activity	2.78	2.80	2.86	Up
	Parasympath activity	6.11	6.11	6.07	Down

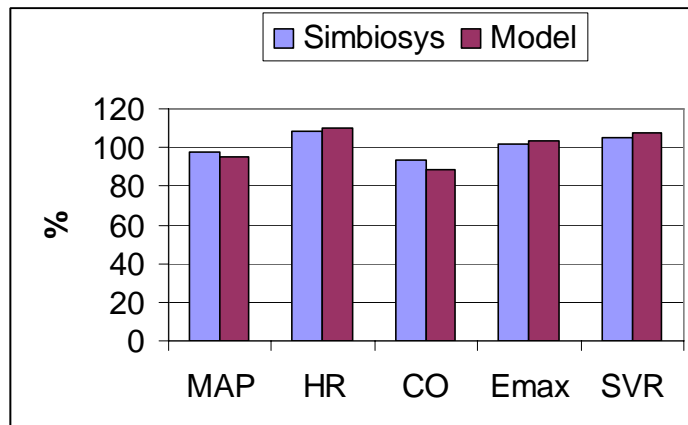


a. 20% Blood withdrawal for Simbiosys.

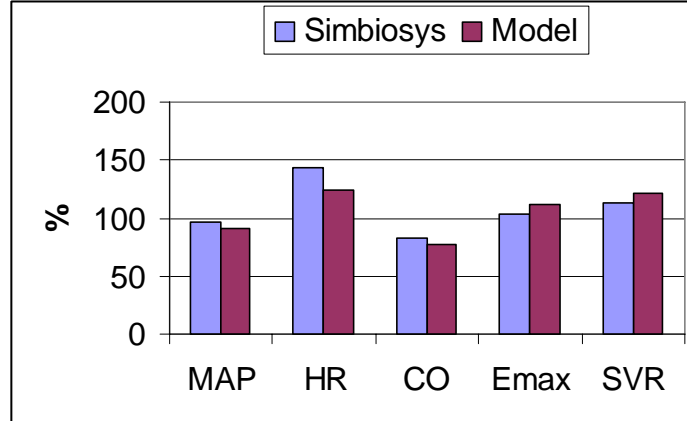


b. 20% Blood withdrawal for the model.

Figure 3.12. Change in P-V loop for 20% blood withdrawal.



a. 10 % loss of blood.



b. 20 % loss of blood.

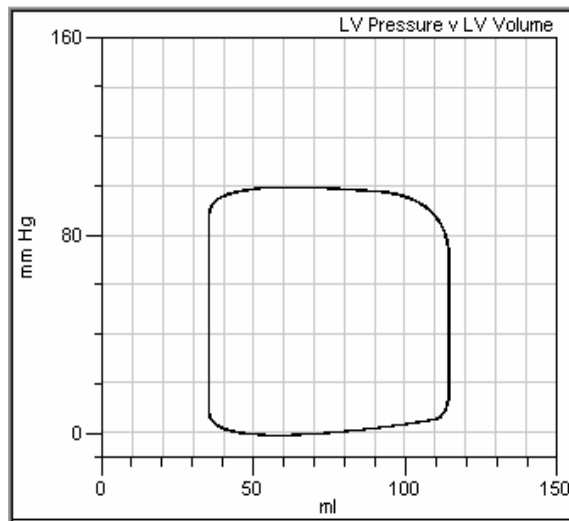
Figure 3.13. Changes in hemodynamics for loss of blood.

With loss of blood, CO and MAP decrease; HR, SVR, and Emax increase.

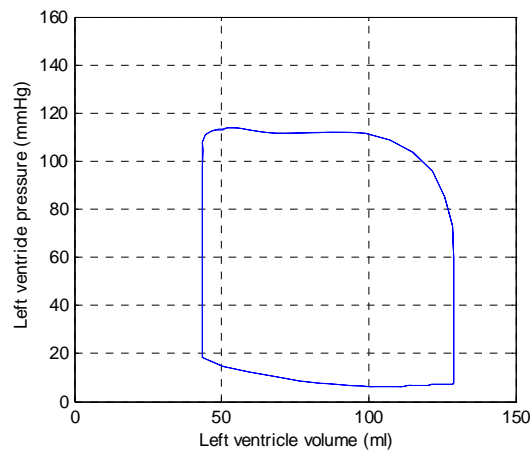
For both Simbiosys and the model, when preload decreases, (1) P-V loops shrink towards the left bottom corner of the coordinate; (2) stroke volume decreases and heart rate increases but cardiac output decreases; (3) mean arterial pressure decreases even though systemic vascular resistance increases; (4) left ventricular contractility and sympathetic activity increases, parasympathetic activity decreases.

3.4.2 Response to change in afterload (SVR)

This subsection will examine the response of the model to forced change in afterload by using forced change in SVR. The change in SVR for Simbiosys is induced by forced change in arterial contractility. For the model, it is induced by forced change in SVR directly. The steady state values are recorded in Table 3.8 after the changes. P-V loops in Figure 3.14 and Figure 3.15 are shown respectively for -20% and +20% change in SVR for Simbiosys and the model. Figure 3.16 shows the changes in hemodynamic variables compared with corresponding baseline values.

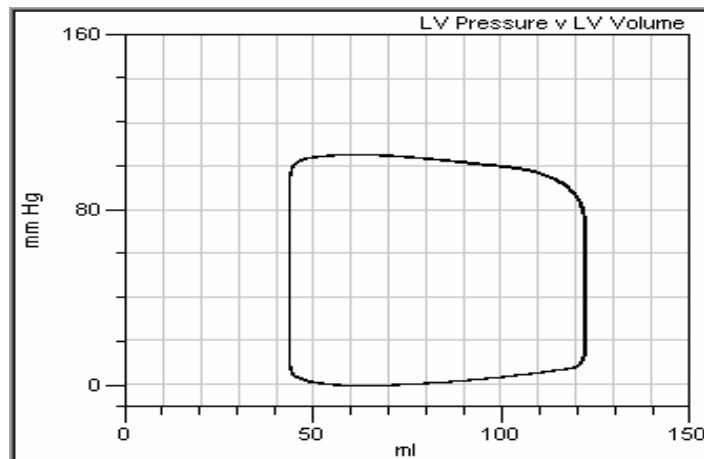


a. -20% in SVR for Simbiosys.

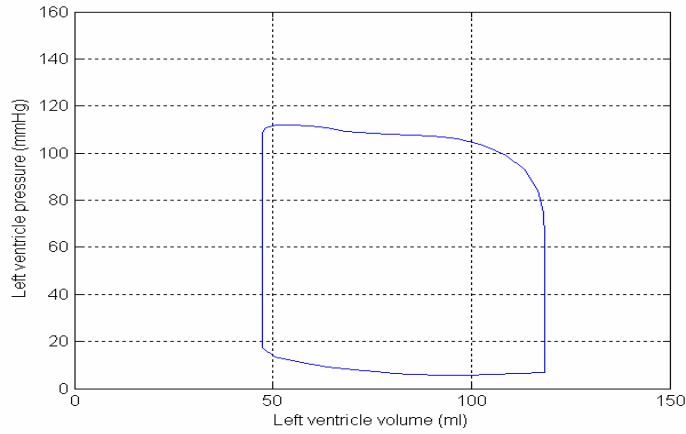


b. -20% in SVR for the model.

Figure 3.14. Change in P-V loop for -20% in SVR.



a. +20% in SVR for Simbiosys.



b. +20% in SVR for the model.

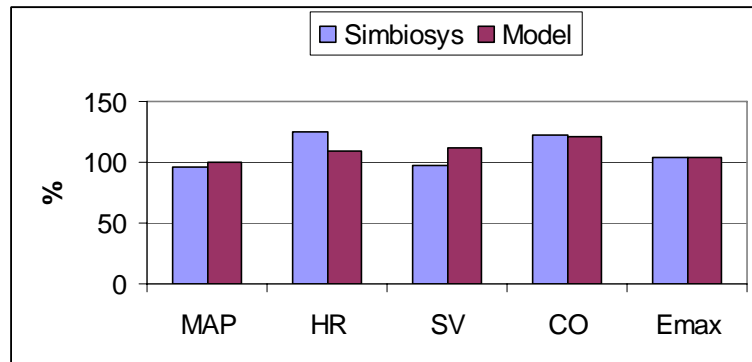
Figure 3.15. Change in P-V loop for +20% in SVR.

Table 3.8. Response to change in afterload

	Hemo-dynamics	-20% in SVR	-10% in SVR	Base line	+10% in SVR	+20% in SVR	Tendency
Sim biosys	LVEDP (mmHg)	5	6	7	7	7	Up
	LVESP (mmHg)	84	87	90	92	93	Up
	EDV (ml)	111	116	118	119	119	Up
	ESV (ml)	35	38	40	42	44	Up
	MAP (mmHg)	85	87	88	89	90	Up
	SV (ml)	76	78	78	77	75	Down
	HR (bpm)	85	75	68	64	60	Down
	CO (l/min)	6.5	5.9	5.3	4.9	4.5	Down
	LV contractility	1.07	1.05	1.03	1.03	1.03	Down
	Arterial contractility	0.87	1.02	1.16	1.26	1.40	Up
	Sympathetic tone	0.262	0.186	0.137	0.112	0.080	Down
	Parasympathetic	0.360	0.360	0.360	0.360	0.360	same

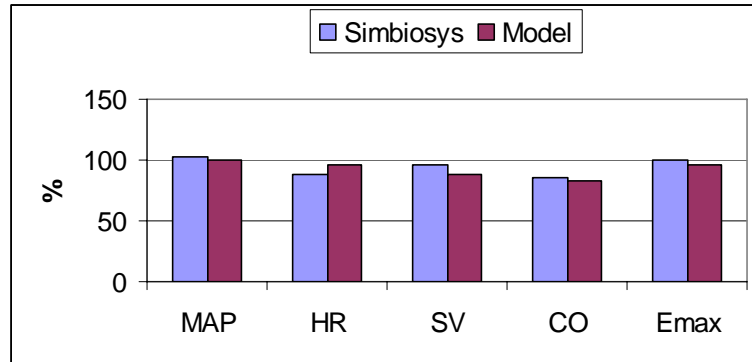
Table 3.8. (continued)

Model	LVEDP (mmHg)	7	7	7	7	7	same
	LVESP (mmHg)	89	89	89	89	89	
	EDV (ml)	129	125	121	117	113	Down
	ESV (ml)	43	44	44	45	45	Up
	MAP (mmHg)	89	89	89	89	89	
	SV (ml)	86	81	77	72	68	Down
	HR (bpm)	75	72	69	67	66	Down
	CO (l/min)	6.4	5.8	5.3	4.9	4.4	Down
	Emax (mmHg/ml)	2.8	2.8	2.7	2.7	2.6	Down
	SVR (mmHg/ml/s)	0.73	0.82	0.91	1.0	1.1	Up
	Sympathetic activity	2.85	2.81	2.78	2.76	2.77	
	Parasympathetic activity	6.07	6.09	6.12	6.12	6.12	Up



a. -20 % in SVR.

HR, CO and Emax increase with decrease in SVR.



b. +20 % in SVR.

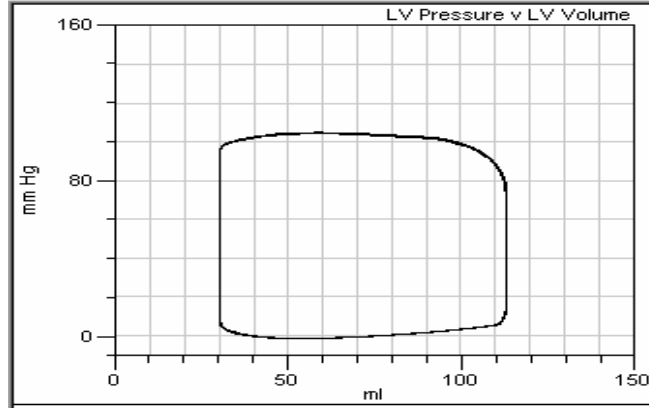
HR, CO and Emax decrease with increase in SVR.

Figure 3.16. Changes in hemodynamics for changes in SVR.

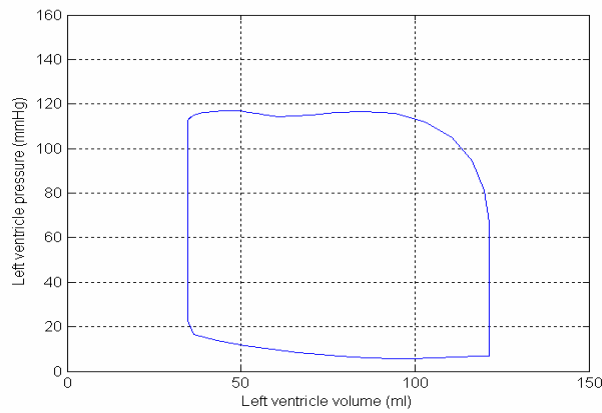
For both Simbiosys and the model, when afterload increases, (1) P-V loops do not change greatly; (2) stroke volume, heart rate and cardiac output decrease; (3) mean arterial pressures do not increase greatly; (4) left ventricular contractility (or Emax) and sympathetic activity decrease. The difference is that: when afterload increases, the parasympathetic tone does not change in Simiosys, but it increases in the model.

3.4.3 Response to change in left ventricular contractility (or Emax)

This subsection will examine the response of the model to forced change in left ventricular contractility by using forced change in Emax. The change in Emax for Simbiosys is induced by forced change in left ventricular contractility. For the model, it is induced by forced change in Emax directly. The steady state values are recorded in Table 3.9 after the changes. P-V loops in Figure 3.17 are shown +40% for change in left ventricular contractility for Simbiosys and +40% changes in Emax for the model. Figure 3.18 shows the changes in hemodynamic variables compared with corresponding baseline values.



a. +40% change in left ventricular contractility for Simbiosys.



b. +40% change in Emax in the model.

Figure 3.17. Change in P-V loop for +40% in Emax in the model.

Table 3.9. Response to change in left ventricle contractility

	Hemodynamics	Base line	+20% in Emax	+40% in Emax	Tendency
	LVEDP (mmHg)	7	6	5	Down
	LVESP (mmHg)	90	91	92	Up
	EDV (ml)	118	113	110	Down
	ESV (ml)	40	35	30	Down
	MAP (mmHg)	88	88	89	Up
	SV (ml)	78	78	80	Up

Table 3.9. (continued)

Simbio sys	HR (bpm)	68	67	67	Down
	CO (l/min)	5.3	5.2	5.4	
	LV contractility	1.03	1.20	1.40	Up
	Arterial contractility	1.16	1.16	1.15	Down
	Sympathetic tone	0.137	0.134	0.131	Down
	Parasympathetic tone	0.360	0.360	0.360	Same
Model	LVEDP (mmHg)	7	7	7	Same
	LVESP (mmHg)	89	90	92	Up
	EDV (ml)	121	119	117	Same
	ESV (ml)	44	39	33	Down
	MAP (mmHg)	89	90	92	Up
	SV (ml)	77	80	84	Up
	HR (bpm)	69	68	67	Down
	CO (l/min)	5.3	5.5	5.6	Up
	E _{max} (mmHg/ml)	2.7	3.24	3.78	Up
	SVR (mmHg/ml/s)	0.91	0.90	0.88	Down
	Sympathetic activity	2.78	2.78	2.76	Down
	Parasympath activity	6.12	6.12	6.13	Up

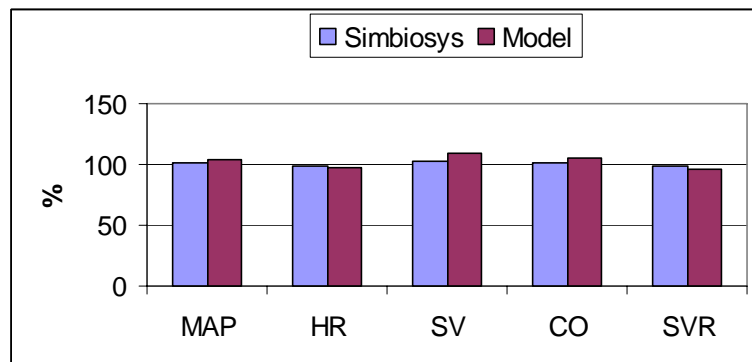


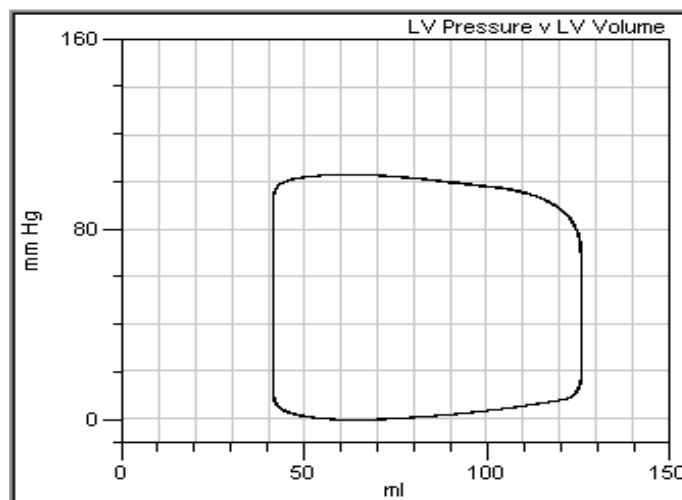
Figure 3.18. Changes in hemodynamics for +40 % in E_{max}.

MAP and CO increase; HR and SVR decrease with increase in E_{max}.

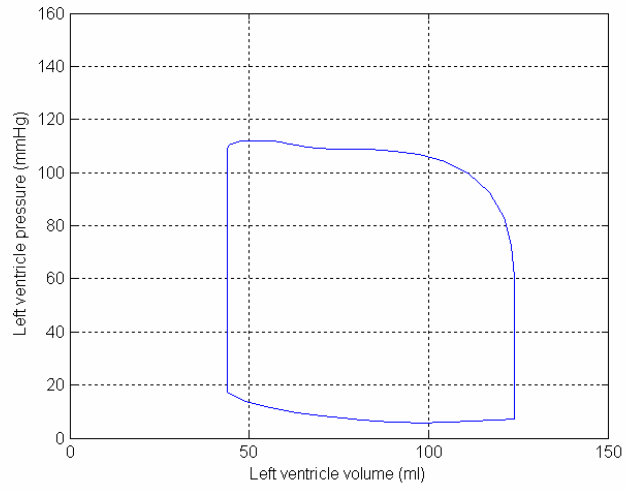
For both Simbiosys and the model, when left ventricular contractility (or E_{max}) increases, (1) P-V loops expand to the left; (2) stroke volume increases and heart rate decreases; (3) systemic vascular resistance decreases; (4) sympathetic activity decreases.

3.4.4 Response to change in heart rate

This section will examine the response of the model to forced change in heart rate by using forced change in heart rate (to simulate drug intervention). The forced change in heart rate for Simbiosys is induced by forced change in sinus rate. For the model, it is induced by forced change in heart rate directly. The steady values are recorded in Table 3.10 after the changes. P-V loops in Figure 3.19 are shown for -10% changes in heart rate for Simbiosys and the model. P-V loops in Figure 3.20 are shown for +40% changes in heart rate for Simbiosys and the model. Figure 3.21 shows the changes in hemodynamic variables compared with corresponding baseline values.

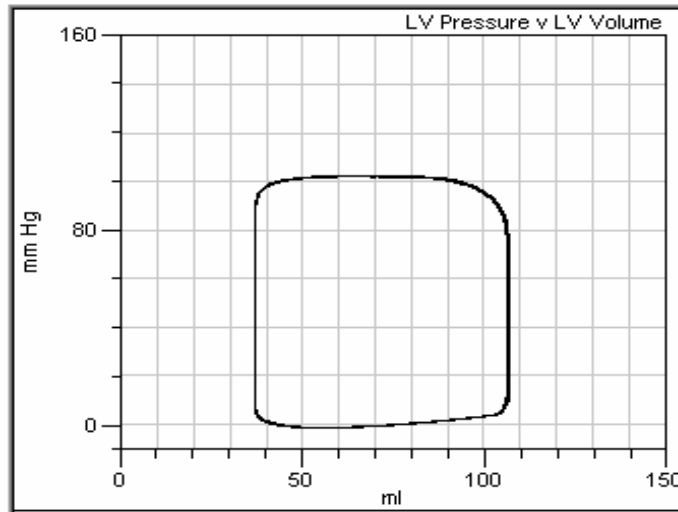


a. -10% change in heart rate for Simbiosys.

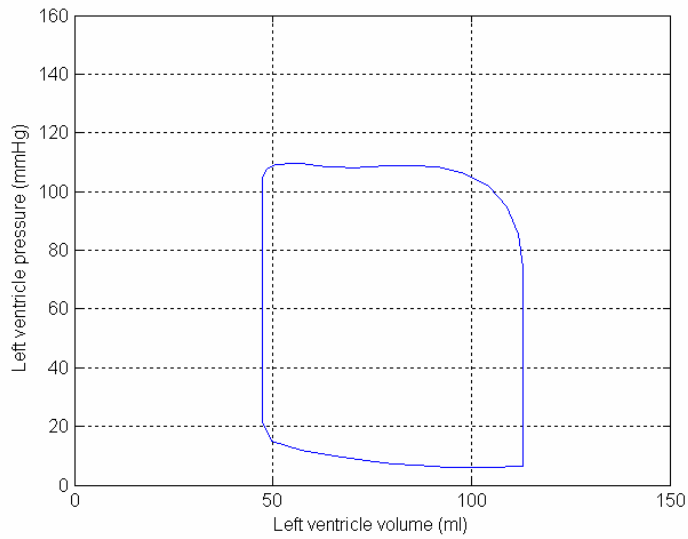


b. -10% change in heart rate for the model.

Figure 3.19. Change in P-V loop for -10% in HR.



a. +40% change in heart rate for Simbiosys.



b. +40% change in heart rate for the model.

Figure 3.20. Change in P-V loop for +40% in HR.

Table 3.10. Response to change in heart rate

	Hemo-dynamics	-10% in HR	Base line	+10% in HR	+20% in HR	+40% in HR	Tend-ency
Symbiosys	LVEDP (mmHg)	8	7	6	5	4	Down
	LVESP (mmHg)	91	90	89	88	86	Down
	EDV (ml)	122	118	114	110	103	Down
	ESV (ml)	41	40	39	38	37	Down
	MAP (mmHg)	87	88	88	89	90	Up
	SV (ml)	81	78	75	72	66	Down
	HR (bpm)	61	68	75	82	95	Up
	CO (l/min)	4.9	5.3	5.6	5.9	6.3	Up
	LV contractility	1.04	1.03	1.03	1.03	1.02	Down

Table 3.10. (continued)

	Arterial contractility	1.21	1.16	1.10	1.05	0.98	Down
	Sympathetic tone	0.176	0.137	0.121	0.112	0.099	Down
	Parasympathetic tone	0.359	0.360	0.360	0.360	0.360	Same
Model	LVEDP (mmHg)	7	7	7	7	6	Down
	LVESP (mmHg)	90	89	89	88	89	
	EDV (ml)	126	121	115	111	104	Down
	ESV (ml)	44	44	44	44	44	Same
	MAP (mmHg)	90	89	89	88	88	Up
	SV (ml)	82	77	71	67	60	Down
	HR (bpm)	62	69	76	83	97	Up
	CO (l/min)	5.1	5.3	5.4	5.6	5.8	Up
	E _{max} (mmHg/ml)	2.8	2.7	2.7	2.6	2.6	Down
	SVR (mmHg/ml/s)	0.94	0.91	0.88	0.86	0.82	Down
	Sympathetic activity	2.80	2.77	2.77	2.76	2.74	Down
	Parasympath activity	6.10	6.12	6.12	6.13	6.14	Up

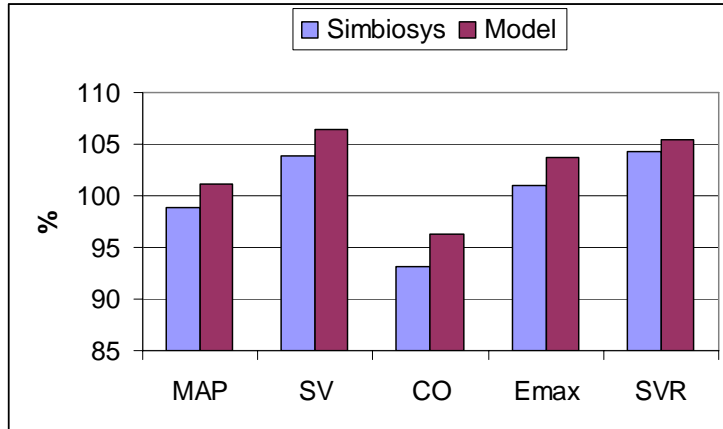


Figure 5.15a -10 % in HR.

CO decreases; SVR and Emax increase with decrease in heart rate.

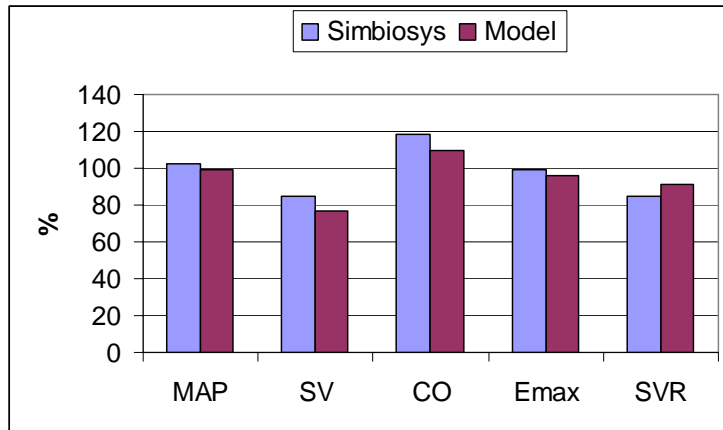


Figure 5.15b +40 % in HR.

CO increases; SVR and Emax decrease with increase in heart rate.

Figure 3.21. Changes in hemodynamics for change in HR.

For both Simbiosys and the model, when heart rate increases, (1) P-V loops shrink to the left; (2) left ventricular contractility decreases; (3) stroke volume decreases but cardiac output increases; (4) systemic vascular resistance decreases; (5) mean arterial pressure does not increase greatly; (6) sympathetic activity decreases. The difference is that: when heart rate increases, the parasympathetic tone does not change in Simbiosys, but parasympathetic activity increases in the model.

3.5 RESPONSE TO EXERCISE

This section will examine the response of the model to exercise. The exercise level is determined by the combination of nervous offsets (central command) and forced change in active muscle resistance. The exercise experiment hemodynamic data for healthy people (9 subjects) from [52] are used as reference for tuning the combinations. The simulation results are compared to the data from [52].

3.5.1 Single level exercise

In the simulation of a certain level of exercise, the set point change is induced by adding offsets to efferent pathways progressively, by changing the sympathetic offset $offset_es$ in (3.23) and the vagal offset $offset_ev$ in (3.24) linearly in 5 seconds. In Figure 3.22, the offsets start changing progressively from 10s with values in Table 3.11. At 15 s, the exercise begins, R_{13} starts decreasing due to local mechanism in active muscle (forced change from 7.1 mmHg/ml/s to 0.8 mmHg/ml/s linearly in 10 seconds), but heart rate and left ventricle contractility increase continually until they achieve new steady values. The complex of changes is shown in Figure 3.22. The new set point consists of higher pressure, higher heart rate and lower SVR which is consistent with exercise physiology [53].

Table 3.11. Offsets in sympathetic and vagal activity

	Rest (steady)	Exercise (steady)
$offset_es$	0	0.24
$offset_ev$	0	0.2

As shown in Figure 3.23, the changes in P-V loops from rest to exercise include increases in end diastolic volume and end systolic pressure. The hemodynamic changes are listed in Table 3.12. Since the blood flow is inverse proportional to resistance, the changes in resistances imply the redistribution of the blood flow. The redistribution of blood flow is shown in Table 3.13.

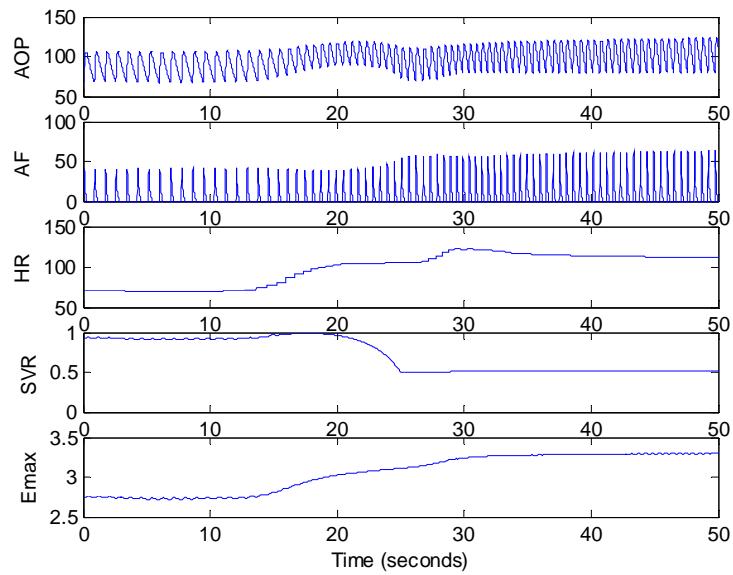


Figure 3.22. Response to exercise.

MAP in mmHg, AF (aortic flow) in L/min, HR in bpm, SVR in mmHg/ml/s, (MAP, CO, SVR) changes from (89, 5.3, 0.91) to (106, 10.8, 0.51) during exercise.

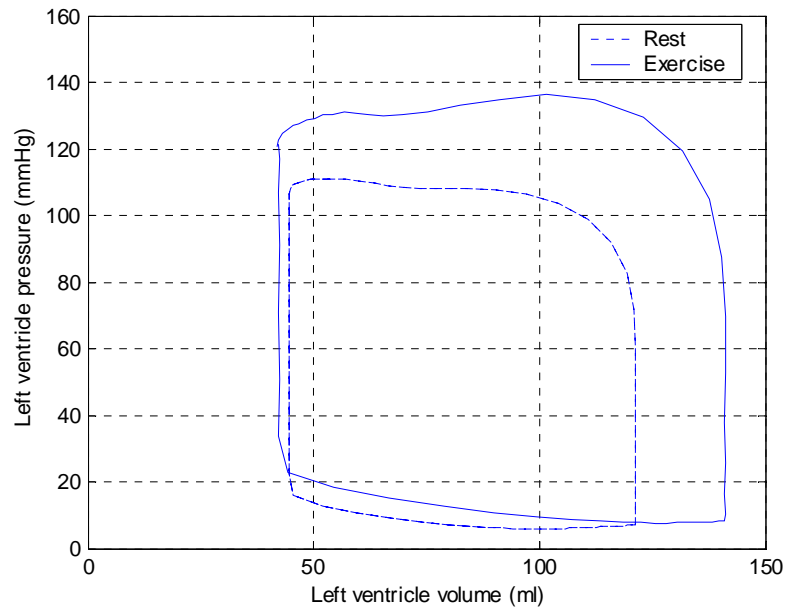


Figure 3.23. P-V loops of rest and exercise.

The loop for exercise expands to the right. The end diastolic volume increases and end systolic volume decreases.

Table 3.12. Hemodynamic changes

Experiment data from [52]	Rest	Exercise	Tendency
MAP (mmHg)	86 ± 3	96 ± 3	Up
HR (bpm)	68 ± 4	111 ± 4	Up
SV	93 ± 6	114 ± 8	Up
CO (l/min)	6.2 ± 0.4	12.8 ± 1.2	Up
SVR* (mmHg/ml/s)	0.811	0.451	Down
LVR** (mmHg/ml/s)		0.77	
SVR/LVR (%)		58.6	
Simulation results	Rest	Exercise	Tendency
LVEDP (mmHg)	7	6	Down
LVESP (mmHg)	89	106	Up
EDV (ml)	121	140	Up
ESV (ml)	44	42	Down
MAP (mmHg)	89	106	Up
SV (ml)	77	98	Up
HR (bpm)	69	110	Up
CO (l/min)	5.3	10.8	Up
E _{max} (mmHg/ml)	2.7	3.3	Up
SVR (mmHg/ml/s)	0.91	0.51	Down
Sympathetic activity	2.77	2.92	Up
Parasympath activity	6.12	5.97	Down

*: calculated from systemic vascular conductance.

** : leg vascular resistance, also calculated from systemic vascular conductance.

Table 3.13. Changes in resistances

Resistance	Rest	Exercise
R_{11}	3.2	4.1
R_{12}	1.5	2.2
R_{13}	7.1	0.8
SVR	0.91	0.51

3.5.2 Multiple levels of exercise

Multiple exercise levels are simulated by using the experimental data from [52] as reference to tweak the combinations of nervous offsets and forced change in R_{13} (muscle resistance) to make the hemodynamic variables in the simulation close to the real data. The simulation results are shown in Table 3.14. The hemodynamic changes in percentage from rest to different levels of exercise (ratio of exercise to rest) are illustrated in Figure 3.24, compared to that of experiment data from [52].

Table 3.14. Multiple exercise levels

Exercise level	0	1	2	3
Data from [52] (9 subjects)	Rest	71 w	97 w	125 w
MAP (mmHg)	86 ± 3	96 ± 3	98 ± 3	107 ± 2
HR (bpm)	68 ± 4	111 ± 4	131 ± 4	149 ± 3
SV (ml)	93 ± 6	114 ± 8	114 ± 6	118 ± 6
CO (L/min)	6.2 ± 0.4	12.8 ± 1.2	14.9 ± 0.9	17.6 ± 0.8
SVR* (mmHg/ml/s)	0.811	0.451	0.390	0.361
LVR** (mmHg/ml/s)		0.77	0.6	0.6
SVR/LVR (%)		58.6	65.0	60.0

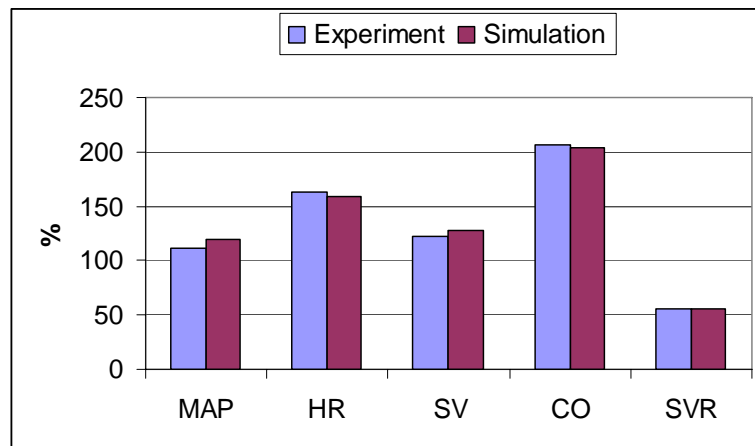
Table 3.14. (continued)

Simulation result	0	1	2	3
Offsets (O1,O2)***	(0,0)	(0.24,0.2)	(0.30,0.24)	(0.33,0.24)
MAP (mmHg)	89	106	115	116
HR (bpm)	69	110	131	148
SV (ml)	77	98	94	91
CO (L/min)	5.3	10.8	12.3	13.5
SVR (mmHg/ml/s)	0.91	0.51	0.48	0.44
R13 (mmHg/ml/s)	7.1	0.8	0.7	0.6
SVR/R13 (%)	12.7	63.8	68.4	72.4

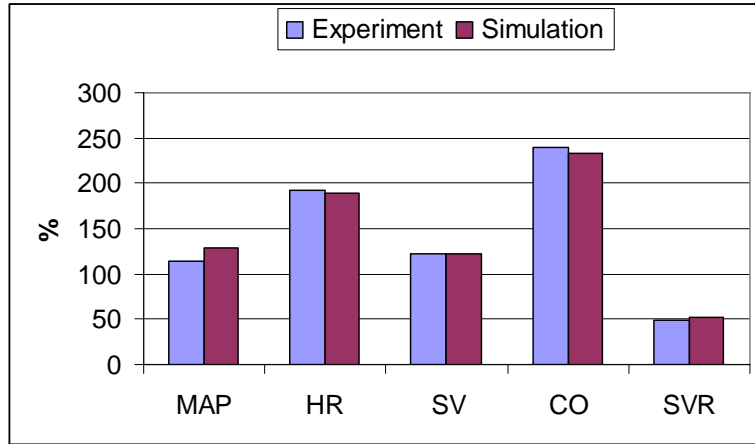
*: calculated from systemic vascular conductance.

** : leg vascular resistance, also calculated from systemic vascular conductance.

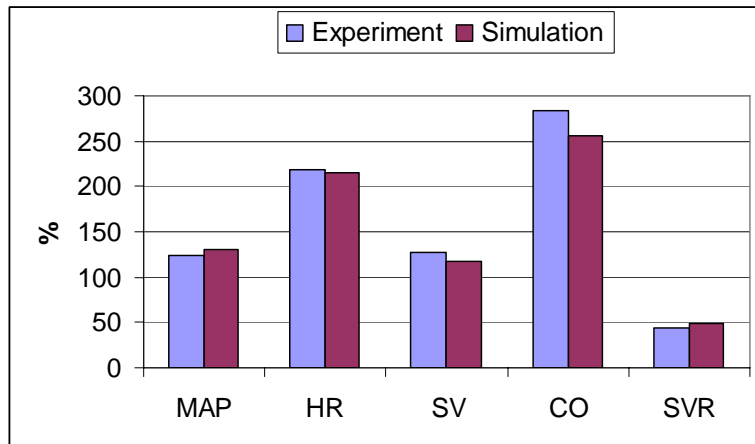
***: outbound nervous signals offsets: O1 (sympathetic offset), O2 (parasympathetic offset).



Exercise level 1



Exercise level 2



Exercise level 3

Figure 3.24. Hemodynamic changes from rest to exercise.

MAP, CO, and HR increase SVR decreases.

According to exercise physiology [52-54], for the human exercise experiment, there is an increase in stroke volume (SV) accompanying the increase in blood pressure at low level exercise, and stroke volume reaches a plateau at a submaximal exercise level. Other hemodynamic variables (MAP, HR, CO) increase with exercise levels. To demonstrate the trends in hemodynamics with exercise intensity, comparable exercise experimental data from [54] are listed in Table 3.15. The experiment data in Table 3.14 and Table 3.15 from [52, 54] and simulation results for multiple exercise levels are illustrated in Figure 3.25.

Table 3.15. Exercise experiment data

Exercise level	0	1	2	3
MAP (mmHg)	98	107	112	122
HR (bpm)	75	101	114	132
SV (ml)	75	96	96	97
CO (L/min)	5.4	9.8	12.0	14.2
SVR(mmHg/ml/s)	1.0	0.65	0.55	0.5

Data read from figures in [54].

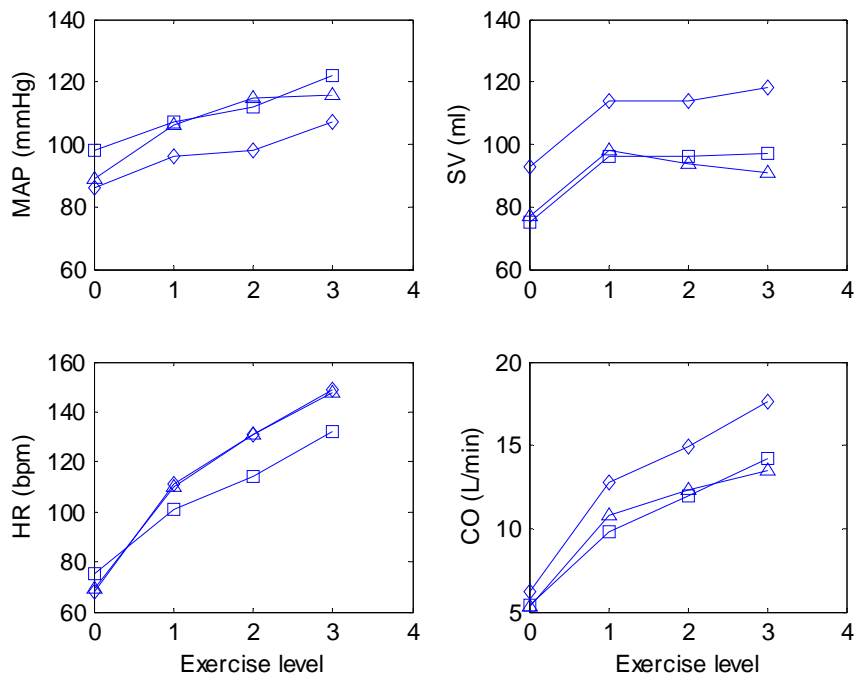


Figure 3.25. Changes in hemodynamics for multiple exercise levels.

Diamond: experiment data from [52]; Square: experiment data from [54]; Triangle: simulation results.

3.6 CONCLUSION

The cardiovascular system model is described and the baroreflex model is coupled to it. Using physiological simulation software Simbiosys and exercise experiment data in the literature as reference, the coupled model of the cardiovascular system and the baroreflex reproduced the hemodynamic response fairly well to single parameter change in preload, afterload, left ventricular contractility and heart rate. The responses to multiple levels of exercise are simulated and the results are consistent with exercise experiment data. Thus this coupled model can be considered as a model for a healthy person. The next chapter is to determine the parameters for the people with heart failure based on this healthy heart model.

4.0 FAILING HEART WITH BAROREFLEX

In this chapter, the qualitative and quantitative changes in the cardiovascular system and the baroreflex will be found out by surveying the literature for patients with heart failure, and these changes will be mapped into the model. The parameters are tuned by using heart failure hemodynamic data in the literature as reference. The responses of the model to multiple levels of exercise are examined and compared to that in the literature.

4.1 HEART FAILURE AND ASSOCIATED PHYSIOLOGICAL CHANGES

Heart failure is the inability of the heart to supply adequate blood flow and therefore oxygen delivery to peripheral tissues and organs. Heart failure is the final result of a variety of primary cardiovascular diseases [1]. The common cause of heart failure is coronary artery disease (CAD). CAD reduces coronary blood flow and oxygen delivery to the myocardium and thus causes impaired function. Another common cause of heart failure is myocardial infarction which needs to be compensated by non-infarcted regions for the loss of function. The other factors like valvular disease and congenital defects place increased demands upon the ailing heart and precipitate failure. External factors for heart failure include increased afterload and increased body demands. There are a series of changes associated with heart failure which include the changes in the cardiovascular system and the changes in the baroreflex [1, 55].

4.1.1 Changes in cardiovascular system

1) Cardiac Changes

The changes in cardiac function associated with heart failure result in a decrease in stroke volume as well as cardiac output. The decline in stroke volume is due to systolic dysfunction, diastolic dysfunction, or a combination of the two [1, 55]. Simply stated, systolic dysfunction is the result of decreased left heart contractility. Diastolic dysfunction means that the ventricle becomes less compliant and impairs ventricular filling. As illustrated in Figure 4.1, the systolic dysfunction is usually caused by the dilated myocardium, which is characterized by increased end diastolic volume and decreased ejection fraction. The diastolic dysfunction is usually caused by the hypertrophic myocardium, which is characterized by decreased end diastolic volume.

2) Neurohumoral Changes

Neurohumoral responses include increased sympathetic nervous activities and increased release of antidiuretic hormone. The net effect of these neurohumoral responses is to help maintain arterial pressure and increase heart rate and blood volume. Otherwise, the arterial pressure will drop out of acceptable range due to decreased stroke volume and cardiac output.

3) Systemic Vascular Resistance changes

To compensate for reduced cardiac output associated with heart failure, some feedback mechanisms within the body will try to maintain normal arterial pressure by constricting arterial resistance vessels thus increase the systemic vascular resistance. The baroreflex is an important component of this feedback system.

4) Blood Volume changes

In heart failure, the compensatory increase in blood volume can increase ventricular preload and stroke volume. Blood volume is augmented by decreased urine output and retention of fluid. There is also an increase in circulating anti-diuretic hormone that contributes to renal retention of water. The resulting increase in blood volume helps to maintain cardiac output. On the other

hand, the increased volume can be deleterious because it increases venous pressures and leads to pulmonary and systemic edema.

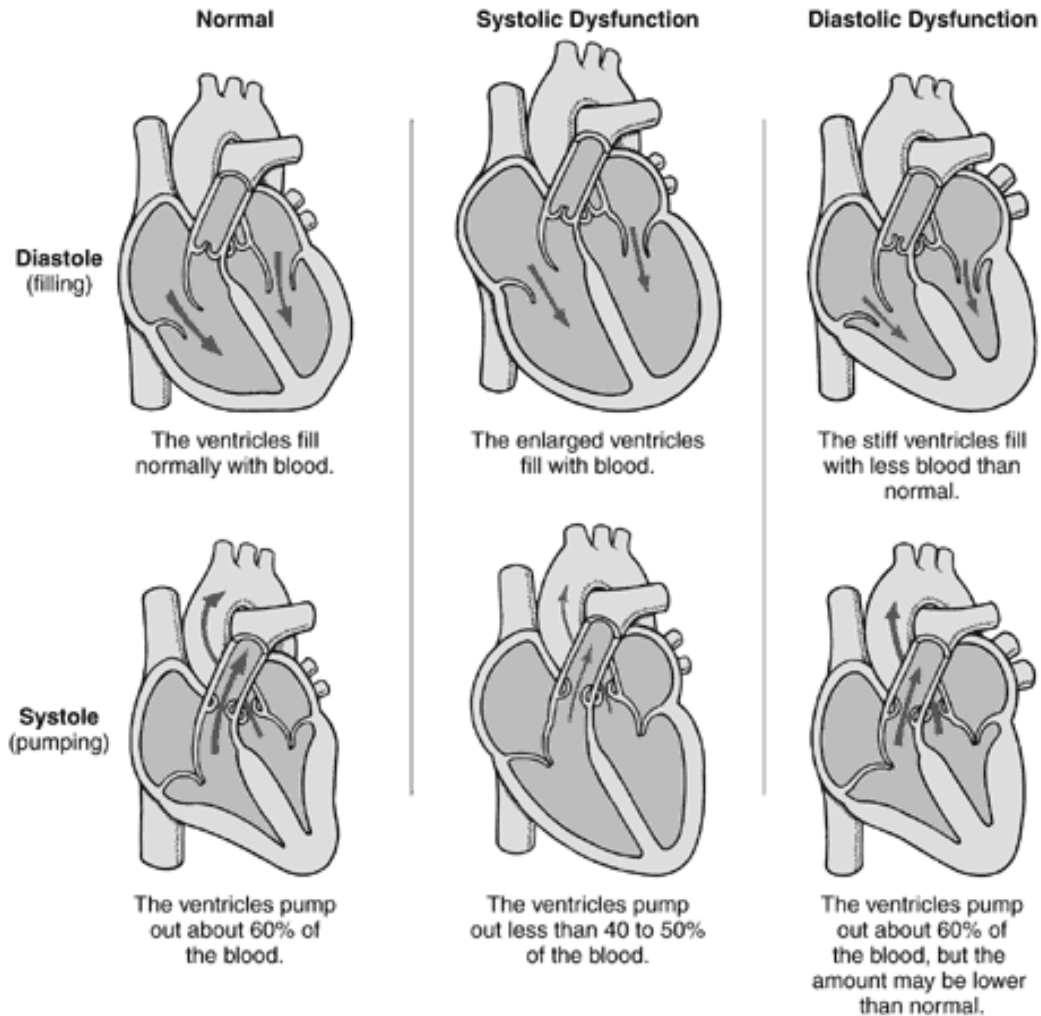


Figure 4.1. Systolic dysfunction and diastolic dysfunction (Adopted from [56]).

4.1.2 Changes in baroreflex

Initially, a reduction in cardiac output associated with heart failure leads to a decrease in the arterial pressure applied to the baroreceptors which, in turn, cause increased heart rate and

systemic vascular resistance through sympathetic and vagal systems. The sympathetic excitation is in effect for the duration of the failure [57].

In neck chamber experiment for examining carotid baroreceptor-cardiac reflex mechanisms in patients with congestive heart failure, the shape of the sigmoid baroreceptor stimulus-cardiac response relation is qualitatively normal in heart failure patients and the time delay of the baroreflex is not changed, but the baroreflex sensitivity is depressed [58]. It was reported that there was a diminished sensitivity of the afferent limb while the gain of the central portion of the reflex was normal in rats with cardiac failure [59]. Patients with heart failure have increased sympathetic nerve activity. In addition, the increase in sympathetic activity is well related to severity of the heart failure and the sympathetic nerve activity progressively increases from mild to severe heart failure [60]. It is suggested that the depressed end-organ response of the baroreflex and the blunted response at the receptor level account for the decrease in baroreflex gain [61, 62]. It has been reported that the vasodilatory response is impaired in patients with congestive heart failure [63]. Reduced baroreflex sensitivity for heart failure is well known where baroreflex sensitivity is defined as the ratio of change in cardiac cycle to change in the arterial pressure [64-66].

In summary, there are some changes in the cardiovascular system and the baroreflex with heart failure. These changes can be mapped into the changes in parameters of the heart failure model. The tendencies of parameters changes for heart failure model are listed in Table 4.1. The parts with parameter change in the baroreflex loop are illustrated in Figure 4.2.

Table 4.1. Changes in parameters of the heart failure model

	Parameters	Tendency
Cardiovascular System	E _{max}	Down
	E _{min}	Up
	SVR	Up
	Heart rate	Up
Baroreflex	Baroreceptor sensitivity	Down
	Sympathetic heart rate gain	Down
	Parasympathetic heart rate gain	Down
	Resistances gains	Down

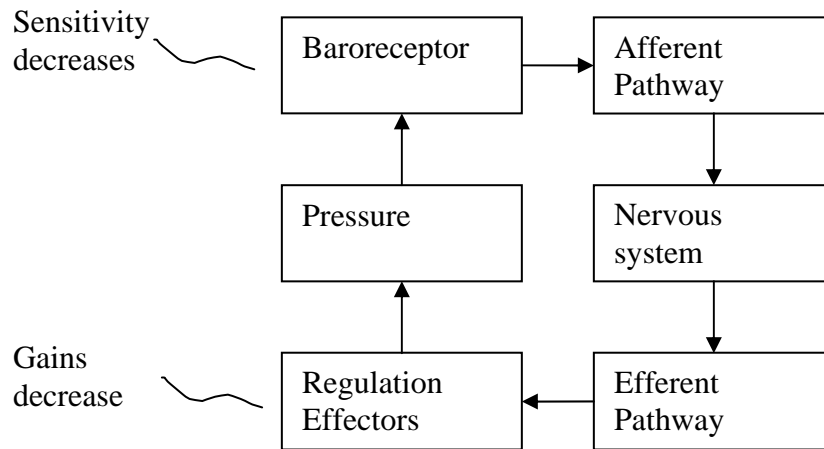


Figure 4.2. Changes in baroreflex.

The baroreceptor gain, and regulation effectors gains (sympathetic heart rate and parasympathetic gain, resistances gains) decrease for patients with heart failure.

4.2 EFFECTS OF CHANGES IN HEART FOR HEART FAILURE MODEL

The change in heart contractility and/or compliance is the primary change of heart failure. As shown in Figure 4.3, the left ventricular contractility (E_{max}) refers to the slope of end systolic pressure volume relationship (ESPVR) and the left ventricular compliance ($1/E_{min}$) refers to the reciprocal of the slope of end diastolic pressure volume relationship (ESPVR). There are basically two types of physical changes with heart failure: decrease in the left ventricular contractility and decrease in the left ventricular compliance. The change in ejection fraction (defined as the ratio of stroke volume to the end diastolic volume) is usually a result of the systolic dysfunction. In the following examples, it is assumed that change in heart contractility and/or compliance is the only change and other parameters (heart rate, systemic vascular resistance and total blood volume) are fixed.

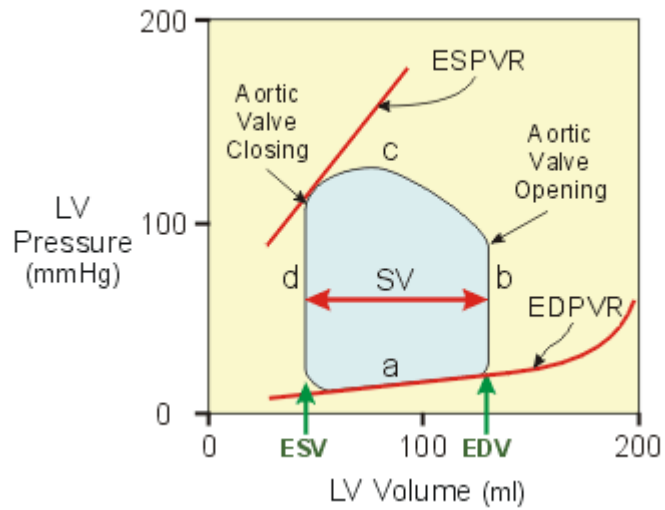


Figure 4.3. Left ventricle pressure volume loop (adopted from [55]).

Four phases in a cardiac cycle: a. filling, b. isovolumetric contraction, c. ejection, d. isovolumetric relaxation. EDV: end diastolic volume. ESV: end systolic volume. SV: stroke volume, the difference between EDV and ESV.

4.2.1 Systolic dysfunction: decrease in E_{max}

As shown in Figure 4.4, the slope of the end systolic pressure volume relationship (ESPVR) decreases with loss of left ventricular contractility (E_{max}). This causes an increased end systolic

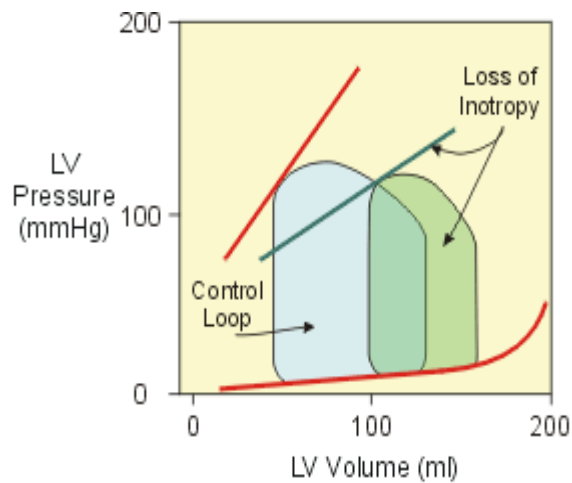


Figure 4.4. Systolic dysfunction (adopted from [55]).

E_{max} decreased (loss of contractility), E_{min} and heart rate unchanged.

volume and an increased end diastolic volume; however the increase in end diastolic volume is not as great as the increase in end systolic volume. Thus the resulting stroke volume decreases. Since stroke volume decreases and end diastolic volume increases, there is a decrease in ejection fraction (EF).

4.2.2 Diastolic dysfunction: increase in E_{min}

As shown in Figure 4.5, a decrease in ventricular compliance (increase in E_{min}) accompanies with diastolic dysfunction, as occurs in ventricular hypertrophy. This will result in a decreased end diastolic volume and a greater end diastolic pressure as shown by changes in the ventricular pressure-volume loop. As a result of these changes, stroke volume decreases. Dependant on the relative change in stroke volume and end diastolic volume, there may or may not be a small change in ejection fraction.

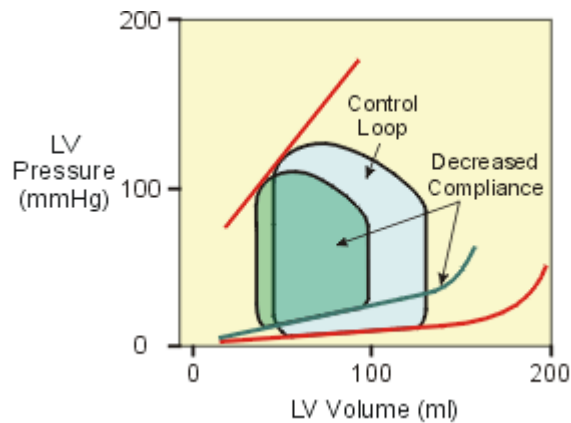


Figure 4.5. Diastolic dysfunction (adopted from [55]).

E_{min} increased, E_{max} and heart rate unchanged.

4.2.3 Combination of systolic dysfunction and diastolic dysfunction: decrease in E_{max} and increase in E_{min}

As shown in Figure 4.6, the slope of the ESPVR is decreased (E_{max} decreased) and the slope of the passive filling curve is increased (E_{min} increased). There is a significant decrease in stroke

volume because of decreased EDV and increased ESV. As a result, the ejection fraction decreased.

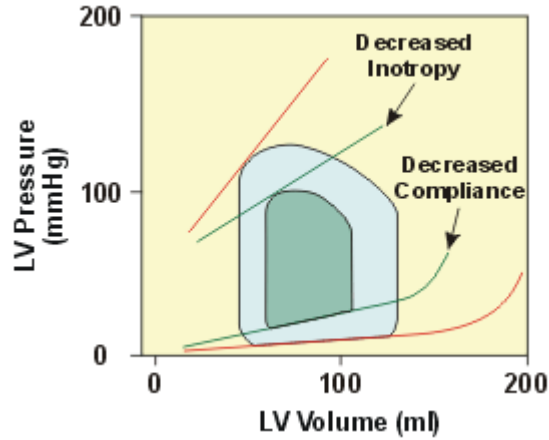


Figure 4.6. Combination of systolic dysfunction and diastolic dysfunction (adopted from [55]).
Emax decreased, Emin increased and heart rate unchanged.

4.3 DETERMINE THE PARAMETERS OF HEART FAILURE MODEL

The parameters for heart failure model are tuned by using heart failure hemodynamic data in the literature as reference. These changes are made according to section 4.1 including both the cardiovascular model and the baroreflex model.

1) Hemodynamic data for heart failure in the literature

The hemodynamics data for patients with heart failure in [67-69] are listed in Table 4.2 as reference for tuning the parameters of heart failure model. These data of heart failure was collected before the implants of LVADs.

Table 4.2. Clinical hemodynamics data for heart failure

Hemodynamic	Data from [67] (23 patients)	Data from [68] (10 patients)	Data from [69] (20 patients)
Systolic pressure (mmHg)	100.6 ± 12.4	No	97 ± 11
Diastolic pressure (mmHg)	56.8 ± 10.4	No	59 ± 12

Table 4.2. (continued)

Mean arterial pressure (mmHg)	74.8 ± 10.7	79.8 ± 11.4	No
Systemic vascular resistance (mmHg/ml/s)	1.20 ± 0.32	0.93 ± 0.25	No
Heart rate (bpm)	89.1 ± 17.6	No	103 ± 14
Cardiac output (L/min)	3.54 ± 0.48*	4.1 ± 2.0	4.6 ± 1.4*
Left ventricle end diastolic volume (ml)	No	241 ± 67	No
Left ventricle end systolic volume (ml)	No	173 ± 28	No
Ejection fraction (%)	No	17 ± 5.7	17.2 ± 5.8

*: calculated by assuming body surface area = 2 m^2 , original data are in cardiac output index (cardiac output normalized by the body surface area).

2) Tune the parameters of heart failure model

Based on the model for healthy people, the parameters of heart failure model are tuned by using the clinical data in Table 4.2 as reference, according to the changes in section 4.1. The changes in parameters for the baroreflex of heart failure model are listed in Table 4.3.

Table 4.3. Parameters for the heart failure baroreflex

Parameter	Meaning	Healthy people	People with heart failure
K_a	1/Baroreceptor sensitivity	11.758	14
g_1	Splanchnic resistance effector gain	0.695	0.63
g_2	The rest resistance effector gain	0.53	0.48
g_3	Muscle resistance effector gain	2.81	2.3
g_4	Sympathetic heart rate gain	-0.6	-0.4
g_5	Vagal heart rate gain	0.1	0.08

4.4 SIMULATIONS RESULTS OF HEART FAILURE MODEL

For different types of heart failure, realistic heart failure hemodynamics can be reproduced with simulations by simultaneously changing E_{max} , E_{min} , V_o and V_T (total blood volume) [70]. Based on the heart failure model, systolic dysfunction is simulated by decreased constant value of E_{max} and diastolic dysfunction by increased constant value of E_{min} . In other words, E_{max} is not under the control of the baroreflex any more due to impaired heart muscle for the case of systolic dysfunction. As shown in Table 4.4, two combinations of V_o and V_T are simulated. As mentioned before, a certain steady value of V_T is achieved by tweaking V_{T0} .

Table 4.4. Heart failure model combinations

Variable or Parameter	Healthy heart	Heart failure 1	Heart failure 2
V_o (ml)	5	5	35
V_T (ml)	250	275	300

To demonstrate the differences between heart failure model with baroreflex and the case without baroreflex, the simulation results of heart failure without baroreflex are presented and compared to the case with baroreflex. For the case of heart failure with baroreflex, the heart rate and systemic vascular resistance are still under the control of the baroreflex; for the case of the heart failure without baroreflex, the values of heart rate and systemic vascular resistance are the same as that of the healthy heart, the total blood volume is the same as the steady total blood volume for the heart failure with baroreflex.

4.4.1 Simulation result 1 ($V_o = 5$ ml, $V_T = 275$ ml)

The P-V loops for different types of heart failure are shown in Figure 4.7, Figure 4.8 and Figure 4.9. The corresponding hemodynamics data are listed in Table 4.5. The changes in

hemodynamics in the simulations with respect to that of the healthy heart are shown in Figure 4.10.

1) Systolic dysfunction

As shown in Figure 4.7, the systolic dysfunction is simulated by reduced $E_{max} = 1.2$ mmHg/ml (normal value 2.7 mmHg/ml). The steady total blood volume for both cases is 275 ml. $V_{T0} = 210$ ml. The P-V loops for failing hearts shift to the right and the ejection fractions decrease which is the same as that in subsection 4.2.1. The case of heart failure with baroreflex has less end diastolic volume and less stroke volume than that of the case without baroreflex, but higher end systolic pressure.

2) Diastolic dysfunction

As shown in Figure 4.8, the diastolic dysfunction is simulated by increased $E_{min} = 0.2$ mmHg/ml (normal value 0.06 mmHg/ml). $V_{T0} = 225$ ml. The P-V loops for failing hearts shift to the left which is the same as that in subsection 4.2.2. The case of heart failure with baroreflex has less end diastolic volume and less stroke volume than that of the case without baroreflex, but higher end systolic pressure.

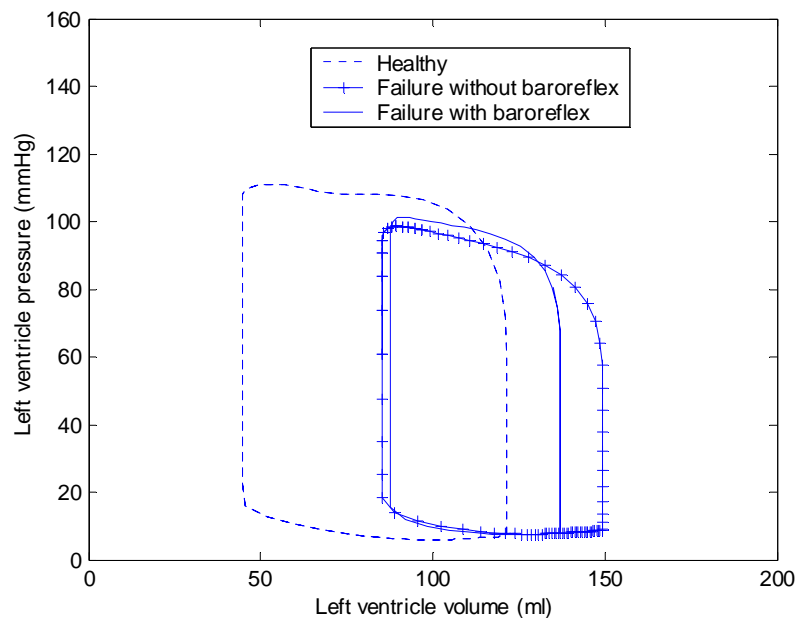


Figure 4.7. P-V loops for healthy heart and systolic dysfunction heart.

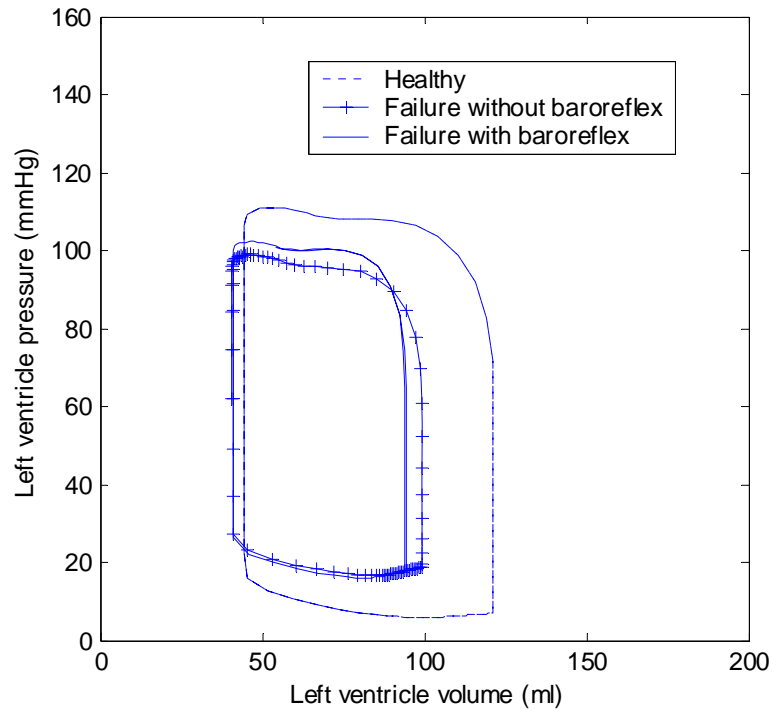


Figure 4.8. P-V loops for healthy heart and diastolic dysfunction heart.

3) The combination of systolic dysfunction and diastolic dysfunction

As shown in Figure 4.9, the combination of systolic dysfunction and diastolic dysfunction is simulated by the combination of $E_{max} = 1.4$ and $E_{min} = 0.2$ mmHg/ml. $V_{T0} = 190$ ml. The P-V loops for failing hearts shrink towards the center of the healthy one and the ejection fractions decrease which is the same as that in section 4.2.3. The case of heart failure with baroreflex has less end diastolic volume and less stroke volume than that of the case without baroreflex, but higher end systolic pressure.

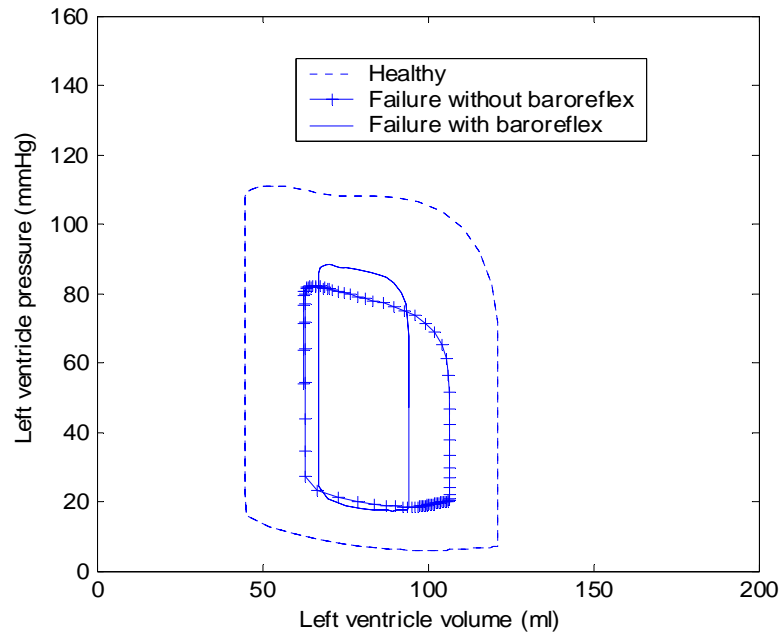


Figure 4.9. P-V loops for healthy and the combination of both failure cases.

Table 4.5. Simulation results for heart failure (1)

($V_o = 5$ ml, $V_T = 275$ ml)

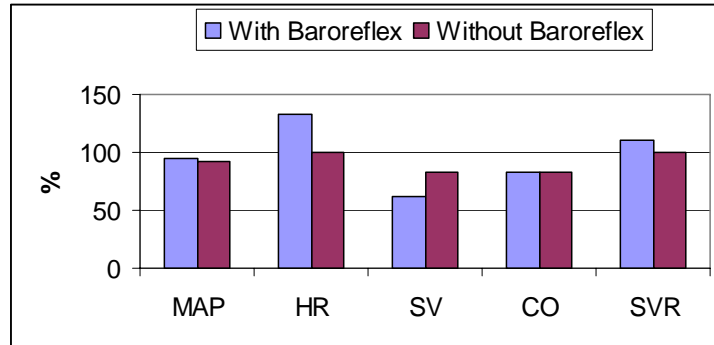
With baroreflex	Healthy heart	Systolic dysfunction (1)	Diastolic dysfunction (2)	Combination of (1) and (2)	Clinical data from [67] (23 patients)
DP(mmHg)	72	71	73	71	56.8 ± 10.4
SP(mmHg)	108	97	100	85	100.6 ± 12.4
LVEDP (mmHg)	7	8	18	18	No
LVESP (mmHg)	89	84	87	79	No
MAP (mmHg)	89	84	87	79	74.8 ± 10.7
EDV (ml)	121	135	92	96	No
ESV (ml)	44	87	41	67	No
SV (ml)	77	48	51	28	No
EF (%)	63.6	35.4	56.7	29.2	No
HR (bpm)	69	92	86	107	89.1 ± 17.6

Table 4.5 (continued)

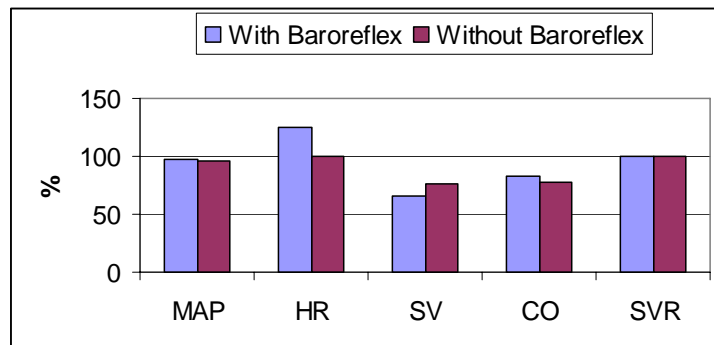
HR (bpm)	69	92	86	107	89.1 ± 17.6
CO (l/min)	5.3	4.4	4.4	3.0	3.54 ± 0.48
SVR (mmHg/ml/s)	0.91	1.01	0.91	1.17	1.20 ± 0.32
E _{max} (mmHg/ml)	2.7	1.2	2.8	1.4	No
E _{min} (mmHg/ml)	0.06	0.06	0.2	0.2	No
Sympathetic activity	2.77	2.84	2.80	2.92	No
Parasympath activity	6.12	6.08	6.11	6.04	No
Without baroreflex	Healthy heart	Systolic dysfunction (1)	Diastolic dysfunction (2)	Combination of (1) and (2)	Clinical data from [67] (23 patients)
DP (mmHg)	72	62	67	57	56.8 ± 10.4
SP (mmHg)	108	100	101	83	100.6 ± 12.4
LVEDP (mmHg)	7	8	18	20	No
LVESP (mmHg)	89	82	86	71	No
MAP (mmHg)	89	82	86	71	74.8 ± 10.7
EDV (ml)	121	149	99	107	No
ESV (ml)	44	85	40	63	No
SV (ml)	77	64	59	44	No
EF (%)	63.6	42.9	59.1	41.3	No
HR (bpm)	69	69	69	69	89.1 ± 17.6
CO (l/min)	5.3	4.4	4.1	3.0	3.54 ± 0.48
SVR (mmHg/ml/s)	0.91	0.91	0.91	0.91	1.20 ± 0.32
E _{max} (mmHg/ml)	2.7	1.2	2.7	1.4	No
E _{min} (mmHg/ml)	0.06	0.06	0.2	0.2	No

DP: diastolic pressure; SP: systolic pressure; LVEDP: left ventricular end diastolic pressure; LVESP: left ventricular end systolic pressure; EDV: end diastolic volume; ESV: end systolic volume; MAP: mean arterial pressure; SV: stroke volume; EF: ejection fraction; HR: heart rate; CO: cardiac output; E_{max}: peak left ventricular contractility; SVR: systemic arterial resistance. Sympathetic activity and parasympathetic activity are in mean value (spikes/s). ESP for the model is hard to read thus assumed the same as MAP.

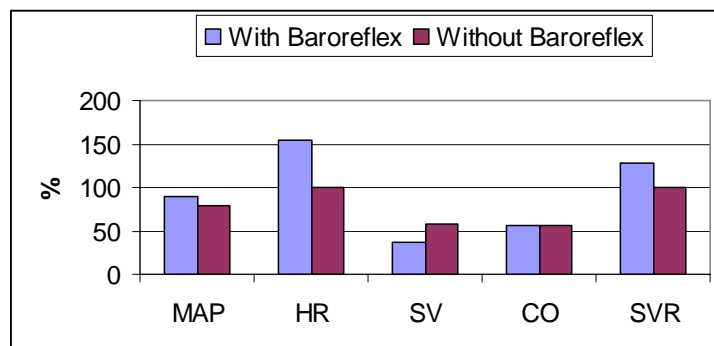
The different types of heart failure in section 4.2 can be reproduced very well by decreased E_{max} and/or increased E_{min} . It can also be seen from Figure 4.10 that, because of the control of the baroreflex, the heart rate and systemic vascular resistance increase to compensate the decrease in the cardiac output due to changes in heart contractility (or compliance) and keep the blood pressure in acceptable range.



a. Systolic dysfunction.



b. Diastolic dysfunction.



c. Combination of systolic dysfunction and diastolic dysfunction.

Figure 4.10. Comparison of simulation results with baroreflex and without baroreflex.

The MAP of the case with baroreflex is higher than that of the case without baroreflex due to the increase in HR and SVR.

4.4.2 Simulation result 2 ($V_o = 35$ ml, $V_T = 300$ ml)

Repeat the simulations in subsection 4.4.1 with V_o and V_T changed. The results are shown in Figure 4.11, Figure 4.12, Figure 4.13 and Table 4.6. The effect of changes in V_o and V_T is shift to right of the P-V loops. The changes in hemodynamics in the simulations with respect to that of the healthy heart are shown in Figure 4.14.

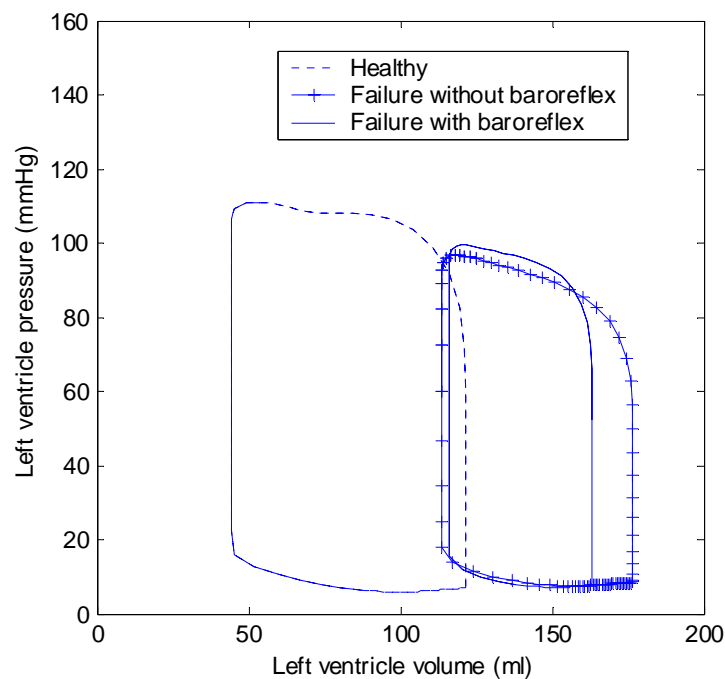


Figure 4.11. Systolic dysfunction P-V loops. ($V_{T0} = 240$ ml)

P-V loops shift to the right because of increased V_o .

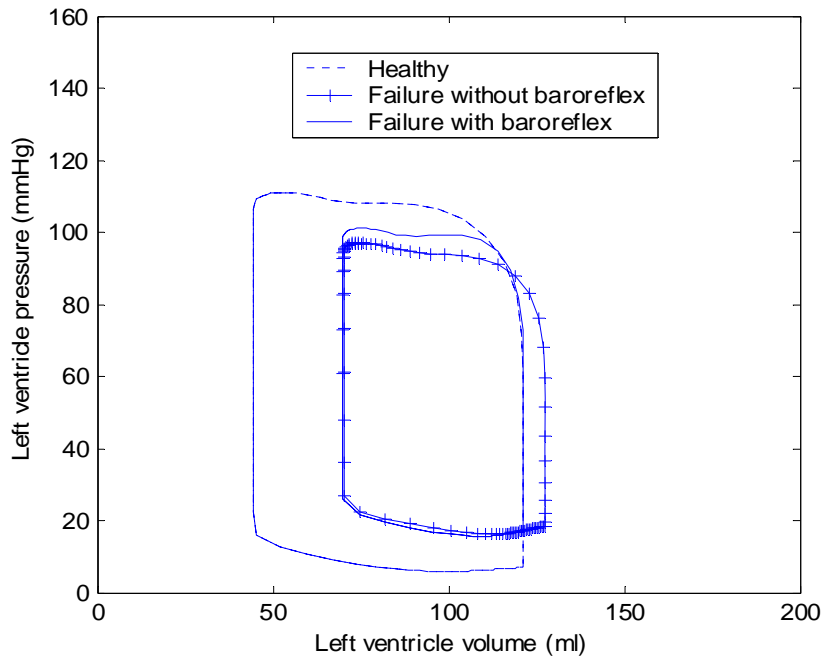


Figure 4.12. Diastolic dysfunction P-V loops. ($V_{T0} = 250$ ml)

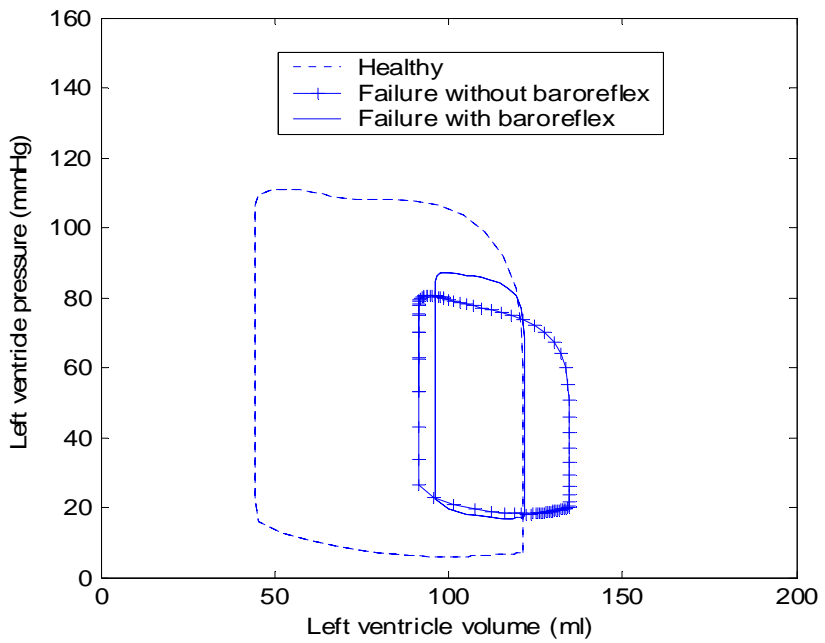


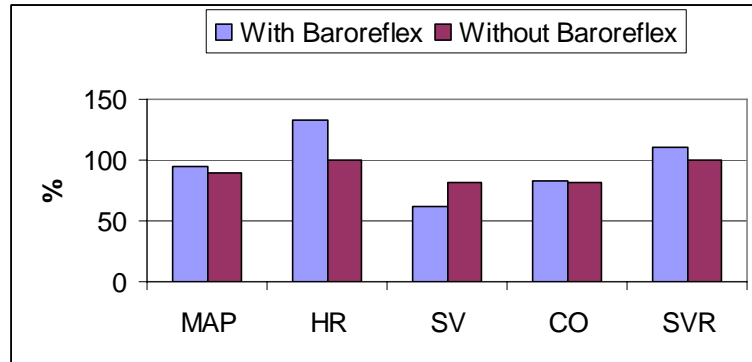
Figure 4.13. P-V loops of combination of systolic and diastolic dysfunctions. ($V_{T0} = 205$ ml)

Table 4.6. Simulation results for heart failure (2) $(V_o = 35 \text{ ml}, V_T = 300 \text{ ml})$

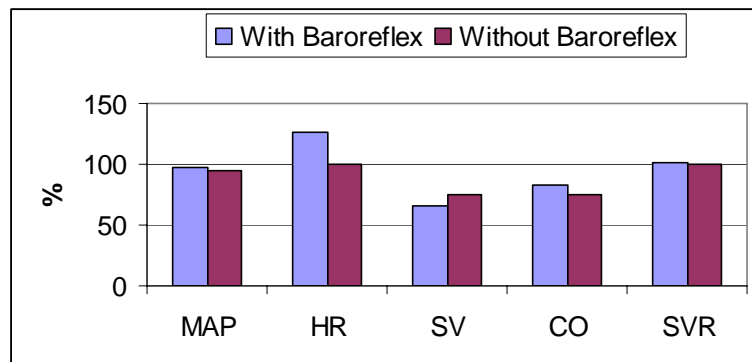
With baroreflex	Healthy heart	Systolic dysfunction (1)	Diastolic dysfunction (2)	Combination of (1) and (2)	Clinical data from [67] (23 patients)
DP(mmHg)	72	71	72	71	56.8 ± 10.4
SP(mmHg)	108	96	98	85	100.6 ± 12.4
LVEDP (mmHg)	7	8	17	17	No
LVESP (mmHg)	89	84	87	78	No
MAP (mmHg)	89	84	87	78	74.8 ± 10.7
EDV (ml)	121	165	121	122	No
ESV (ml)	44	117	70	96	No
SV (ml)	77	48	51	26	No
EF (%)	63.6	28.7	42.3	21.2	No
HR (bpm)	69	92	87	111	89.1 ± 17.6
CO (l/min)	5.3	4.4	4.4	2.9	3.54 ± 0.48
SVR (mmHg/ml/s)	0.91	1.01	0.92	1.21	1.20 ± 0.32
E _{max} (mmHg/ml)	2.7	1.2	2.8	1.4	No
E _{min} (mmHg/ml)	0.06	0.06	0.2	0.2	No
Sympathetic activity	2.77	2.84	2.80	2.95	No
Parasympath activity	6.12	6.08	6.11	6.02	No
Without baroreflex	Healthy heart	Systolic dysfunction (1)	Diastolic dysfunction (2)	Combination of (1) and (2)	Clinical data from [67] (23 patients)
DP (mmHg)	72	60	66	56	56.8 ± 10.4
SP (mmHg)	108	98	99	82	100.6 ± 12.4
LVEDP (mmHg)	7	8	18	18	No
LVESP (mmHg)	89	80	84	70	No
MAP (mmHg)	89	80	84	70	74.8 ± 10.7
EDV (ml)	121	176	128	135	No
ESV (ml)	44	113	70	92	No

Table 4.6 (continued)

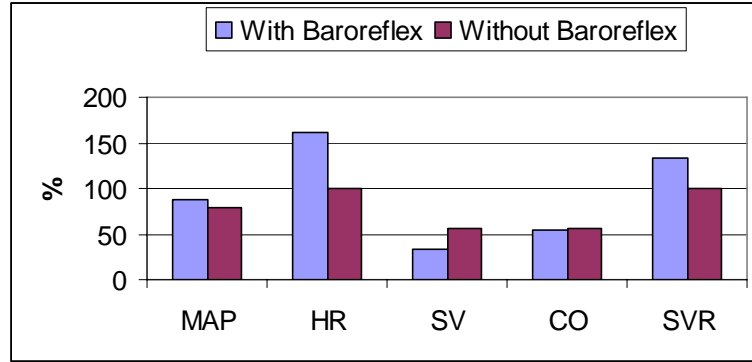
SV (ml)	77	63	58	43	No
EF (%)	63.6	35.6	45.2	32.1	No
HR (bpm)	69	69	69	69	89.1 ± 17.6
CO (l/min)	5.3	4.3	4.0	3.0	3.54 ± 0.48
SVR (mmHg/ml/s)	0.91	0.91	0.91	0.91	1.20 ± 0.32
E _{max} (mmHg/ml)	2.7	1.2	2.7	1.4	No
E _{min} (mmHg/ml)	0.06	0.06	0.2	0.2	No



a. Systolic dysfunction.



b. Diastolic dysfunction.



c. Combination of systolic dysfunction and diastolic dysfunction.

Figure 4.14. Comparison of simulation results with baroreflex and without baroreflex.

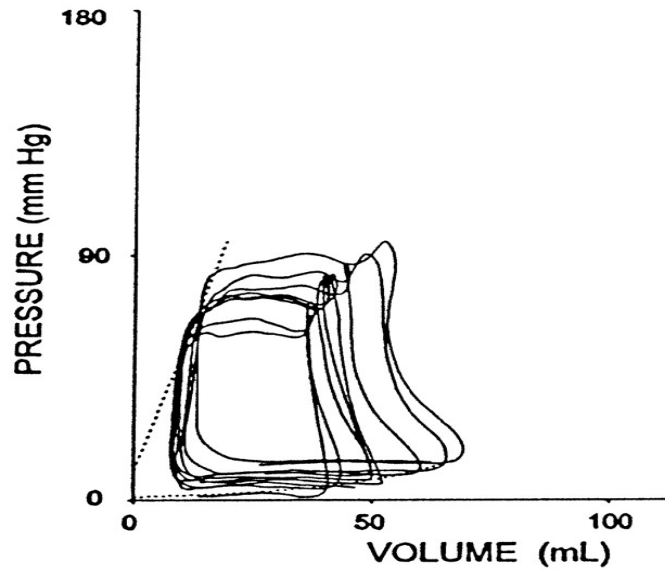
The MAP of the case with baroreflex is higher than that of the case without baroreflex due to the increase in HR and SVR.

Similar to that in subsection 4.4.1, because of the control of the baroreflex, the heart rate and systemic vascular resistance increase to compensate the decrease in the cardiac output due to changes in heart contractility (or compliance) and keep the blood pressure in acceptable range.

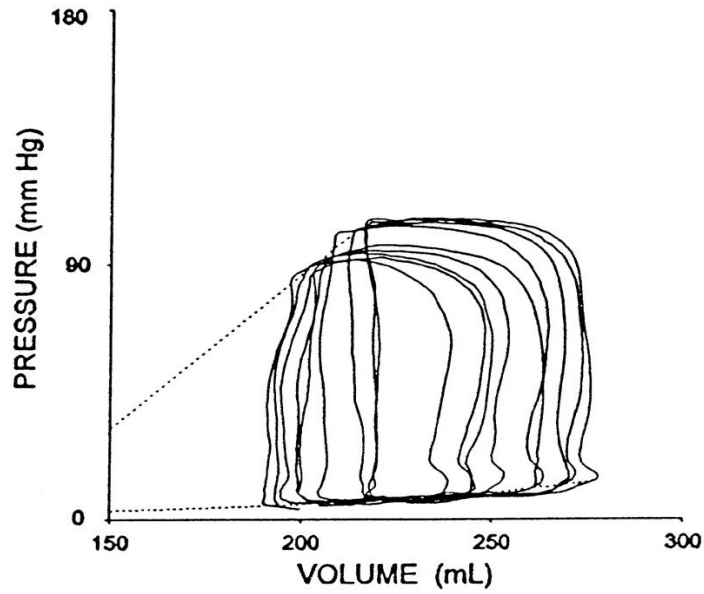
4.4.3 Simulations results of specific clinical heart failure

Some cases of failing heart P-V loops from [71] in Figure 4.15 are reproduced by changing parameters of the heart failure model with the baroreflex. In Figure 4.16, the hypertrophic heart failure is simulated by increased $E_{min}=0.2$ mmHg/ml (normal 0.06), decreased $V_o = -5$ ml (normal 5) and $V_{T0} = 145$ ml. the steady total $V_T = 220$ ml (normal 250). The dilated heart failure is simulated by decreased $E_{max}=1.0$ mmHg/ml (normal 2.7), increased $V_o = 100$ ml (normal 5) and $V_{T0} = 345$ ml. the steady total $V_T = 400$ ml (normal 250). Figure 4.17 shows the two cases of heart failure responses to reduction in preload. In this simulation of response to preload, the total blood volume is not under the control of the baroreflex.

Comparing the simulations results in Figure 4.16 and Figure 4.17 to that in Figure 4.15, it can be seen that both hypertrophic and dilated heart failure can be reproduced fairly well. With reduction in preload, MAP decreases and heart rate increases in the simulation. The simulation result is consistent with the clinical experiment.

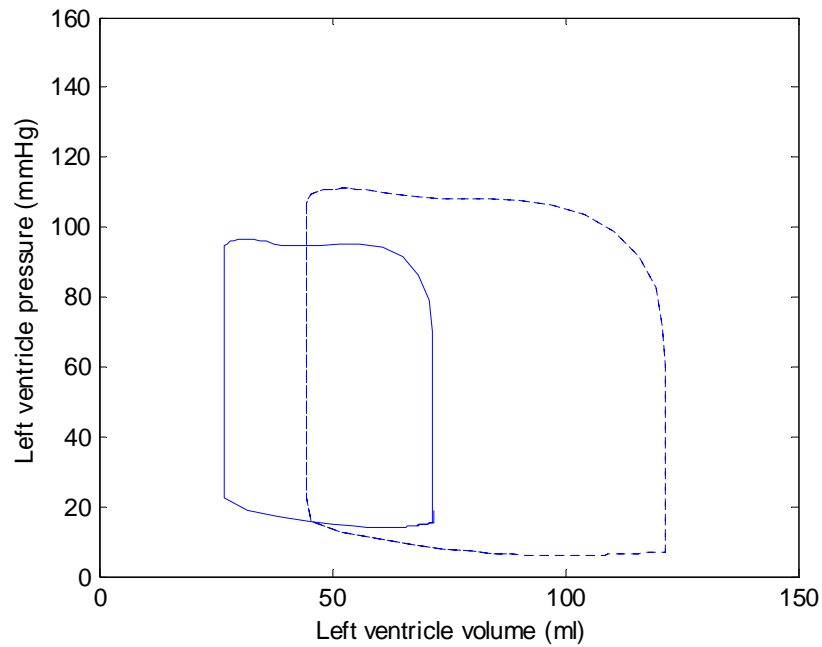


a. Hypertrophic cardiomyopathy. The right most is the P-V loop of baseline.

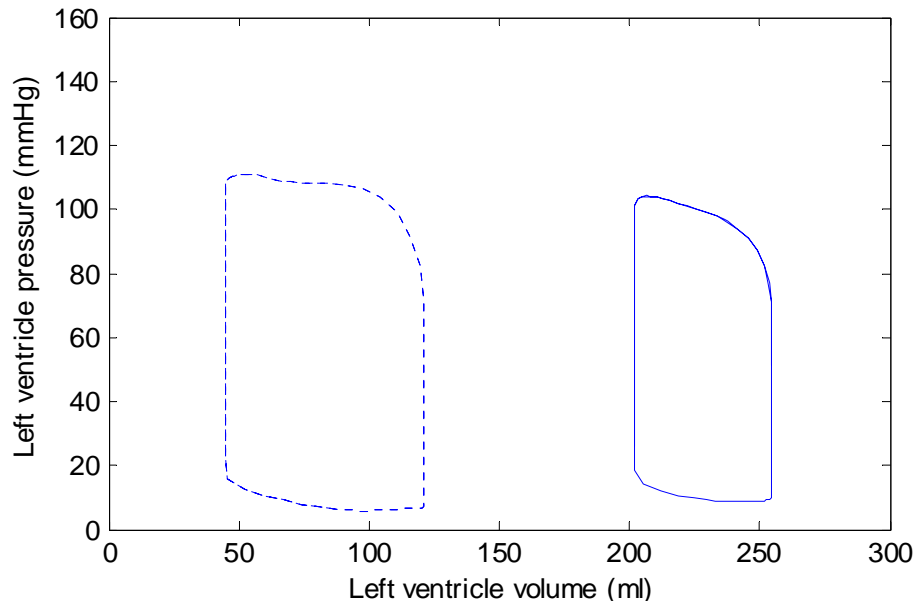


b. Dilated cardiomyopathy. The right most is the P-V loop of baseline.

Figure 4.15. P-V loops of failing heart responses to changes in preload (adopted from [71]).

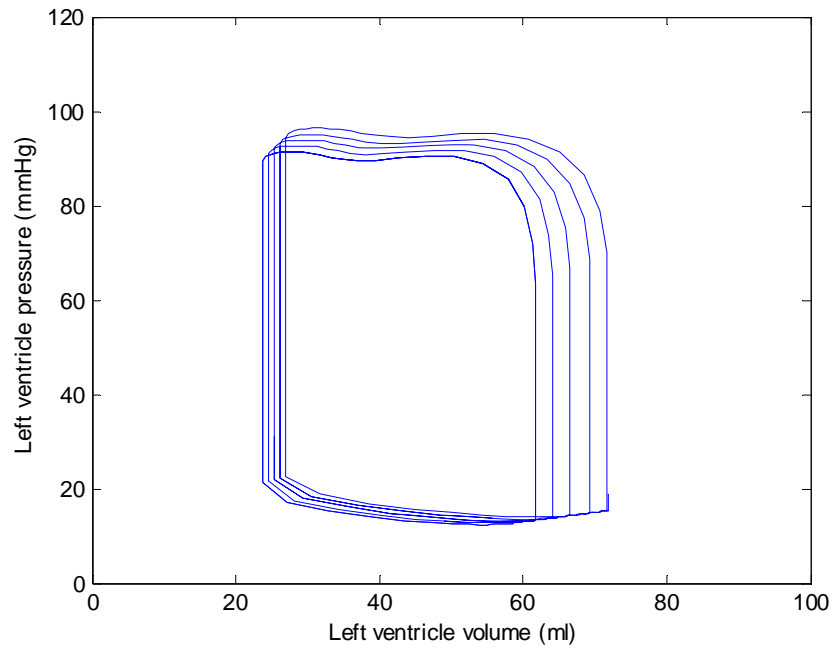


a. Reproduced P-V loop (solid line) of hypertrophic cardiomyopathy ($V_o = -5$ ml, $V_T = 220$ ml, $E_{min} = 0.2$ mmHg/ml). Broken line is the normal one.

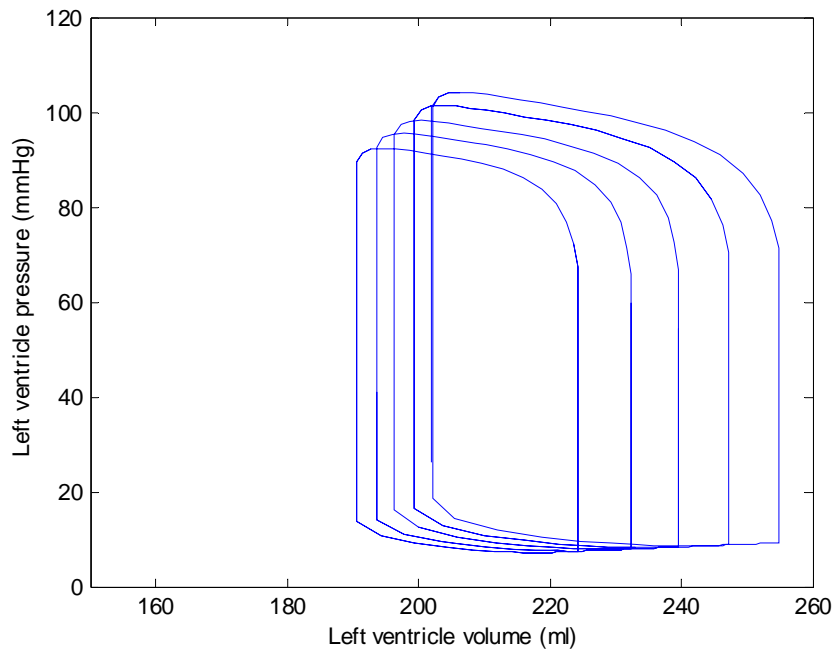


b. Reproduced P-V loop (solid line) of dilated cardiomyopathy ($V_o = 100$ ml, $V_T = 400$ ml, $E_{max} = 1.0$ mmHg/ml). Broken line is the normal one.

Figure 4.16. Model reproduced clinical baseline failing heart P-V loops.



a. Hypertrophic cardiomyopathy response to change in preload (Total blood volume changed from 220 to 200 ml).



b. Dilated cardiomyopathy response to change in preload (Total blood volume changed from 400 to 360 ml).

Figure 4.17. Simulation results of failing heart response to changes in preload.

In this section, some cases of heart failure and clinical experiment are simulated by combinations of decreased E_{max} and/or increased E_{min} , V_o and V_T . It can also be seen from the simulation results that, comparing to the corresponding case without baroreflex, because of the control of the baroreflex, the heart rate and systemic vascular resistance increase to compensate the decrease in the cardiac output due to changes in heart contractility (or compliance) and keep the blood pressure in acceptable range.

4.5 RESPONSES OF HEART FAILURE TO EXERCISE

The responses to exercise for the two types of heart failure in subsection 4.4.3 are simulated. Similar to that of section 3.5, in the simulation of exercise, the set point change is induced by adding offset to efferent pathways (forced changes in $offset_{es}$ and $offset_{ev}$) linearly in 5 seconds. In Figure 6.18, the offsets start changing progressively from 10s. At 15 s, the exercise begins, R_{13} starts decreasing due to local vasodilatation in active muscle (forced change linearly in 10 seconds), but heart rate increases continually until it achieves a new steady value. Because the ability of adjustment of end organs may be damaged for a patient with heart failure, the value of muscle resistance in exercise is set higher than that in the case of simulation of healthy people. This is applied to both hypertrophic and dilated heart failure. Multiple levels exercise responses are examined and compared to the data collected from heart failure patients exercise experiment in [54].

4.5.1 Hypertrophic heart failure

Multiple exercise levels are simulated by using the experimental data from [54] as reference to tweak the combinations of nervous offsets and forced change in R_{13} (muscle resistance). The complex of changes from rest to a certain level of exercise is shown in Figure 4.18 and P-V

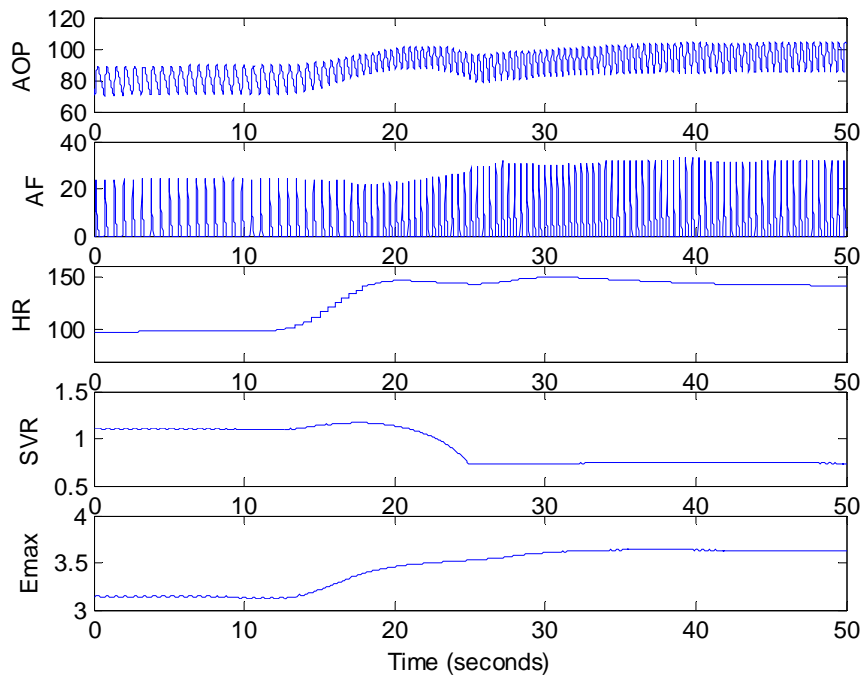


Figure 4.18. Response to exercise for hypertrophic heart failure.

MAP in mmHg, AF (aortic flow) in L/min, HR in bpm, SVR in mmHg/ml/s, (MAP, CO, SVR) changes from (81, 3.6, 1.08) to (97, 6.3, 0.74) during exercise.

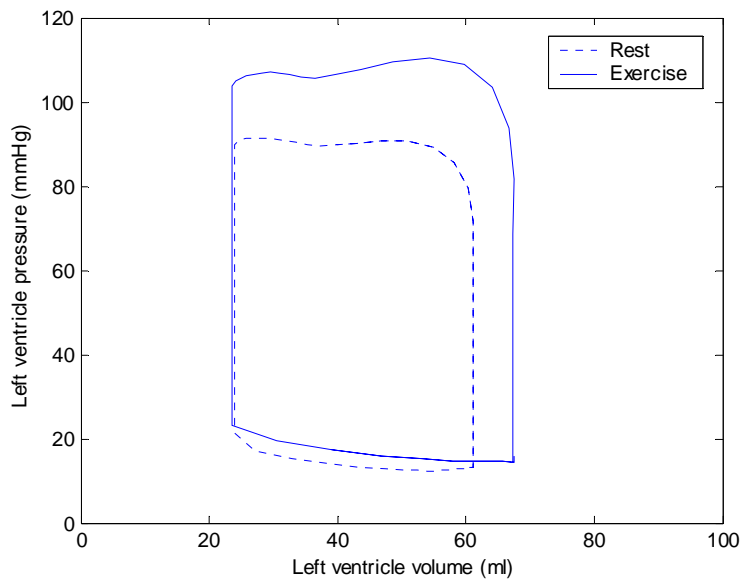


Figure 4.19. P-V loops of rest (dotted line) and exercise (solid line).

The loop for exercise expands to the right. The end diastolic volume and end systolic pressure increase.

loops in Figure 4.19. As shown in Figure 4.19, the changes in P-V loops from rest to exercise include expansion to the right and increase in end diastolic volume and increase in end systolic pressure. The hemodynamic changes are listed in Table 4.7. The hemodynamic changes in percentage from rest to exercise (ratio of exercise to rest) are shown in Figure 4.20.

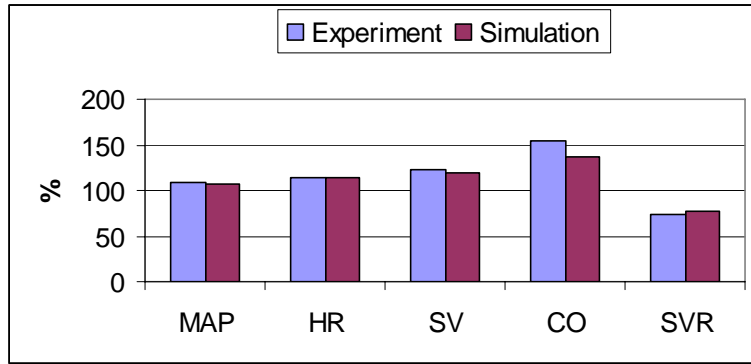
Table 4.7. Hypertrophic heart failure response to exercise

Exercise level	0	1	2	3
Data from [54] (30 subjects)	Rest	150 (kpm)	300 (kpm)	450 (kpm)
MAP (mmHg)	92	100	110	118
HR (bpm)	86 ± 17	98	114	134
SV (ml)	49 ± 15	60	60	58
CO (L/min)	4.0 ± 1.2	6.2	7.0	8.2
SVR (mmHg/ml/s)	1.41	1.05	0.87	0.87
SVR/LVR	13 ± 5	32	48	52
Simulation results	0	1	2	3
(O1,O2)	Rest	(0.16,0.1)	(0.26,0.4)	(0.31,0.6)
MAP (mmHg)	81	87	93	97
HR (bpm)	98	112	129	143
SV (ml)	37	44	44	44
CO (L/min)	3.6	4.9	5.7	6.3
SVR (mmHg/ml/s)	1.08	0.84	0.78	0.74
R13 (mmHg/ml/s)	8.5	2.1	1.6	1.4
SVR/R13 (%)	12.8	40.0	48.2	52.5

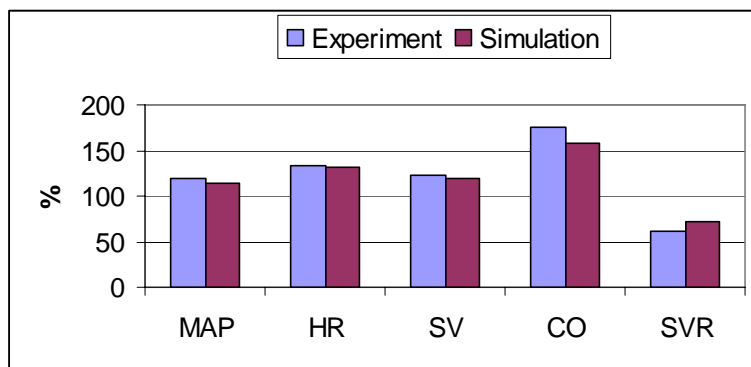
kpm: kilopond meters /min.

O1: offset in sympathetic activity caused by central command.

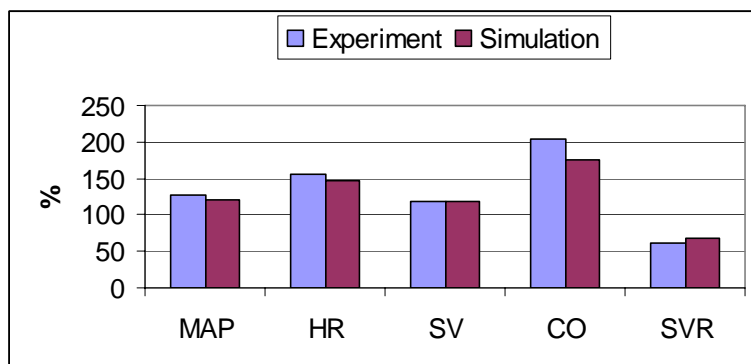
O2: offset in parasympathetic activity caused by central command.



Exercise level 1



Exercise level 2



Exercise level 3

Figure 4.20. Hemodynamic changes from rest to exercise.

MAP, CO, and HR increase, SVR decreases with increasing exercise intensity.

The experiment data from [54] and simulation results for multiple exercise levels are illustrated in Figure 4.21. With increasing exercise intensity, the tendency of changes in

hemodynamics is similar to that of healthy people but with less amounts and intolerance to higher exercise level (the heart rate is relatively high compared to the corresponding possible maximum). The results are consistent with the data in [54].

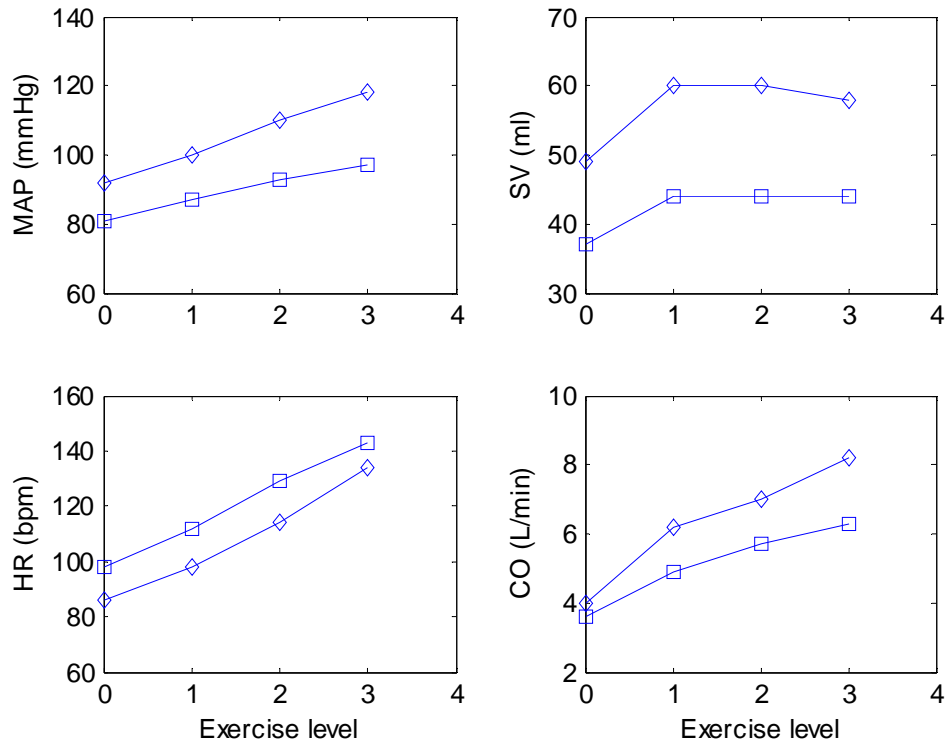


Figure 4.21. Changes in hemodynamics for multiple exercise levels.
Diamond: experiment data from [54]; Square: simulation results.

4.5.2 Dilated heart failure

The complex of changes of dilated heart failure response to exercise is shown in Figure 4.22 and P-V loops in Figure 4.23. As shown in Figure 4.23, the changes in P-V loops from rest to exercise include shift to the right and increase in end diastolic volume and increase in end systolic pressure. The hemodynamic changes are listed in Table 4.8. The hemodynamic changes in percentage from rest to exercise are shown in Figure 4.24. The experiment data from [54] and simulation results for multiple exercise levels are illustrated in Figure 4.25. With increasing

exercise intensity, the changes in hemodynamics are similar to that of healthy people. The results are consistent with the data in [54].

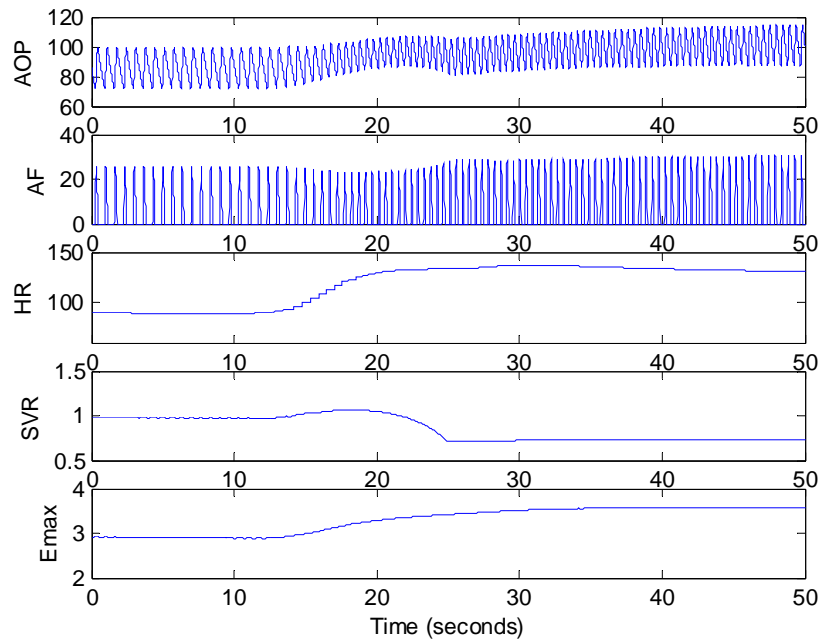


Figure 4.22. Response to exercise for dilated heart failure.

MAP in mmHg, AF (aortic flow) in L/min, HR in bpm, SVR in mmHg/ml/s, (MAP, CO, SVR) changes from (86, 4.5, 0.98) to (88, 5.9, 0.75) during exercise.

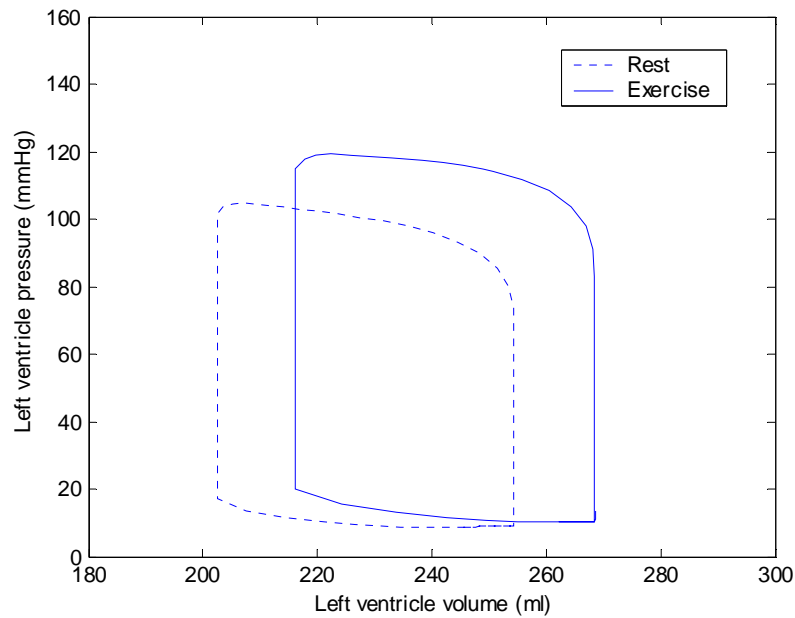
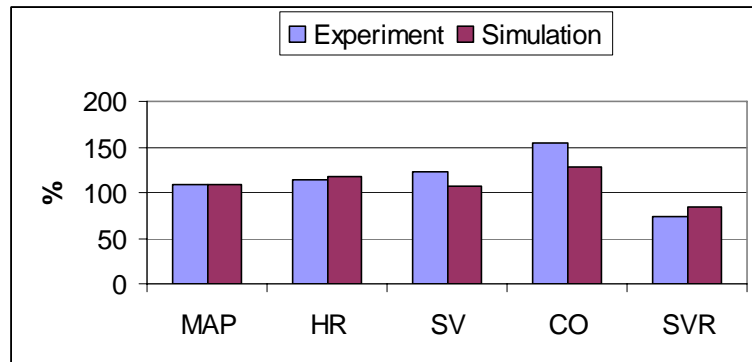


Figure 4.23. P-V loops of rest (dotted line) and exercise (solid line).

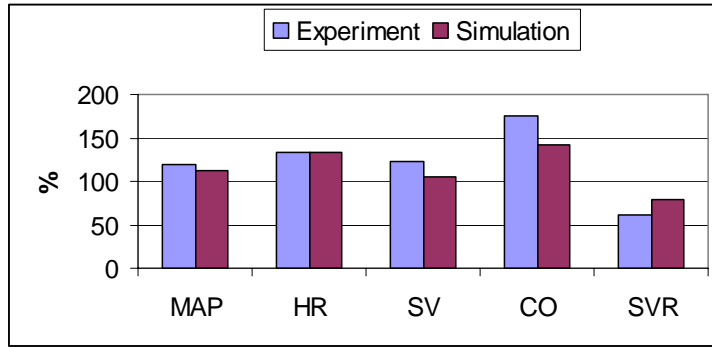
The loop for exercise shifts to the right. The end diastolic volume and end systolic volume increase.

Table 4.8. Dilated heart failure response to exercise

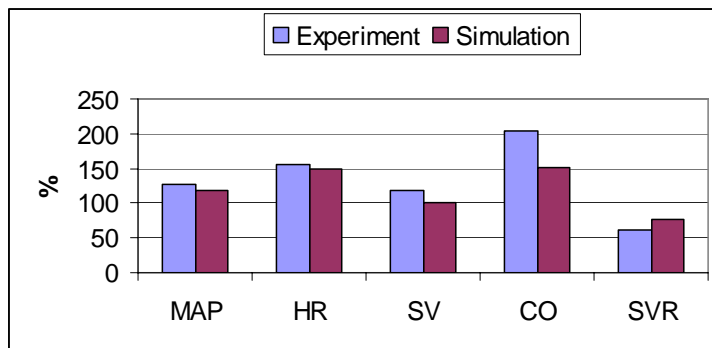
Exercise level	0	1	2	3
Data from [54] (30 subjects)	Rest	150 (kpm)	300 (kpm)	450 (kpm)
MAP (mmHg)	92	100	110	118
HR (bpm)	86 ± 17	98	114	134
SV (ml)	49 ± 15	60	60	58
CO (L/min)	4.0 ± 1.2	6.2	7.0	8.2
SVR (mmHg/ml/s)	1.41	1.05	0.87	0.87
SVR/LVR	13 ± 5	32	48	52
Simulation results	0	1	2	3
(O1,O2)	Rest	(0.17,0.02)	(0.26,0.2)	(0.31,0.6)
MAP (mmHg)	86	93	97	101
HR (bpm)	89	104	118	132
SV (ml)	52	56	55	52
CO (L/min)	4.6	5.9	6.5	7.0
SVR (mmHg/ml/s)	0.96	0.81	0.76	0.74
R13 (mmHg/ml/s)	7.4	2.1	1.6	1.4
SVR/R13 (%)	13.0	38.6	47.5	52.0



Exercise level 1



Exercise level 2



Exercise level 3

Figure 4.24. Hemodynamic changes from rest to exercise.

MAP, CO, and HR increase, SVR decreases with increasing exercise intensity.

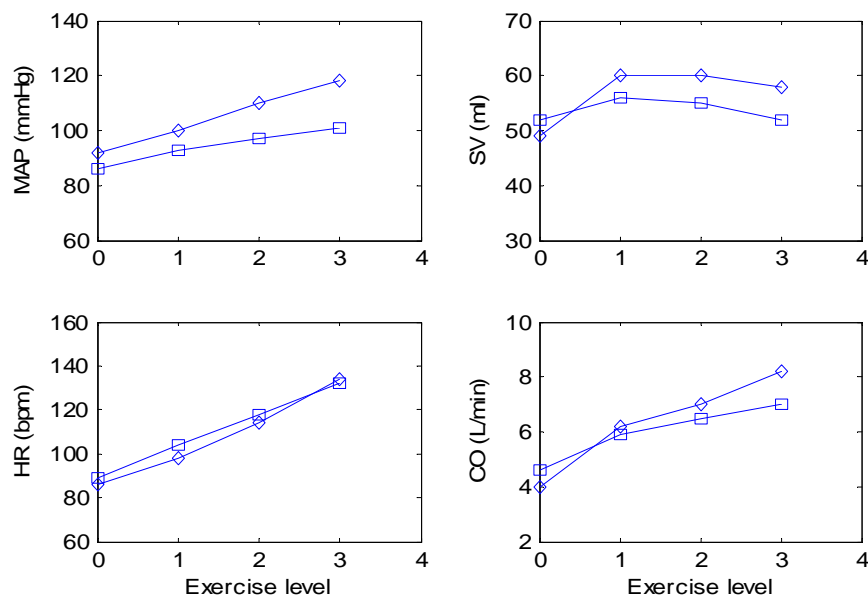


Figure 4.25. Changes in hemodynamics for multiple exercise levels.

Diamond: experiment data from [54]; Square: simulation results.

For both cases of heart failure, from rest to exercise, the tendencies of changes in MAP, CO, and SVR are similar to that of healthy people but the amounts of changes are less than that of healthy people due to physiological changes in the patients with heart failure. The increased HR during exercise (relatively low level for healthy people) nearly achieves the maximal possible value for heart failure patients (exercise intolerance).

4.6 CONCLUSION

Based on the healthy cardiovascular model, some parameters of the cardiovascular system and the baroreflex are changed to simulate heart failure. Because of the control of the baroreflex, the heart rate and the systemic vascular resistance increase to compensate the decrease in the cardiac output due to changes in heart contractility and/or compliance and keep the blood pressure in acceptable range. Some cases of clinical heart failure can be simulated by changing parameters of the model (E_{max} , E_{min} , V_0 , total blood volume). The responses to multiple levels of exercise for two types of heart failure are simulated. From rest to exercise, the tendencies of changes in MAP, CO, HR, and SVR are similar to that of healthy people but the amounts of changes are less than that of healthy people due to pathophysiological changes in the patients with heart failure. As shown in the simulation results, without the baroreflex, the model will not be able to simulate the changes in heart rate and the systemic vascular resistance and the resulting compensation for different physiological states.

5.0 THE COMBINED MODEL OF PUMP AND FAILING HEART

In this chapter, a pump model is introduced first in section 5.1. Then the pump model is coupled to the failing heart to simulate the interaction between the pump and the cardiovascular system in section 5.2. In section 5.3, the behavior of the coupled model of the pump, the heart and the baroreflex is examined.

5.1 THE PUMP MODEL

The rotary pump is a mechanical device driven by a motor. The rotation of the motor and the impellor of the pump force the blood to flow from the inlet of the pump to the outlet of the pump and generate a pressure rise across the pump. The electrical power is converted to mechanical power during this process. Therefore, the pump works under electrical and mechanical and/or hydraulic laws. Figure 5.1 shows the DC motor circuit.

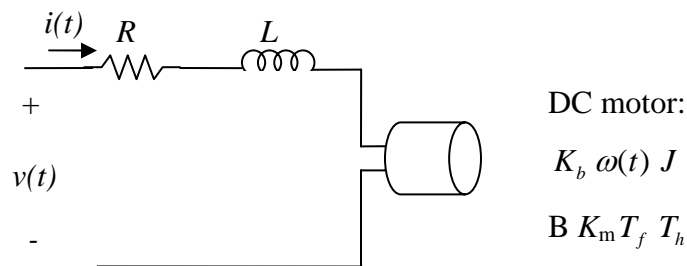


Figure 5.1. DC motor circuit

The electrical part of the DC motor equation (using Kirchhoff's voltage law) satisfies:

$$v(t) = L \frac{di(t)}{dt} + Ri(t) + K_b \omega(t) \quad (5.1)$$

Where

K_b is the EMF constant

$\omega(t)$ is rotating speed

The DC motor's mechanical part (using Newton's law) satisfies:

$$J \frac{d\omega(t)}{dt} = \sum T_i = K_m i(t) - B\omega(t) - T_f - T_h \quad (5.2)$$

Where

J is the inertia load of the rotor

$i(t)$ is current

B is a linear constant approximation for mechanical friction

K_m , the armature constant, is related to physical properties of the motor, such as magnetic field strength, the number of turns of wire around the conductor coil

T_f is a constant friction torque

T_h is the load torque exerted on the pump (coming from the hemodynamic, related to heart)

The load torque is derived from the shaft work performed by the motor upon the impeller, and is related to pump efficiency through:

$$\eta T_h \omega = HQ \quad (5.3)$$

Where

H is pressure difference between the outlet and the inlet of the pump,

Q is flow rate.

The hydraulic efficiency η is a function of speed and flow rate:

$$\eta = \eta(H, Q, \omega) \quad (5.4)$$

Typically,

$$\eta = \eta(N_s) \quad (5.5)$$

Where N_s is so called specific speed expressed as:

$$N_s = \frac{NQ^{1/2}}{H^{3/4}} \quad (5.6)$$

In fact this “specific speed”, a non-dimensional number (normalized by the size and nominal running speed of the pump), is used to describe the characteristic of the pump in the design stage. In other words, the design objective is to achieve the maximal efficiency at a specific speed (once the pump is made, operating speed is the only variable for determining the efficiency). If the pump is not running at nominal speed, the efficiency will drop a little bit.

These ideal equations are derived from electrical and mechanical principles. Note that there are two possibilities for a certain patient status in LVAD application:

1. If the left ventricle has no contractility (the left ventricle in complete failure), T_h becomes a constant, the speed and current of LVAD will become constants eventually.
2. If the left ventricle has contractility (the left ventricle still operating), T_h fluctuates dramatically, speed, current will be under the influence of this term.

For the second case, T_h will oscillate, the difficulty of solving for the desired variables arises. It should be pointed out that when combining these two equations an extra part of energy (or power) should be considered: if the ventricle still has contractility, the cardiac output is the result of the sum of blood pump power and left ventricular contraction power.

These basic equations for the pump are the basis for all VAD simulations and variable estimations. Because of power loss, parameters uncertainty and difficulties of solving these equations for H and Q directly, some researches turn to estimating H and Q with functions of current and speed. The objective of the estimation is to achieve approximate instantaneous waveforms of H and Q in a certain speed range.

The experimental data in Figure 5.2 illustrates a family of static characteristic curves for a typical rotary pump (Nimbus) describing the relationship between the pump flow and the pressure difference across the pump with various rotational speeds [72].

An empirical pump model was developed in [4]. The model describes the relationship of the pump rotational speed, the pump flow and pressure difference across the pump. It is an empirical model with parameters determined from experiments.

$$H = P_o - P_i = B_0Q + B_1 \frac{dQ}{dt} + B_2\omega^2 \quad (5.7)$$

Where

B_0 , B_1 and B_2 are parameters determined from experiments

ω is pump speed

H is pressure difference across the pump (pump head)

Here the pump speed is supposed to be adjusted directly (in fact the speed need to be solved in the pump dynamic equations).

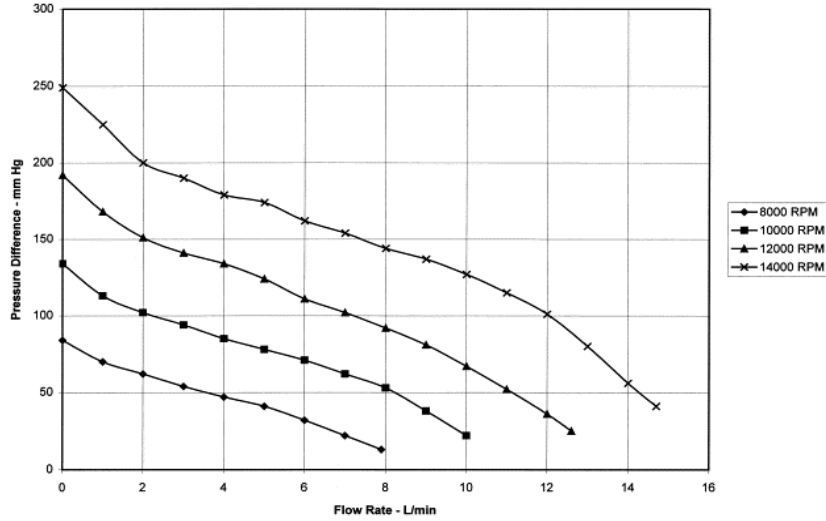


Figure 5.2. Rotary pump characteristic curves [72]

5.2 THE COUPLED MODEL OF THE PUMP AND THE FAILING HEART

In a typical pump implantation, the pump is connected between the left ventricle and the aorta. The flow through the pump and cannula is in parallel with the aortic flow. When the pump and cannula connect to the cardiovascular system model, the pump flow is added to the combined model as another state variable. The combined model is shown in Figure 5.3. In this model, the addition of circuit to the network, four passive parameters L_0 , R_0 , L_1 , and R_5 , is related to the cannula. Resistor R_6 is pressure dependent to simulate the suction phenomena [73].

$$R_6 = \begin{cases} 0 & \text{if } x_1 > P_{th} \\ -3.5LVP + 3.5P_{th} & \text{otherwise} \end{cases} \quad (5.8)$$

where $P_{th} = 1$ mmHg is a threshold.

Table 5.1 lists the state variables and Table 5.2 lists the model parameters. For this combined model, the SVR, HR and E_{max} are under the control of the baroreflex thus it is a time varying system. The resulting model is also a forced system with the pump speed as the primary control variable.

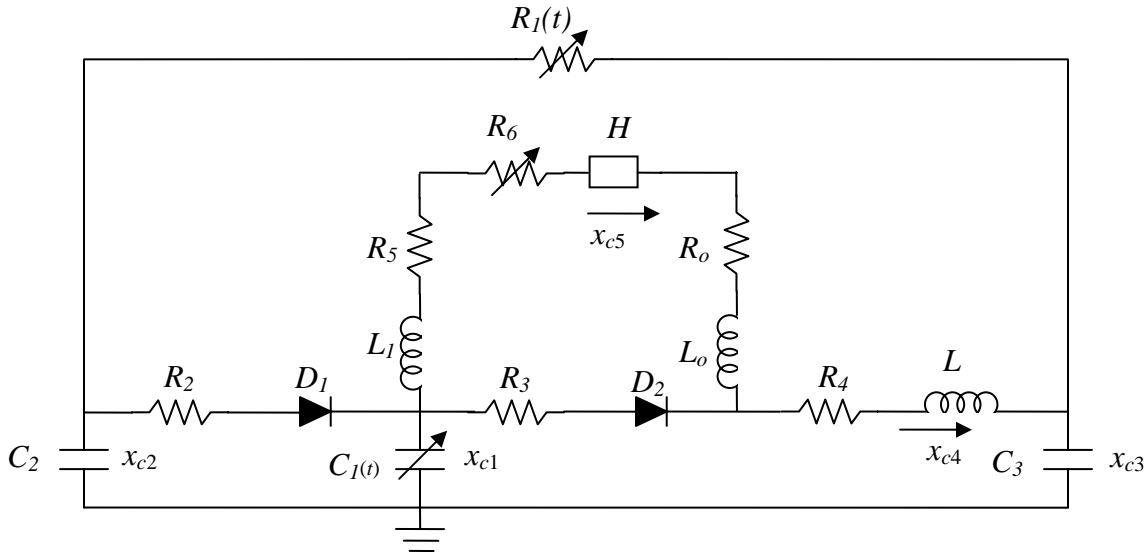


Figure 5.3. The coupled model of pump and failing heart

Table 5.1. State variables

Variables	Physiological meaning (units)
x_{c1}	Left ventricular volume (ml)
x_{c2}	Left atrial pressure (mmHg)
x_{c3}	Arterial pressure (mmHg)
x_{c4}	Total flow (ml/s)
x_{c5}	Pump flow (ml/s)

Table 5.2. Model parameters

Parameters	Value	Physiological Meaning	Units
Resistances			
$R_1(t)$	Time varying	Systemic Resistance	mmHg.s/ml
R_2	0.005	Mitral valve (open)	
	∞	Mitral valve (close)	
R_3	0.001	Aortic valve (open)	
	∞	Aortic valve (closed)	
R_4	0.0398	Characteristic resistance	
R_5	0.0677	Cannulae inlet resistance	
R_0	0.0677	Cannulae outlet resistance	
R_6	Pressure dependent		
Compliances			
$C_1(t)$	Time varying	Left ventricular compliance	ml/mmHg
C_2	4.4	Left atrial compliance	
C_3	1.33	Systemic compliance	
Inertances			
L	0.0005	Inertance of blood in Aorta	mmHg.s ² /ml
L_1	0.0127	Cannulae inlet inertance	
L_0	0.0127	Cannulae inlet inertance	
Valves			
D_1		Aortic valve	
D_2		Mitral valve	

Table 5.2. (continued)

Pump			
B0	-0.1707		
B1	-0.02177		
B2	0.0000903		

Note that $R_{1(t)}$ and $C_{1(t)}$ are under the control of the baroreflex, thus are time varying.

The state equations of the coupled model can be written as

$$\frac{dx}{dt} = A(t)x + bu(t) \quad (5.9)$$

where $u(t) = \omega^2(t)$ is the control variable and $A(t)$ can be either a (4 x 4) or a (5 x 5) time varying matrix, depending on the modes of D_1 and D_2 . The dimension of the vector b , changes accordingly, i.e., it can be (4 x 1) or (5 x 1). The following 3 phases will occur in a cardiac cycle, over four different time intervals.

1) *Isovolumic phase*: In this phase, the aortic and mitral valves are closed. Moreover, total flow is equal to pump flow, i.e., $x_{c4}(t) = x_{c5}(t)$. In this case, we have

$$A(t) = \begin{bmatrix} 0 & 0 & 0 & -1 \\ 0 & -\frac{1}{R_1 C_2} & \frac{1}{R_1 C_2} & 0 \\ 0 & \frac{1}{R_1 C_3} & -\frac{1}{R_1 C_3} & \frac{1}{C_3} \\ \frac{E(t)}{L+L'} & 0 & -\frac{1}{L+L'} & -\frac{R+R_4}{L+L'} \end{bmatrix} \quad (5.10)$$

and

$$b = [0 \ 0 \ 0 \ -b_2/(L' + L)]^T \quad (5.11)$$

where $L' = L_1 + L_0 + b_1$ and $R = R_5 + R_0 + R_6 + b_0$.

2) *Ejection phase*: In this phase, the aortic valve is open, and the mitral valve is closed. In this case, two flows go into the circulatory system, from the aorta and from the pump.

$$A(t) = \begin{bmatrix} 0 & 0 & 0 & -1 & 0 \\ 0 & -\frac{1}{R_1 C_2} & \frac{1}{R_1 C_2} & 0 & 0 \\ 0 & \frac{1}{R_1 C_3} & -\frac{1}{R_1 C_3} & \frac{1}{C_3} & 0 \\ \frac{E(t)}{L} & 0 & -\frac{1}{L} & -\frac{(R_3 + R_4)}{L} & \frac{R_3}{L} \\ 0 & 0 & 0 & -\frac{R_3}{L} & \frac{R - R_3}{L} \end{bmatrix} \quad (5.12)$$

and

$$\mathbf{b} = [0 \ 0 \ 0 \ 0 \ -b_2/L]^T \quad (5.13)$$

3) *Filling phase*: In this phase of the cardiac cycle, the mitral valve is open, and the aortic valve is closed, blood from the left atrium goes into the left ventricle. This again implies $x_{c4}(t) = x_{c5}(t)$. For this phase,

$$A(t) = \begin{bmatrix} -\frac{E(t)}{R_2} & \frac{1}{R_2} & 0 & -1 \\ \frac{E(t)}{R_2 C_2} & -\frac{(R_1 + R_2)}{R_1 R_2 C_2} & \frac{1}{R_1 C_2} & 0 \\ 0 & \frac{1}{R_1 C_3} & -\frac{1}{R_1 C_3} & \frac{1}{C_3} \\ \frac{E(t)}{L + L'} & 0 & \frac{-1}{L + L'} & \frac{-(R + R_4)}{L + L'} \end{bmatrix} \quad (5.14)$$

and

$$\mathbf{b} = [0 \ 0 \ 0 \ -b_2/(L' + L)]^T \quad (5.15)$$

The case with both valves open does not occur for a normal heart and thus is not included in this model. For a sequence of these phases in a normal cardiac cycle, for example, filling-contraction-ejection-relaxation, the end states of the last phase are initial conditions for the next phase. The block diagram Figure 5.4 shows the coupling between the failing heart, the pump and the baroreflex. The arterial pressure is the input for the baroreflex. The contractility (E_{max}) of the left ventricle is fixed at a low value to simulate the heart failure. The SVR , HR and VT (total blood volume) are under the control of the baroreflex. Specifically, the SVR and VT vary

instantaneously; the *HR* (or cardiac cycle) varies cycle by cycle, in other words, the *HR* remains constant in a cardiac cycle.

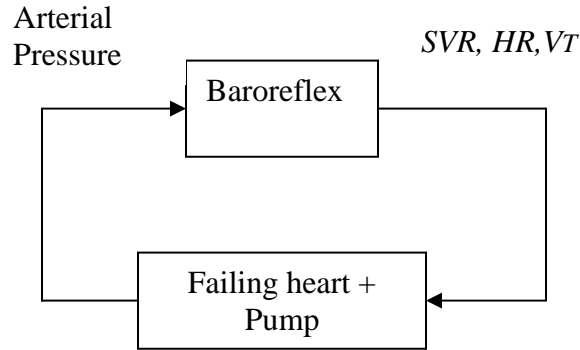
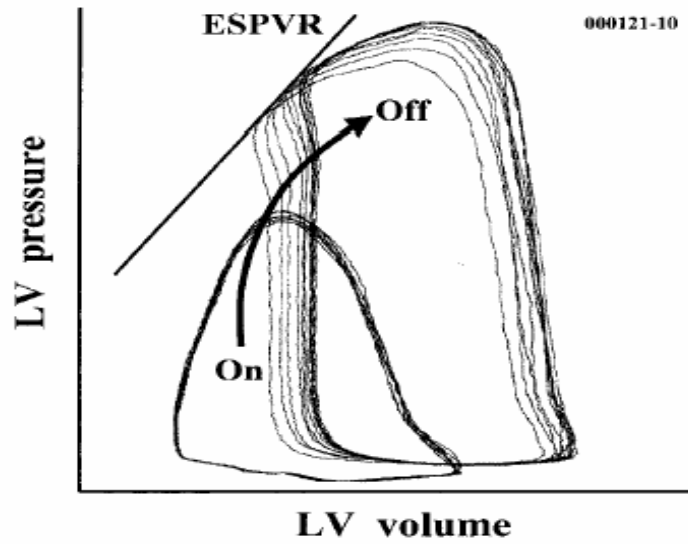


Figure 5.4. Pump augmented failing heart with baroreflex

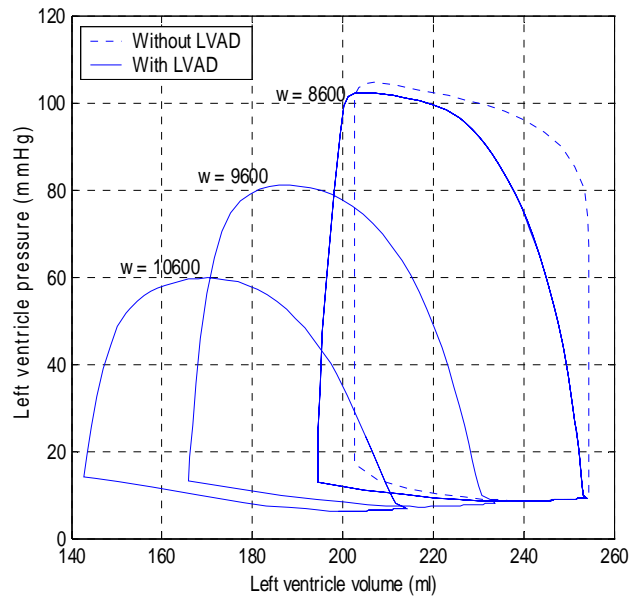
5.3 CHANGES IN HEMODYNAMICS WITH PUMP IMPLANTED

Clearly, an implanted pump will have impact on the native cardiovascular system. Specifically, the hemodynamic variables will vary corresponding to the changes caused by the baroreflex and the pump speed (rotary pumps). Such changes will be simulated and compared to the clinical experiments in the literature.

Figure 5.5 shows changes in P-V loops when the pump speed (or rate) increases for the clinical experiment in [74] and simulation. With increasing pump speed, the P-V loops shrink towards the left bottom corner of the coordinate in both the clinical experiment and simulation. Table 5.3 lists the hemodynamic variables with the increasing pump speed in the simulation.



a. P-V loops for pump on-off test in a clinical experiment (adopted from [74])



b. Simulation with increasing pump speed

Figure 5.5. P-V loops changes with changing pump speed

With increasing pump speed, the P-V loops shrink towards the left bottom corner of the coordinate.

Table 5.3. Hemodynamic changes with increasing pump speed

LVAD operating rate (rpm)	MAP (mmHg)	HR (bpm)	CO (L/min)	SVR (mmHg/ml/s)
8,100	86	87	4.3	0.98
8,600	86	84	4.5	0.94
9,100	88	79	5.1	0.87
9,600	89	75	5.7	0.81
10,100	91	72	6.3	0.76
10,600	94	69	7.0	0.71

CO: total blood flow (pump flow + aortic flow).

It can be seen that with increase in pump speed, the cardiac output and blood pressure increase, heart rate and systemic vascular resistance decrease. These hemodynamic changes with increase in pump speed can be verified by the clinical data. There are some experiments on patients with pulsatile LVADs implanted in [75]. The stroke volume for this implanted pulsatile pump is 80 ml/stroke. For the experiment of partial pump support, the pumps were running at a lower fixed rate and lower pump flow (far below the blood flow requirement of the body). At first, the pump was in full support for the heart. Then the pump was turned to partial support. During this experiment, mean arterial blood pressure decreased, heart rate increased, and cardiac output fell.

For the simulations of the full and partial pump support, the pump speed is adjusted to match the cardiac output in the clinical experiment accordingly. Simulation results with the baroreflex decoupled are listed for comparison. For the case with baroreflex, the heart rate and systemic vascular resistance are under the control of the baroreflex. For the case without baroreflex, the heart rate and systemic vascular resistance are the same for the full and partial pump support. Table 5.4 shows the experiment results (18 patients) and simulation results. Figure 5.6 shows the changes in percentage.

Table 5.4. Full and partial pump support

Clinical data from [75] (18 patients)	Full pump support	Partial pump support
LVAD operating rate (cycles/min)	66 ± 11	28 ± 9
MAP (mmHg)	91 ± 8	71 ± 12
HR (bpm)	94 ± 12	106 ± 17
CO (L/min)	5.3 ± 1.0	4.2 ± 1.2
Simulation results with LVAD	Full pump support	Partial pump support
LVAD operating rate (rpm)	9,300	8,100
MAP (mmHg)	88	86
HR (bpm)	77	87
CO (L/min)	5.4	4.3
SVR (mmHg/ml/s)	0.85	0.98
Simulation results without baroreflex	Full pump support	Partial pump support
LVAD operating rate (rpm)	9,300	8,100
MAP (mmHg)	88	78
HR (bpm)	77	77
CO (L/min)	5.4	4.5
SVR (mmHg/ml/s)	0.85	0.85

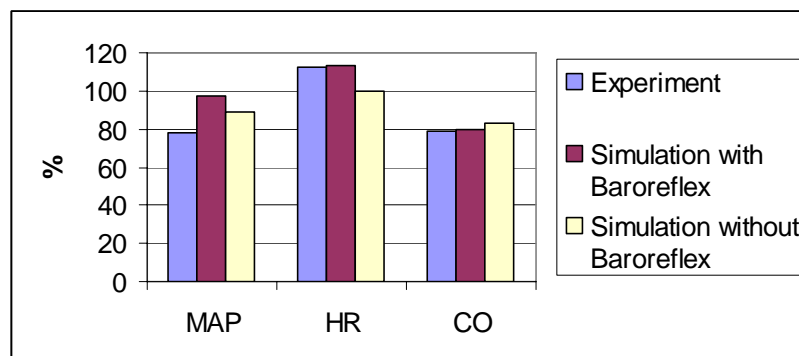


Figure 5.6. Changes in hemodynamics (ratio of partial to full)
Experiment results from [75].

The changes in HR and CO match pretty well but the change in MAP does not. It is apparent that the SVR does not change in the experimental data (MAP and CO have nearly the same percent change).

5.4 CONCLUSION

The pump model is coupled to the failing heart model with built in baroreflex. The simulation results have the same trends for the P-V loops and hemodynamic changes as that of the clinical experiment for the full and partial pump support. With increasing pump speed, the P-V loops shrink to the left bottom corner in the coordinate, mean arterial pressure increased, heart rate decreased, and cardiac output increased.

6.0 PUMP CONTROL BASED ON HEART RATE AND SYSTEMIC VASCULAR RESISTANCE

For a normal heart, the cardiac output (CO) is determined by two factors: stroke volume (SV) and heart rate (HR). From rest to exercise, both stroke volume and heart rate increase, thus the resulting greater CO can meet the increased blood flow requirement. More generally, the physiological status of the patient may demonstrate a wide range of variation, due to exercise intensity and emotional changes. Thus a controller that can detect and adapt to the real time physiological changes of the body is important for the LVAD application.

The baroreflex function is preserved fairly well in the patients with heart failure even though some end organ functions are damaged or attenuated. The increase in stroke volume for healthy people during exercise is the result of a complex of physiological process: increasing blood return, increasing heart contractility and decreasing systemic vascular resistance. The increased heart rate and decreased systemic vascular resistance are observed during exercise in the patients with heart failure. Incorporating this information can make the LVAD controller responsive to the change in physiological state of the body. With the baroreflex model coupled to the cardiovascular system model in the simulation, the controller can use this information to estimate the blood flow requirement of the body and drive the pump to meet this estimated requirement. The feasibility of this controller will be investigated in this chapter. First, the pump operation will be illustrated in section 6.1 by using a superimposed pump characteristic curves and a simplified physiological constraint on the H-Q plane. Second, the pump controller based on HR and SVR will be described in section 6.2. The simulation results will be compared to that of constant speed method, constant pump head method and heart rate related pump speed control method in section 6.3. Third, the performance of this proposed method with respect to changes in parameters and tolerance to noise will be examined in section 6.4.

6.1 PUMP OPERATION

In general, the rotary pump can be simplified as a model in which the pressure rise across the pump is a function of pump speed and pump flow. The pump model

$$H = f(Q, \omega) \quad (6.1)$$

where H is the pressure rise across the pump, Q is pump flow, and ω is pump speed.

For a certain physiological state of the body, a specific pump speed needs to be set for the implanted pump. Figure 6.1 illustrates a family of the static pump characteristic curves and an operating point (H_o, Q_o, ω_o) . When the pump is coupled to a failing cardiovascular system, (H_o, Q_o) is constrained by the coupled cardiovascular system and the pump, and also needs to meet the physiological requirement of the body. In the illustration, the physiological state is simplified by a certain SVR; a prescribed Q_o will result in a certain H_o and ω_o . The corresponding pump speed ω_o is the desired operating speed for this prescribed Q_o . Similarly, a prescribed H_o will result in a certain Q_o and ω_o . The corresponding pump speed ω_o is the desired operating speed for the prescribed H_o .

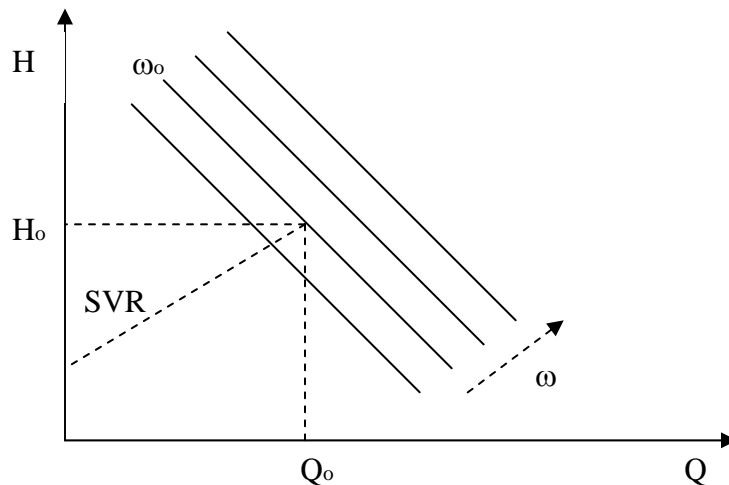


Figure 6.1. Static pump characteristic curves and operating point.

Superimposed pump characteristic curves and physiological state of the body. H is the pump head and Q is the pump flow, ω is the pump speed.

If both H and Q are prescribed and are not coincident, as shown in Figure 6.2, no single operating point can satisfy both of them at the same time.

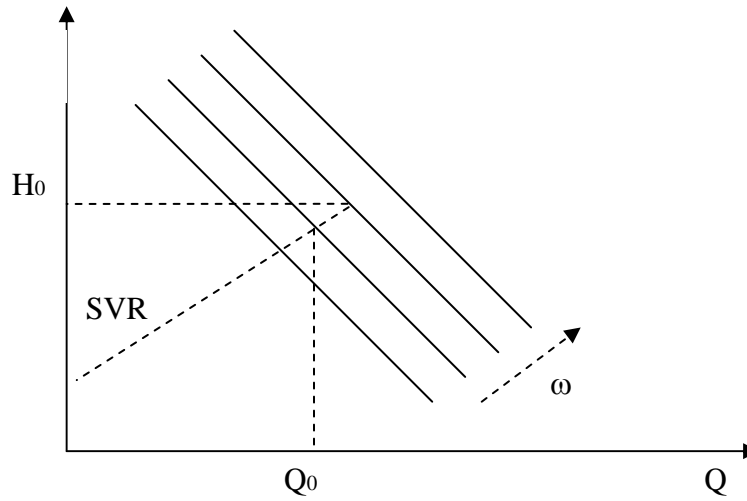


Figure 6.2. Same SVR and different operating points.

The operating point may move in the H-Q plane for different physiological states. From rest to exercise, SVR decreases, both H and Q increase, the operating point moves right upward, as illustrated in Figure 6.3.

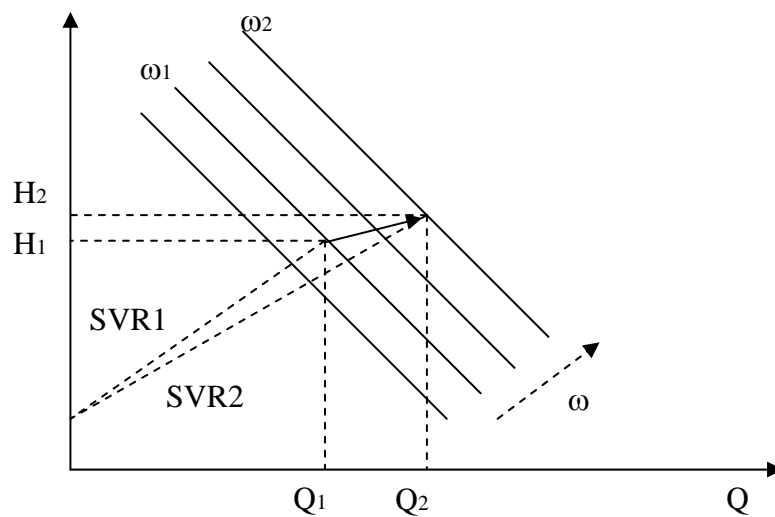


Figure 6.3. Change in operating points from rest (1) to exercise (2).

6.2 PROPOSED PUMP CONTROL BASED ON HR AND SVR

As mentioned before, the increased HR and decreased SVR are observed from rest to exercise for patients with heart failure. Thus it is reasonable to assume that HR and SVR are still under the control of the baroreflex for the patients with heart failure. We further assume that HR and SVR of the patient can be measured or estimated with a pump implanted [10]. The pump speed is chosen to match the physiological state of the body, which is estimated by using the HR and SVR. Figure 6.4 shows the closed-loop block diagram.

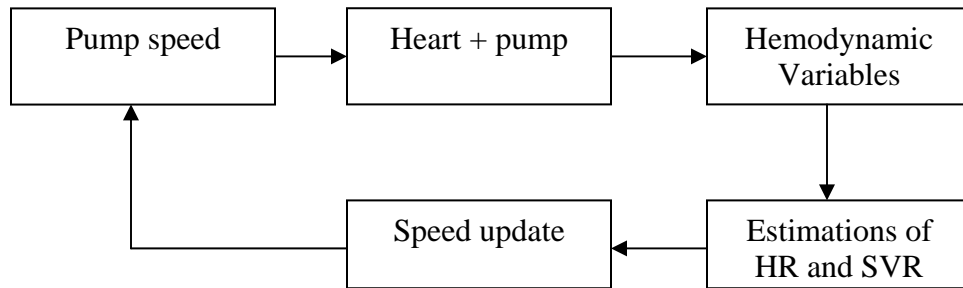


Figure 6.4. Block diagram for the closed-loop control based on HR and SVR.

Since the left ventricle contractility for severe heart failure is decreased significantly, it is reasonable to assume that the aortic valve is always closed when the pump takes the role of the left ventricle pumping the blood out of the chamber. Thus, the combined model of the pump and the cardiovascular system in Figure 5.2 can be simplified as Figure 6.5. The aortic valve is open-circuited and is taken out in Figure 6.5.

This proposed controller will be manipulated by using mean hemodynamic variables. Thus the circuit in Figure 6.5 can be further reduced to a circuit in mean sense by eliminating the constant capacitors and inductors. The reduced circuit diagram in mean sense is shown in Figure 6.6 (LVP: left ventricular pressure, AOP: aortic pressure).

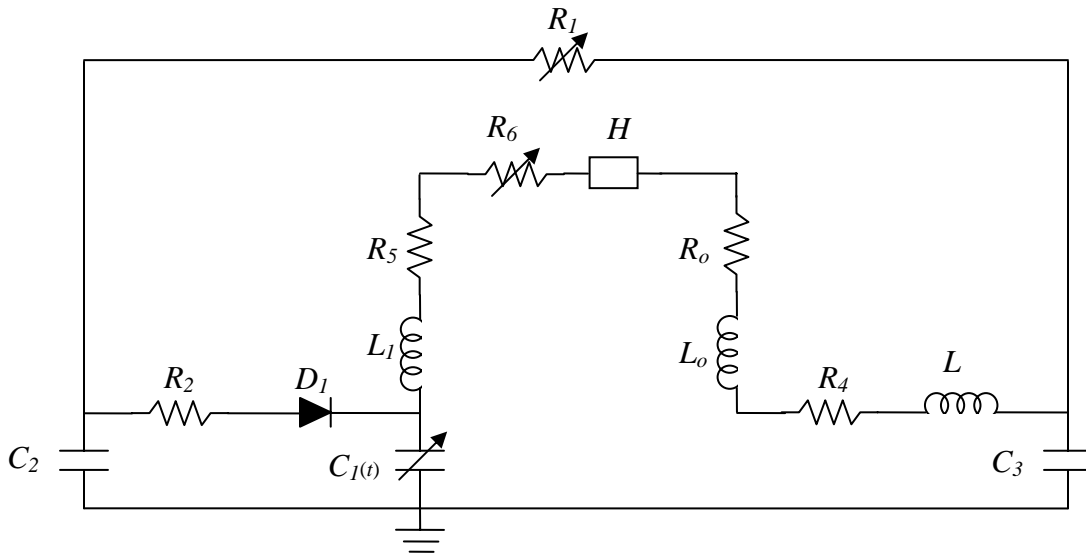


Figure 6.5. Simplified version of the combined model (aortic valve is taken out).

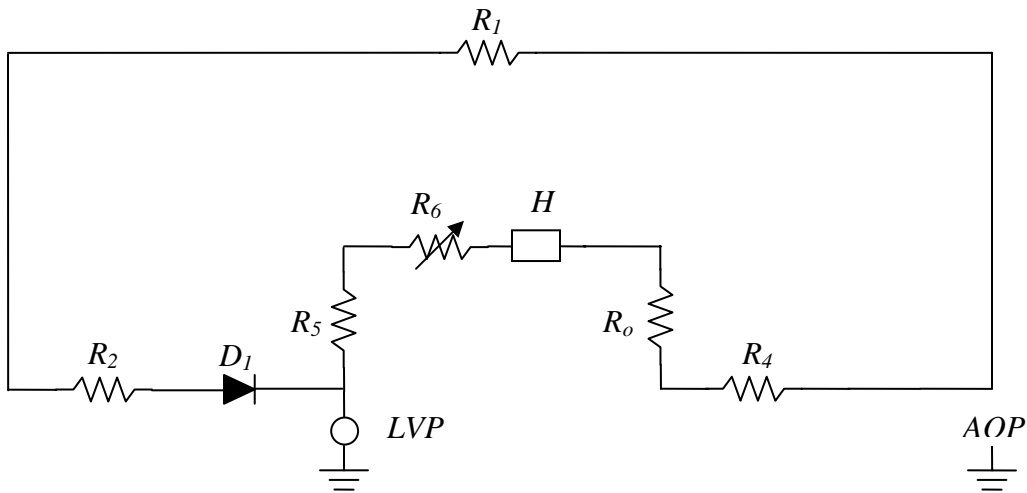


Figure 6.6. Reduced circuit diagram in mean sense.

For a healthy human, the cardiac output (CO) is the product of the stroke volume (SV) and the heart rate (HR),

$$CO = HR * SV \tag{6.2}$$

When exercise starts, both HR and SV increase thus CO increases.

With the pump coupled to a failing heart, if ignore the small resistances in the circuit, the pressure rise across the pump H is the difference between the aortic pressure (AOP) and the left ventricular pressure (LVP),

$$H = AOP - LVP \quad (6.3)$$

To mimic the healthy heart response to exercise, we want the pump to operate in a similar fashion to that of the healthy heart. In other words, we want pump to generate estimated reference amounts of H and CO : H_0 and CO_0 . If the failing left ventricle does not have enough contractility to open the aortic valve, thus CO is equal to the pump flow. In this case, the estimated references pump flow, arterial pressure and pump head

$$CO_0 = HR * SV_r \quad (6.4)$$

$$AOP_0 = CO_0 * SVR \quad (6.5)$$

$$H_0 = AOP_0 - LVP_r \quad (6.6)$$

where SV_r and LVP_r are preset values. Especially, SV_r has a different value for rest and exercise.

The block diagram of this control scheme is shown in Figure 6.7. In this diagram, the variables HR , H and CO are averaged value over a cardiac cycle. With these estimated reference values for the pump head and flow, the errors between the real ones and these reference values will be used to change the pump speed towards the desired value.

To mimic the change in stroke volume for different states of a healthy person (rest and exercise), the stroke volume is set as a function of the heart rate (to mimic the increase in stroke volume during exercise) in the simulation,

$$SV_r = \begin{cases} 70ml & HR \leq 85bpm \\ 80ml & HR > 85bpm \end{cases} \quad (6.7)$$

The instantaneous left ventricular pressure depends on the volume and the contractility of the left ventricle, both of which are time varying. Here a constant mean value is used in the simulation,

$$LVP_r = 50 \text{ mmHg} \quad (6.8)$$

Considering the arterial pressure can not increase or decrease beyond some reasonable range, the estimated reference value H_0 is set to be saturated at a certain value (160 mmHg here), thus (6.6) becomes

$$H_0 = \begin{cases} AOP_0 - LVP_r & AOP_0 \leq 160 \\ 160 - LVP_r & AOP_0 > 160 \end{cases} \quad (6.9)$$

Given (6.8), this implies that H_0 is saturated at 110 mmHg.

In the block diagram, the pump speed is updated with:

$$\omega_{k+1} = \omega_k + \Delta\omega \quad (6.10)$$

$$\Delta\omega = K1 * (H_0 - H) + K2 * (CO_0 - CO) \quad (6.11)$$

where K1 and K2 are constants. The values for them are chosen to be the possible maximum not to cause overshoot in the transition from rest to exercise.

To simulate the failing heart the contractility index E_{max} is set equal to 0.7 mmHg/ml (normal value is 2.7 mmHg/ml). The exercise in the simulation is induced by adding offsets to efferent nervous signals and forced change in active muscle resistance. Figure 6.8 shows the response of the controller to a certain level of exercise. Figure 6.9 shows the errors between the estimated reference values and actual values for H and Q in a certain simulation run. Figure 6.10 shows the trajectory of the operating point in the pump H-Q plane. Figure 6.11 shows the LVP and LVPr, and Figure 6.12 shows LVP and AOP.

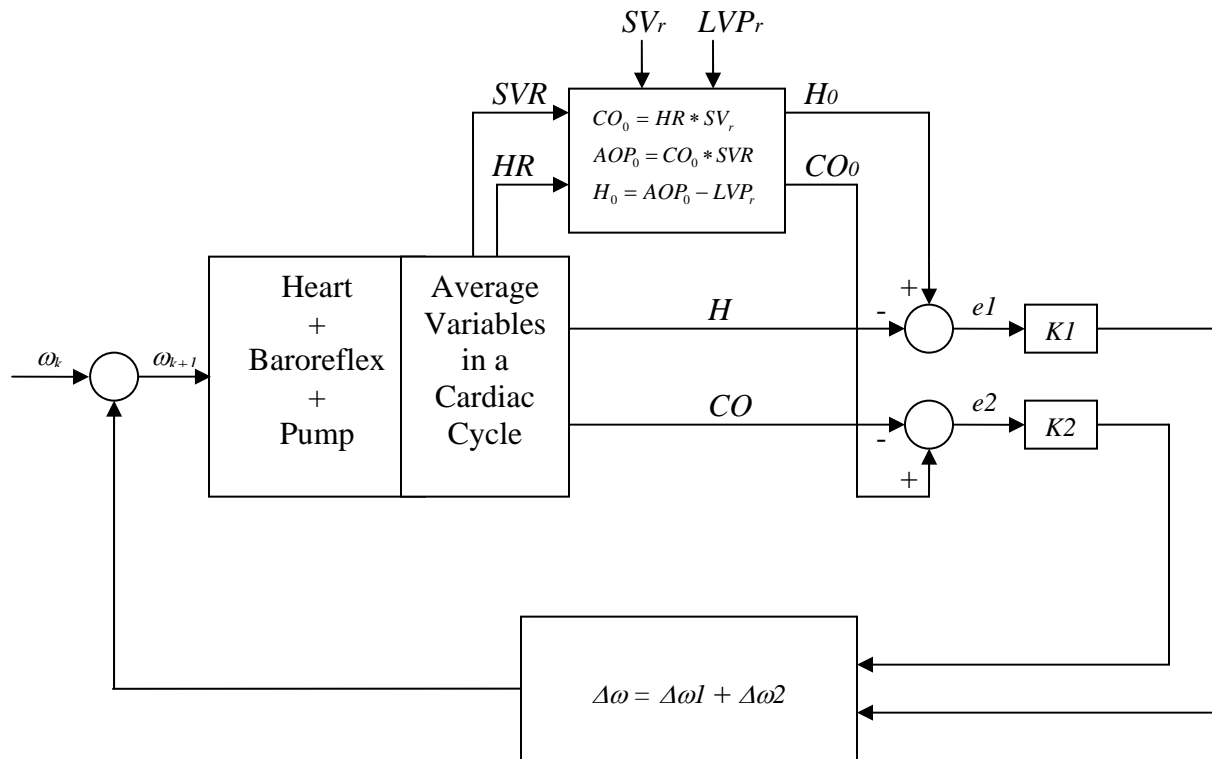
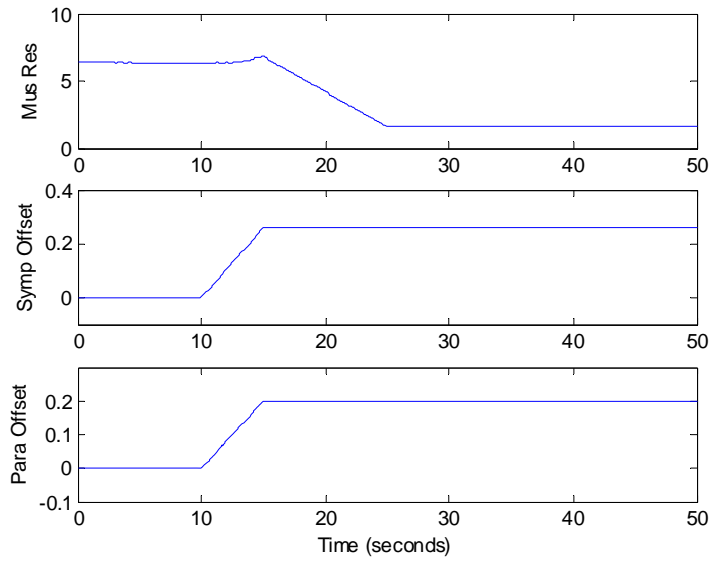
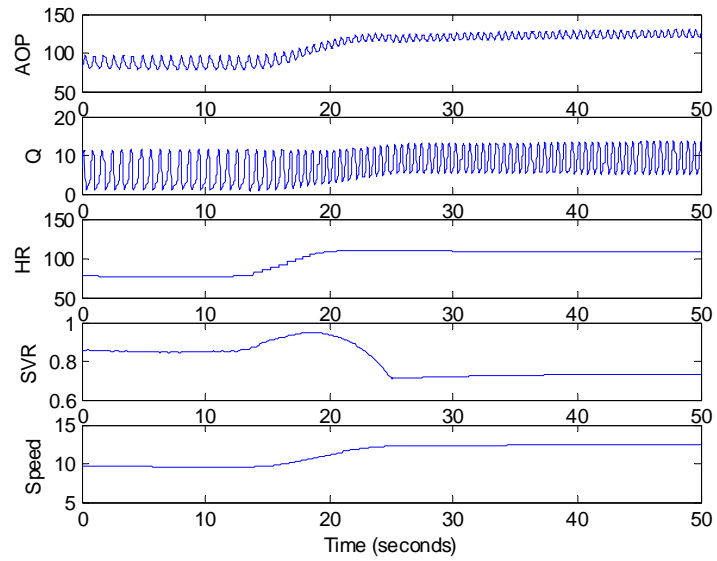


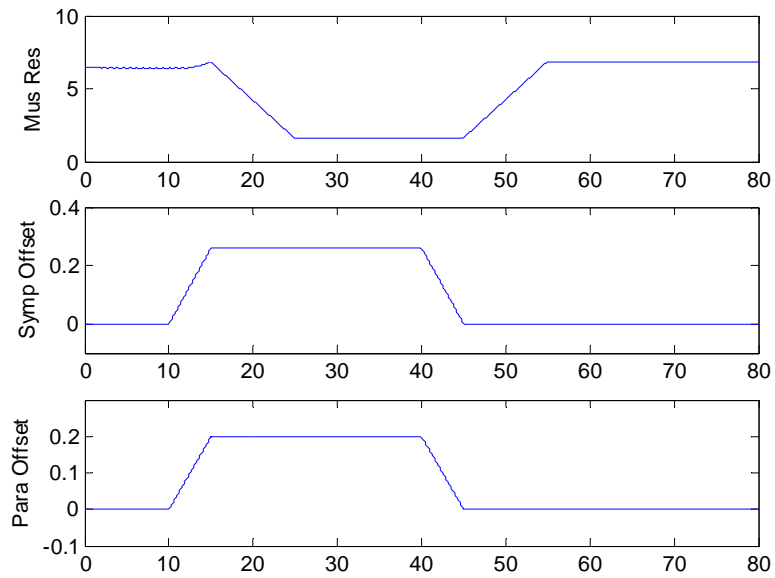
Figure 6.7. Block diagram for the controller based on the HR and SVR.



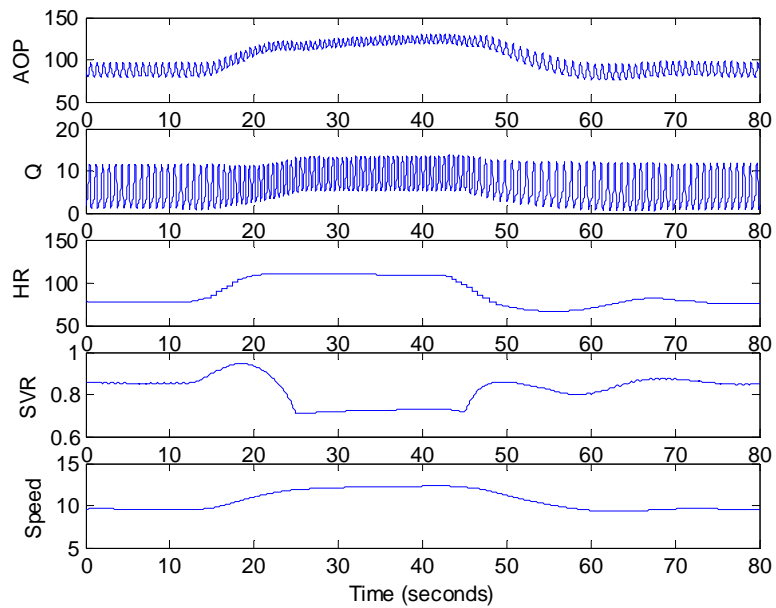
a. Forced changes to induce the exercise



b. Hemodynamic variables



c. Forced changes for rest-exercise-rest



d. Hemodynamic variables for rest-exercise-rest

Figure 6.8. Controller responses to exercise level 2.

At 15s, exercise starts. $K1=0.004$, $K2=0.004$, $LVP_r=50$ mmHg . AOP: aortic pressure in mmHg; Q: pump flow in L/min; HR: heart rate in bpm; SVR: systemic vascular resistance in mmHg/ml/s; Speed: pump speed in krpm. Operating point for exercise: $H = 98$ mmHg, $CO = 9.3$ L/min, Speed = 12.4 krpm.

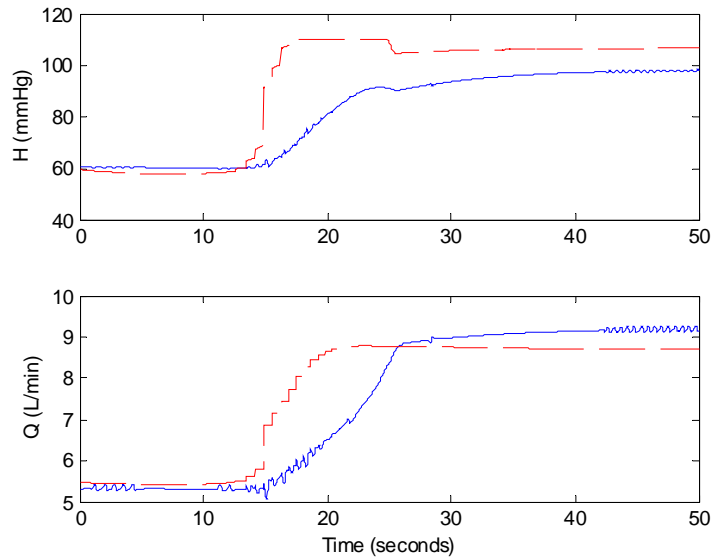


Figure 6.9. Control errors for H and Q from rest to exercise level 2.

Broken lines are estimated reference values and solid lines are actual values. $K1=0.004$, $K2=0.004$, $LVP_r=50$ mmHg . The portion from 17s to 25s for estimated reference H_0 is saturated.

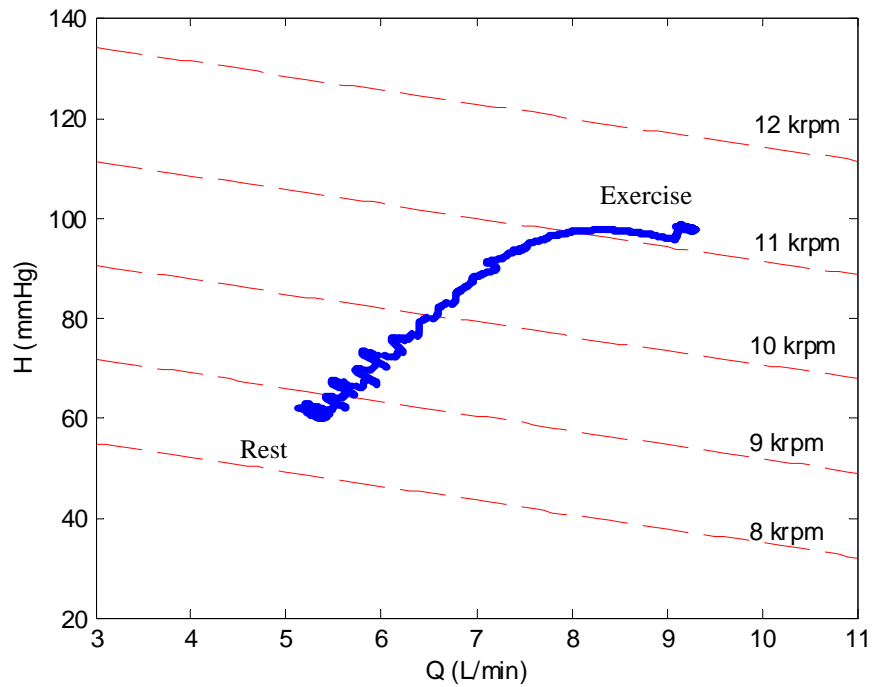


Figure 6.10. Operating point trajectory from rest to exercise

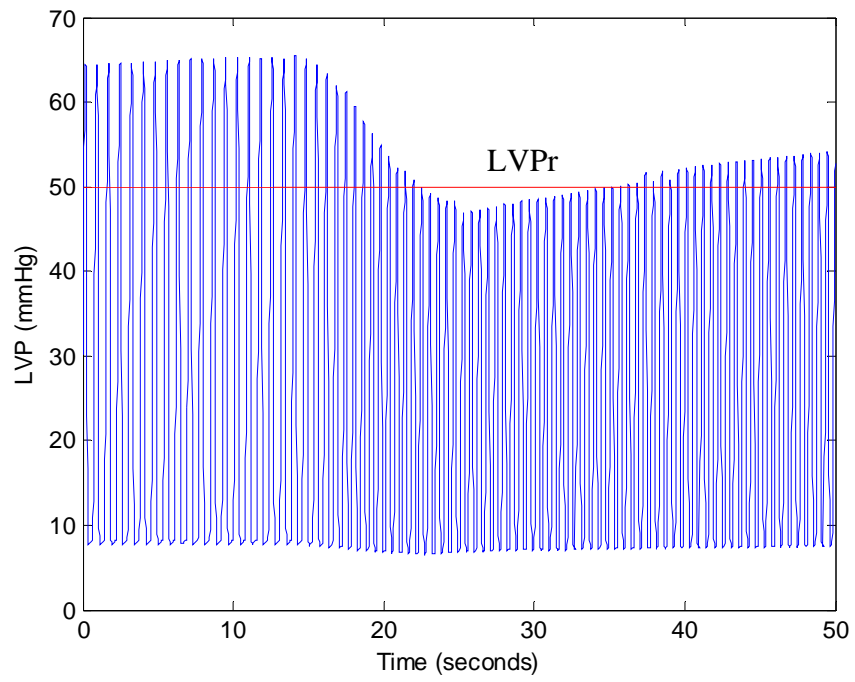


Figure 6.11. LVP and LVPr

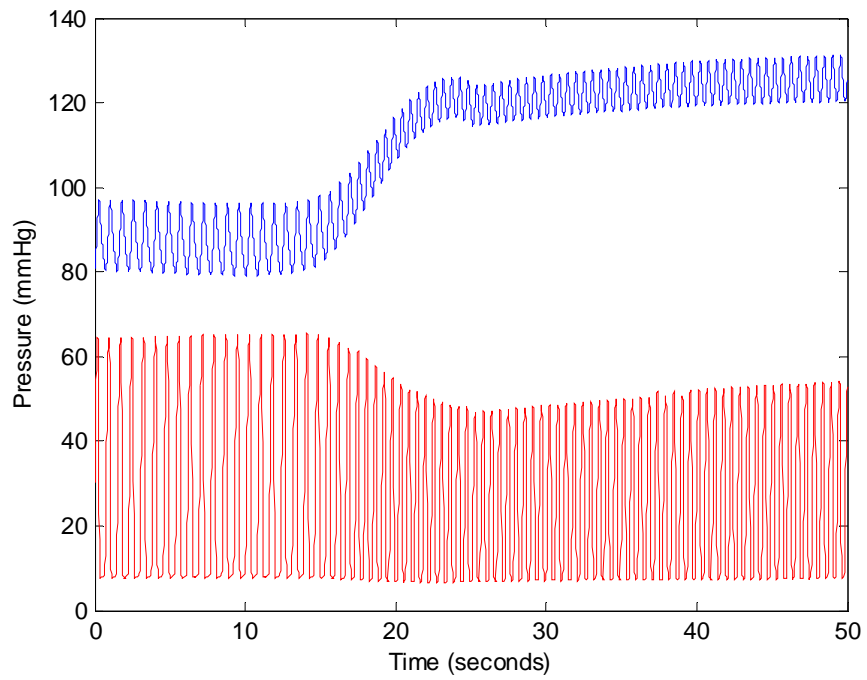


Figure 6.12. AOP and LVP

The simulation results are consistent with the analysis in Figure 6.3. From rest to exercise, (1) the blood pressure and cardiac output increased; (2) the operating point in the H-Q plane moved right upward; (3) the pump speed increased. It can be seen from the results that there are steady state errors between the estimated reference values and the real values. This is caused by the two not coincident prescribed references values: one for H and the other one for CO. As illustrated in Figure 6.13, for a certain physiological state (simplified by SVR), the two corresponding estimated operating points are different in the H-Q plane. The final actual operating point is located in between these two operating points. The steady errors are the difference between the actual H and Q and the estimated reference H_0 and Q_0 . This can be further clarified by Figure 6.14 and Figure 6.15. In these two cases, only one of the H and CO branches is applied in the closed loop control. For each of the two special cases, the steady error for the applied variable (H or CO) is 0, but for the other unapplied variable the steady error is the maximum.

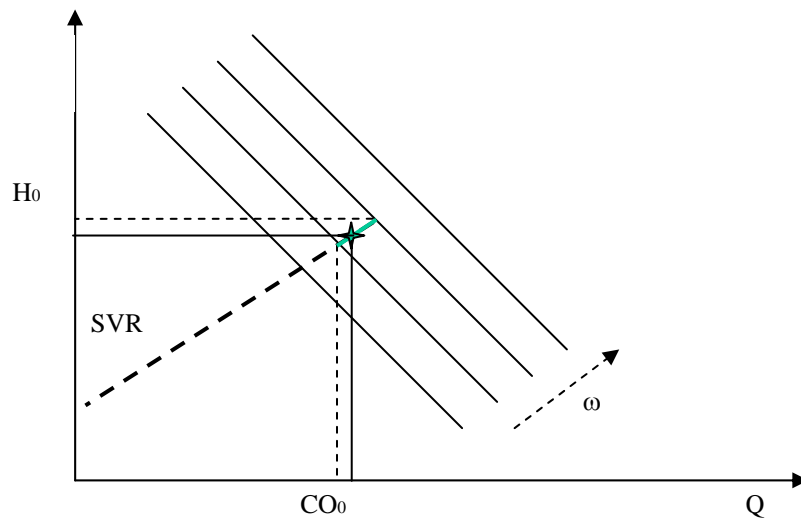
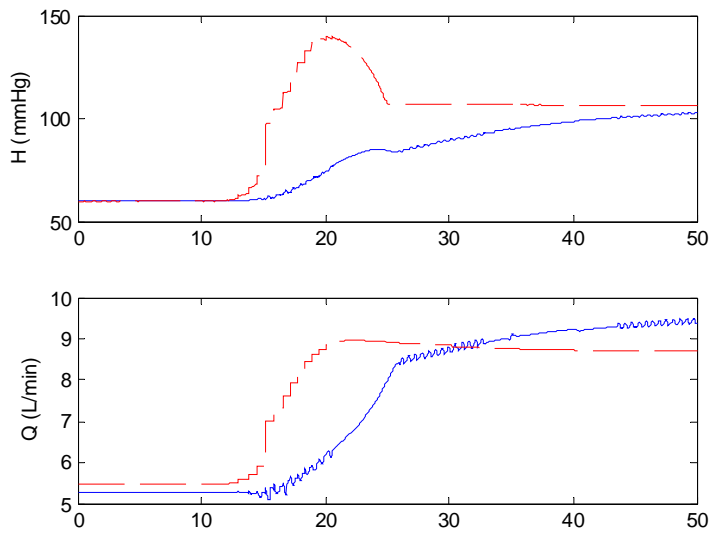
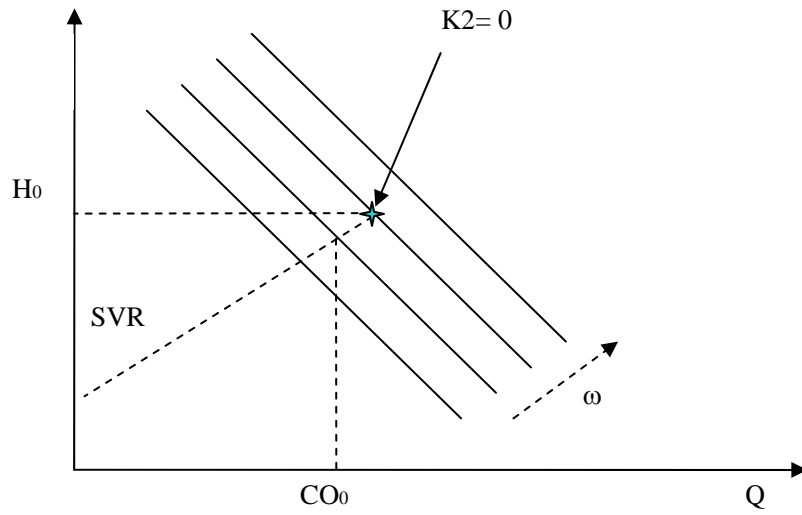


Figure 6.13. Illustration of the operating point and steady errors.

The star is the actual operating point. Solid lines are actual operating values. Broken lines are estimated reference values for H and CO branches in the control diagram.

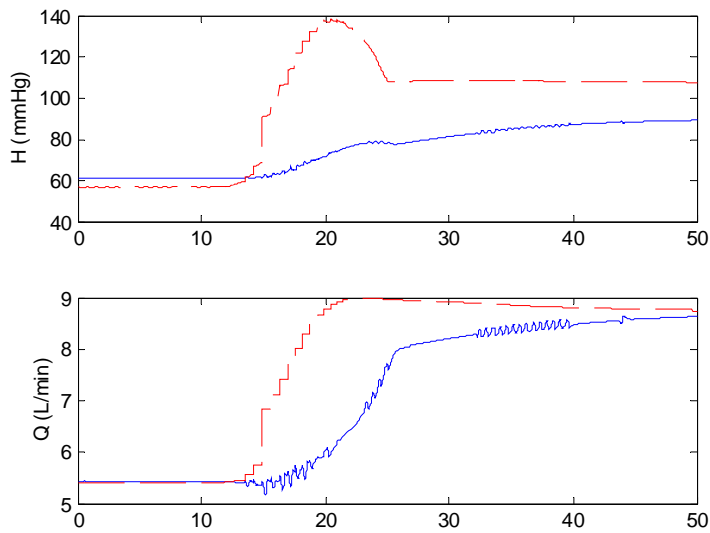


a. Errors for $K2 = 0$

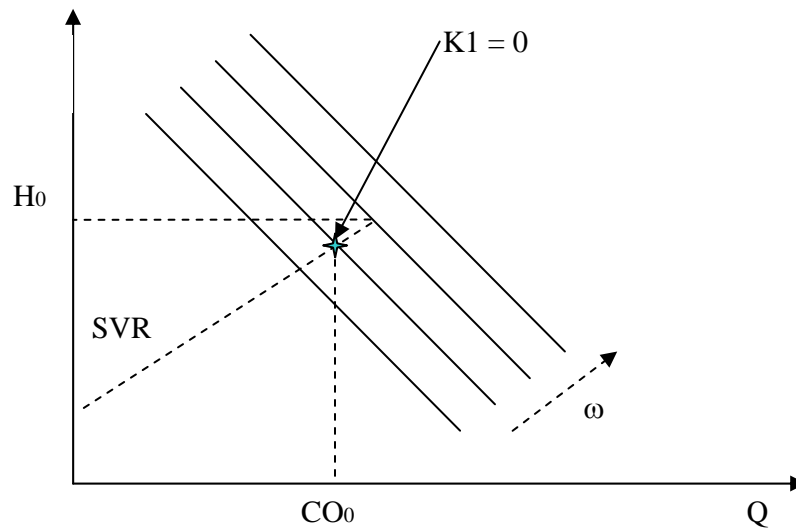


b. Operating point

Figure 6.14. $K2 = 0$ (only H branch is applied)



a. Errors for $K1 = 0$

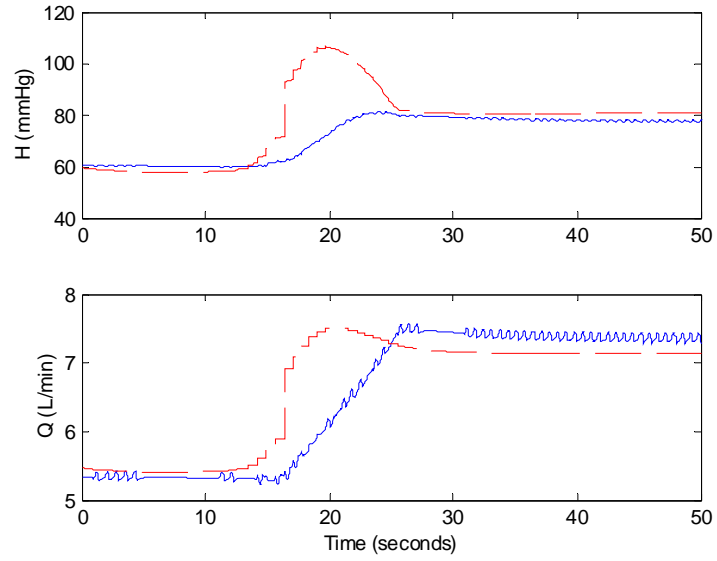


b. Operating point

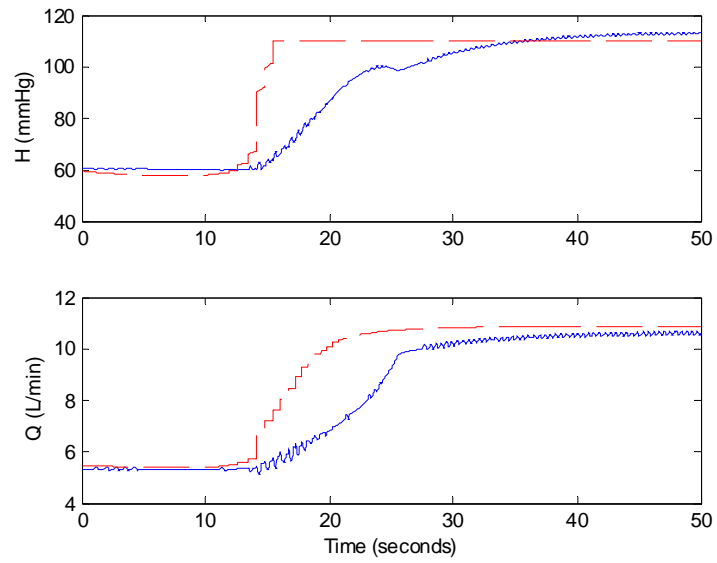
Figure 6.15. $K1 = 0$ (only CO branch is applied)

Also, the estimated operating points for H and CO branches may switch their relative positions. In Figure 6.16, for exercise level 1, the operating position relative to H_0 and CO_0 is similar to that of exercise level 2; for exercise level 3, H_0 and CO_0 switch their positions, as shown in Figure 6.17. Table 6.1 lists hemodynamic variables for multiple levels of exercise.

Figure 6.18 illustrates the results comparing to the experimental heart failure data in the literature [54].



a. Exercise level 1



b. Exercise level 3

Figure 6.16. Steady errors for exercise level 1 and level 3

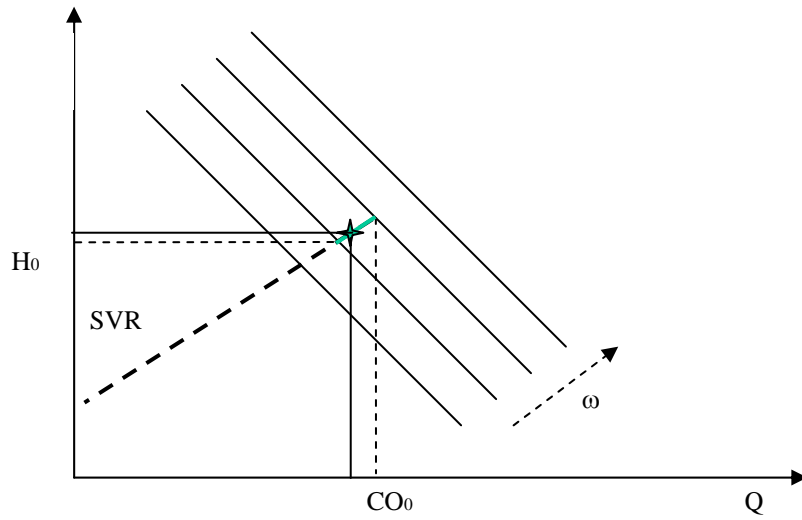


Figure 6.17. Operating point for exercise level 3

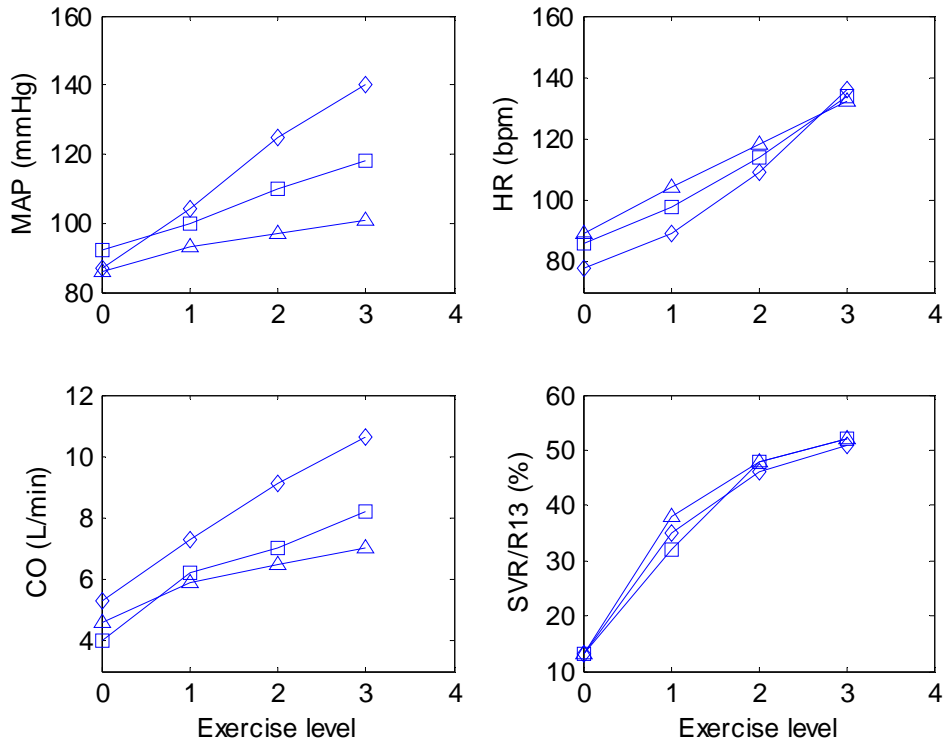


Figure 6.18. Multiple levels of exercise

Diamond: simulation with controller; square: experimental heart failure data from [54]; triangle: heart failure simulation without pump. SVR/R13: ratio of systemic resistance to active muscle resistance.

Table 6.1. Multiple levels of exercise

Exercise level	0	1	2	3
Simulation results (O1,O2)	Rest	(0.17,0.02) R13=2.1	(0.26, 0.2) R13=1.6	(0.31, 0.6) R13=1.4
Pump Speed (rpm)	9,567	11,000	12,347	13,267
MAP (mmHg)	87	104	125	140
HR (bpm)	78	89	109	136
CO (L/min)	5.3	7.3	9.1	10.6
SVR (mmHg/ml/s)	0.85	0.75	0.73	0.71

6.3 COMPARISON OF THE PROPOSED PUMP CONTROL WITH OTHER METHODS

It is desirable to compare the response to exercise of this control method to other methods. The methods considered here include the constant speed and constant pump head method, and the method of pump speed as a linear function of the heart rate. For comparison, the starting points are the same for all these methods, and different levels of exercise will be used to test the responses of these different methods.

6.3.1 Constant speed method

This method is actually used in real life. In the pump characteristic H-Q plane, the operating point will move along a certain pump speed curve. The response of this method to exercise level 2 is shown in Figure 6.19. The simulation results for different levels of exercise are listed in Table 6.2. The pump speed is chosen as the same as that of the controller based on HR and SVR at rest. It can be seen that the MAP and CO increase in spite of the lack of left ventricular contractility; these increases are results of other baroreflex controlled compensation such as increased HR and total blood volume.

Table 6.2. Simulation results for constant speed

Exercise level	0	1	2	3
Simulation results (O1,O2)	Rest	(0.17,0.02) R13=2.1	(0.26, 0.2) R13=1.6	(0.31, 0.6) R13=1.4
Pump Speed (rpm)	9567	9567	9567	9567
MAP (mmHg)	87	92	97	100
HR (bpm)	78	99	119	147
CO (L/min)	5.3	6.1	6.3	7.1
SVR (mmHg/ml/s)	0.85	0.80	0.76	0.73

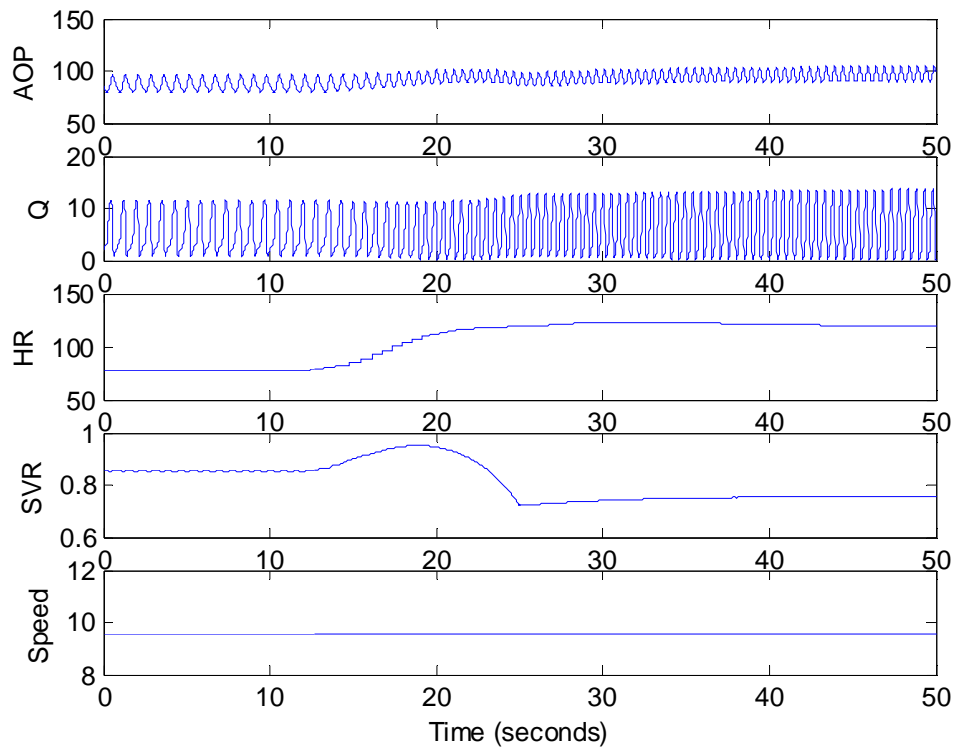


Figure 6.19. Constant speed method response to exercise level 2. At 15s, exercise starts.

6.3.2 Constant pressure head method

By keeping the pump head constant, this method can incorporate the change in SVR automatically [31]. The operating will move to the right horizontally in the pump H-Q plane. In the simulation, only the H branch is used and $K1 = 0.008$. The response of this method to exercise level 2 is shown in Figure 6.20. The simulation results of different levels of exercise are listed in Table 6.3. The pump pressure head is chosen to match the head at rest for the controller based on HR and SVR ($H_0 = 60$ mmHg). The simulation results show that there are some increases in MAP and CO.

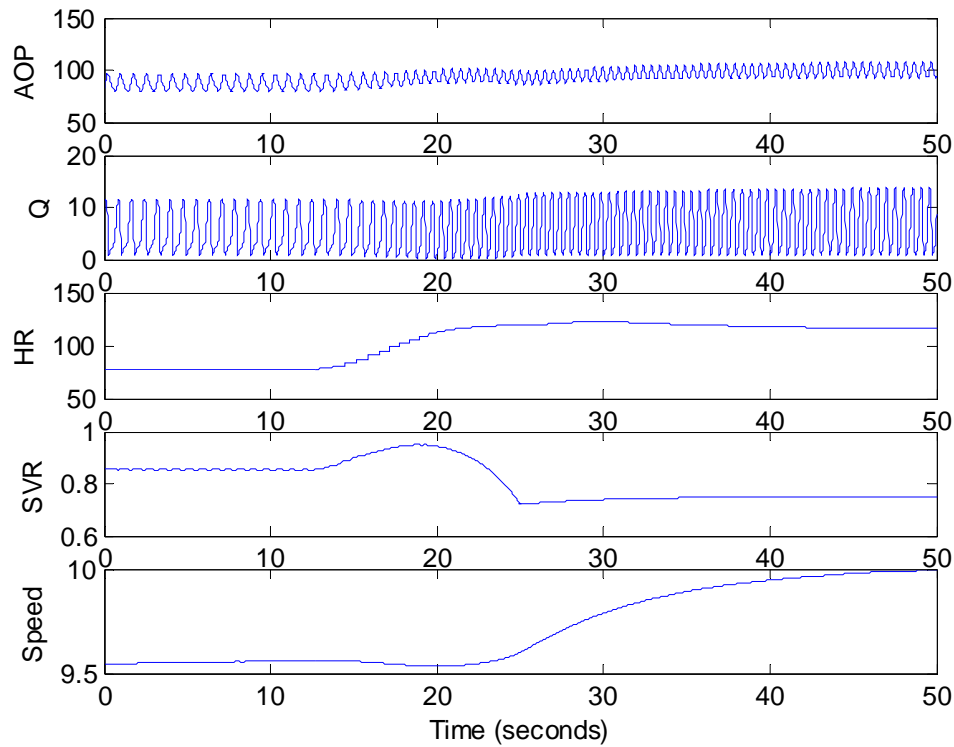


Figure 6.20. Constant pump head method response to exercise level 2. At 15s, exercise starts.

Table 6.3. Simulation results for constant pump head

Exercise level	0	1	2	3
Simulation results (O1,O2)	Rest	(0.17,0.02) R13=2.1	(0.26, 0.2) R13=1.6	(0.31, 0.6) R13=1.4

Table 6.3. Simulation results for constant pump speed (continued)

Pump Speed (rpm)	9567	9812	9995	10164
MAP (mmHg)	87	94	100	105
HR (bpm)	78	96	116	142
CO (L/min)	5.3	6.2	6.9	7.8
SVR (mmHg/ml/s)	0.85	0.79	0.75	0.72

6.3.3 Pump speed as a linear function of heart rate

A control method is reported in [42] using heart rate as the control input. In the animal experiment, the controller adjusted the pump speed in response to increasing or decreasing heart rate in a linear relationship. To examine the performance of this control method, in the simulation,

$$\omega = \omega_0 + k * (HR - HR_0) \quad (6.12)$$

where ω_0 , k , HR_0 are constants. The values of them are chosen to match the cases for rest and exercise level 3. $\omega_0 = 9568$ rpm, $k = 63$ rpm/bpm, $HR_0 = 78$ bpm. The response of this method to exercise level 2 is shown in Figure 6.21. The simulation results of different levels of exercise are listed in Table 6.4.

Table 6.4. Simulation results for heart rate related pump speed method

Exercise level	0	1	2	3
Simulation results (O1,O2)	Rest	(0.17,0.02) R13=2.1	(0.26, 0.2) R13=1.6	(0.31, 0.6) R13=1.4
Pump Speed (rpm)	9542	10439	11590	13243
MAP (mmHg)	87	99	115	140
HR (bpm)	78	92	110	136
CO (L/min)	5.3	6.7	8.4	10.4
SVR (mmHg/ml/s)	0.85	0.77	0.73	0.71

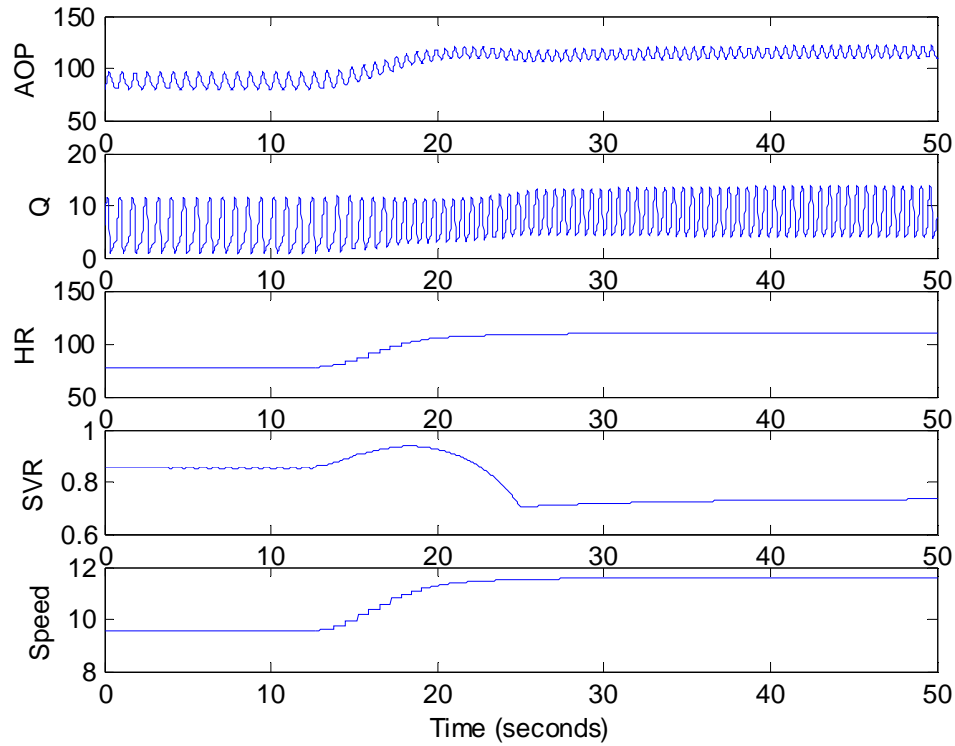


Figure 6.21. Heart rate related pump speed method response to exercise level 2.

Figure 6.22 compares the responses of the different methods to the same set of exercise simulations (the simulation results in Table 6.2 through 6.4). The experimental heart failure exercise data from [54] is also plotted for comparison (Table 4.8). Interestingly, the increase in pump flow for the constant speed method in the simulation is consistent with the animal experiment results in [76]. It can be seen that the pump speed, blood pressure and pump flow generated by the proposed controller is higher than that of the constant speed, constant pump head methods and the heart rate related pump speed method. Therefore the proposed control method can provide better support for the exercise. There is no suction for all the simulations.

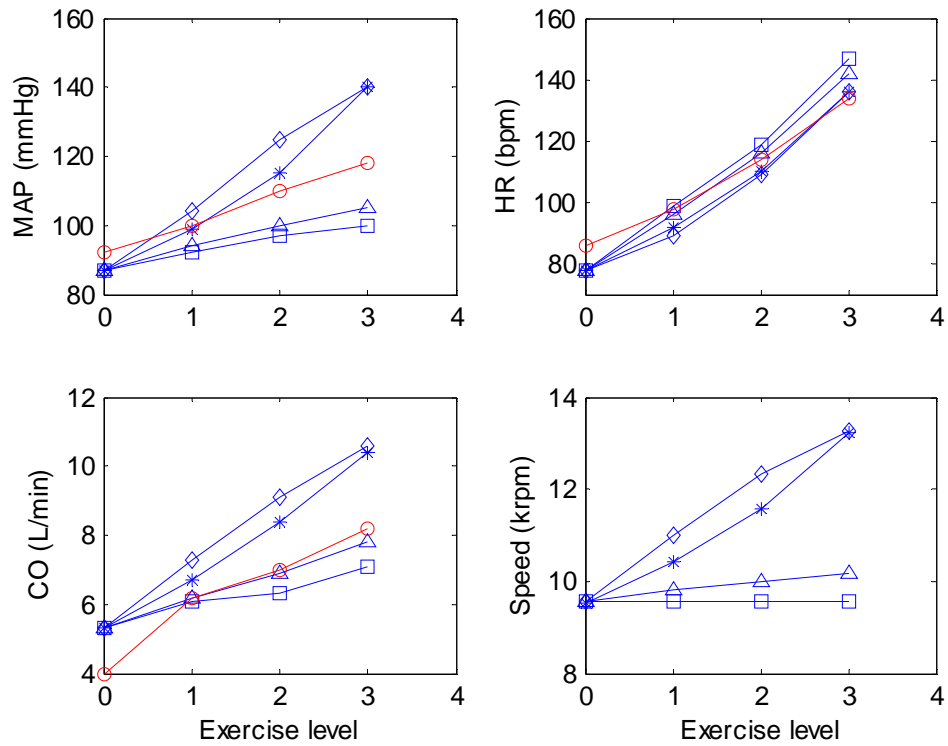


Figure 6.22. Response to the exercise for different control methods

Diamond: control based on HR and SVR; Triangle: constant pump head; Square: constant pump speed; Star: pump speed as a linear function of heart rate; Circle: experimental heart failure data ([54] without pump).

6.4 PERFORMANCES OF THE PROPOSED CONTROLLER

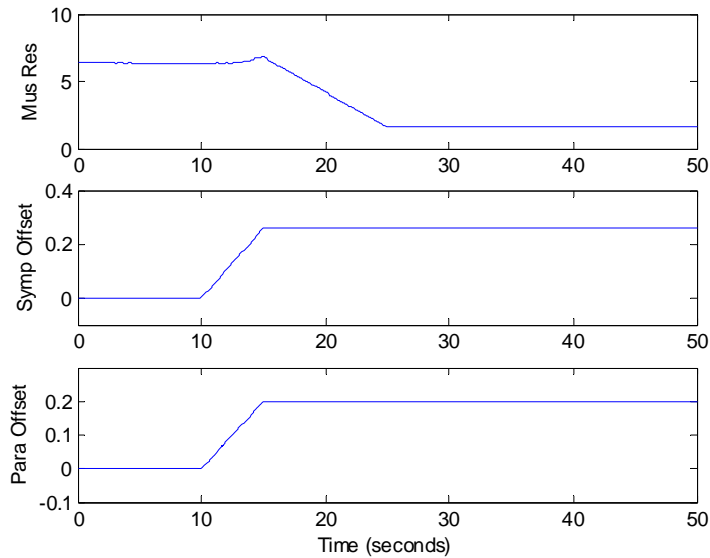
The factors that may affect the performance of the controller include the following:

- K1 and K2
- LVPr
- SVr
- Noise

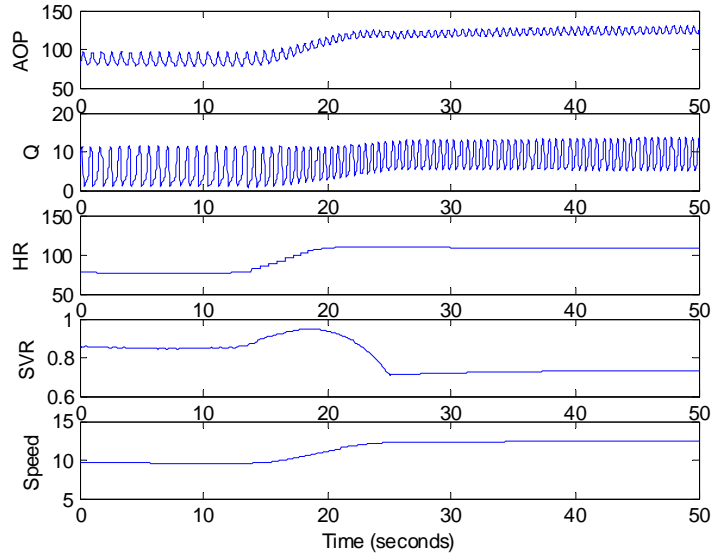
These factors will be examined one by one in this section.

The simulation for a certain exercise level will be used to test the controller. Figure 6.23 shows the simulation from rest to exercise level 2 without noise at $K1 = 0.004$, $K2 = 0.004$,

LVPr = 50 mmHg. Operating point: $H = 98\text{mmHg}$, $CO = 9.3\text{ L/min}$, Speed = 12.4 krpm. Steady
 Errors: $H - H_0 = 98 - 106 = -8\text{mmHg}$, $CO - CO_0 = 9.3 - 8.7 = 0.6\text{L/min}$ (see Figure 6.9).



a. Forced changes to simulate exercise.



b. $K_1=0.004$, $K_2=0.004$, LVPr=50 mmHg.

Noise free (rest to exercise 2 at 15s)

Figure 6.23. Simulation from rest to exercise

6.4.1 K1 and K2

These two gains will determine the responsiveness of the controller and the actual operating point relative to the estimated positions for H and CO branches. Figure 6.24 and Figure 6.25 show the responsiveness of the controller with gains proportionally increased or decreased. The steady operating points are the same for both cases, but the transitions from rest to exercise are different due to different gain values.

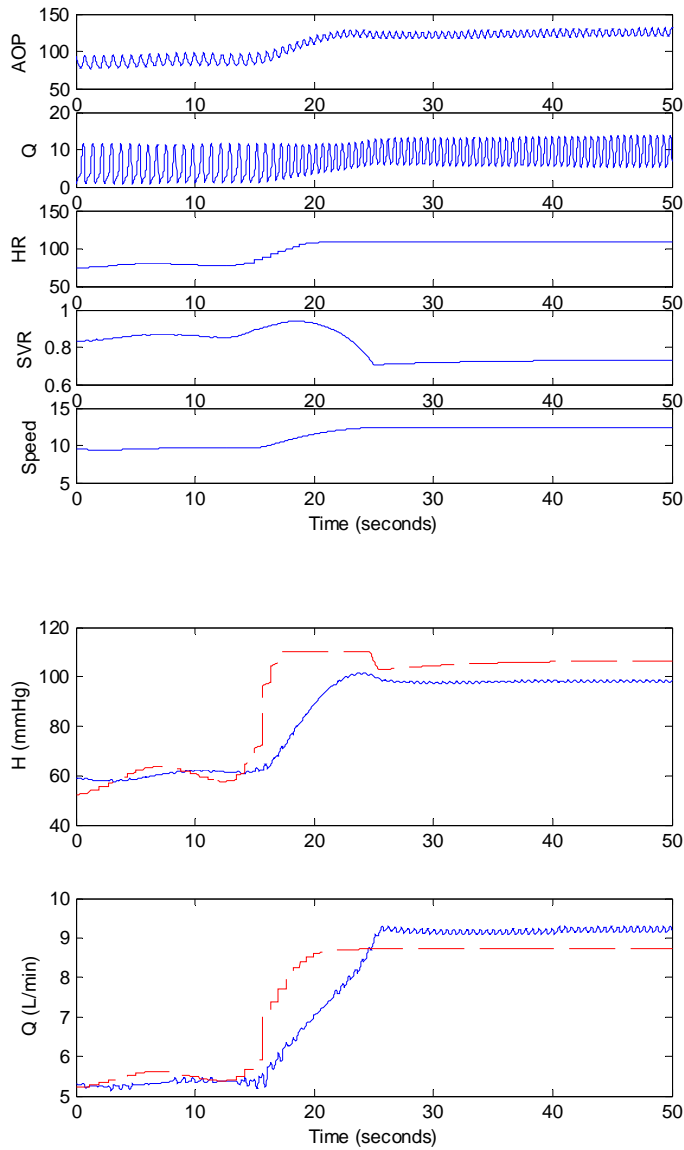


Figure 6.24. $K1=0.007$, $K2=0.007$, $LVP_r=50$ mmHg

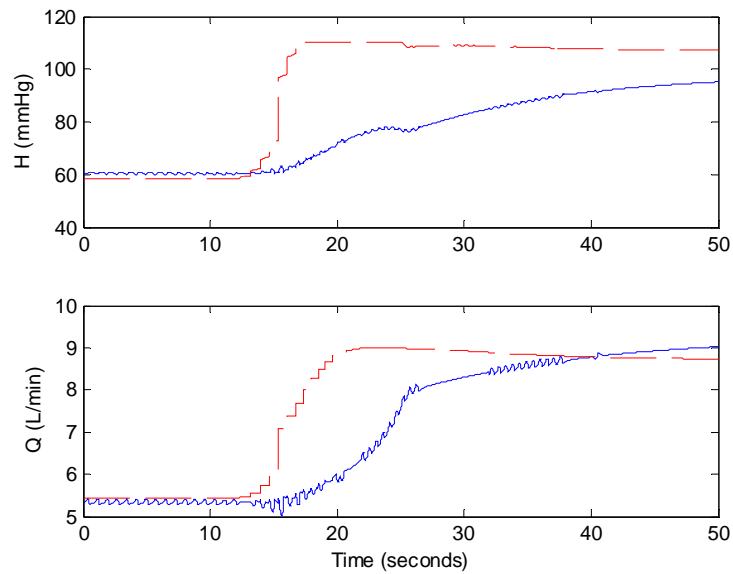
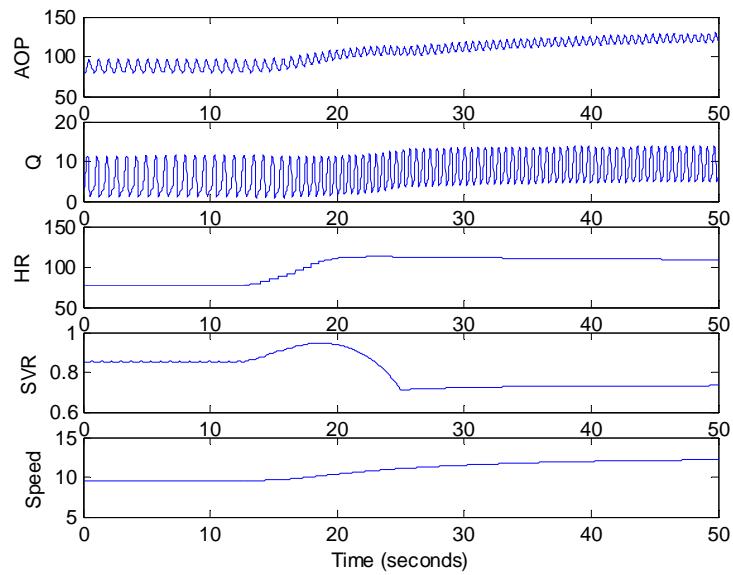


Figure 6.25. $K_1=0.002$, $K_2=0.002$, $LVP_r=50$ mmHg

The relative ratio of K_1 to K_2 will determine the position of the actual operating point in the H-Q plane. In Figure 6.26, the actual operating point is close to the operating point determined by the estimated reference value CO_0 if K_1 is smaller and K_2 is larger. Similarly, in

Figure 6.27, the actual operating point is close to the operating point determined by the estimated reference value H_0 if K_1 is larger and K_2 is smaller.

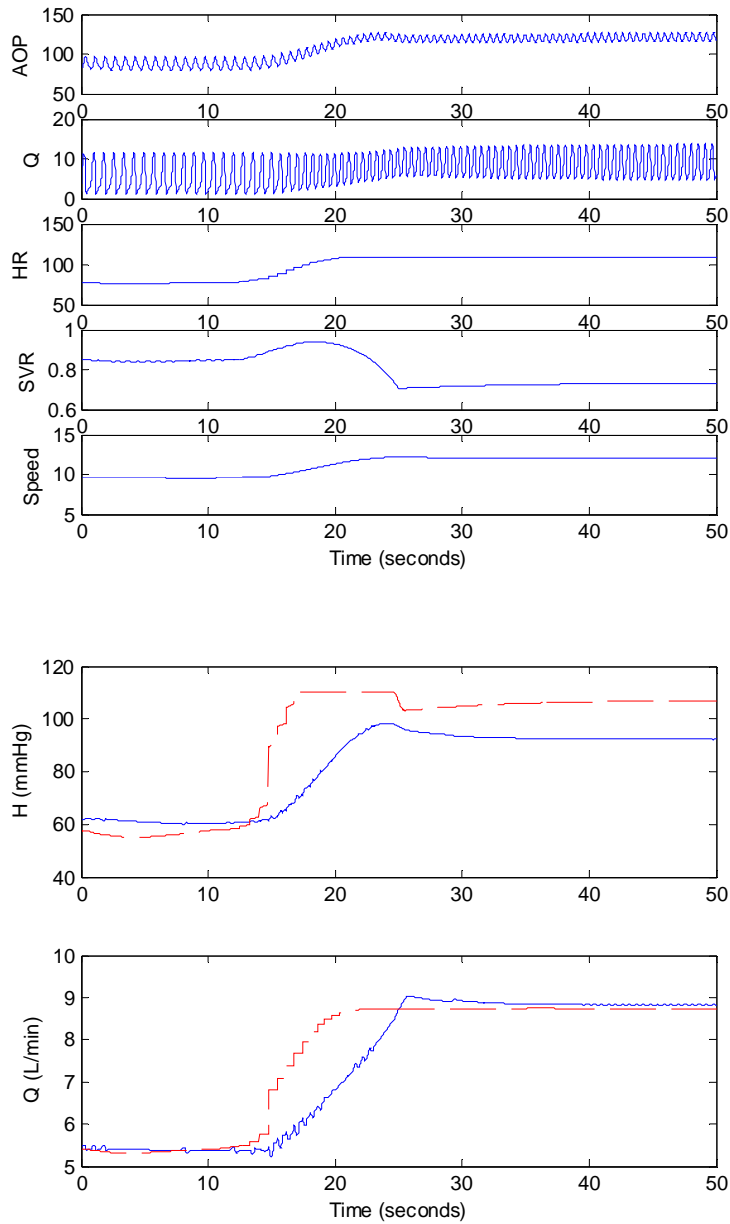


Figure 6.26. $K_1 < 0.004$, $K_2 > 0.004$, noise free (rest to exercise 2)

$K_1 = 0.001$, $K_2 = 0.01$, $LVPr = 50$ mmHg,

Operating point: $H = 92$ mmHg, $CO = 8.8$ L/min, Speed = 12.0 krpm.

The CO branch dominates.

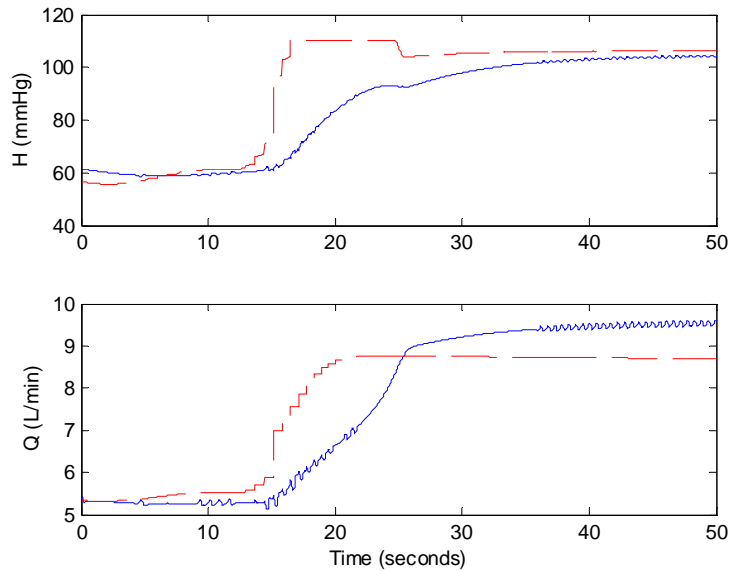
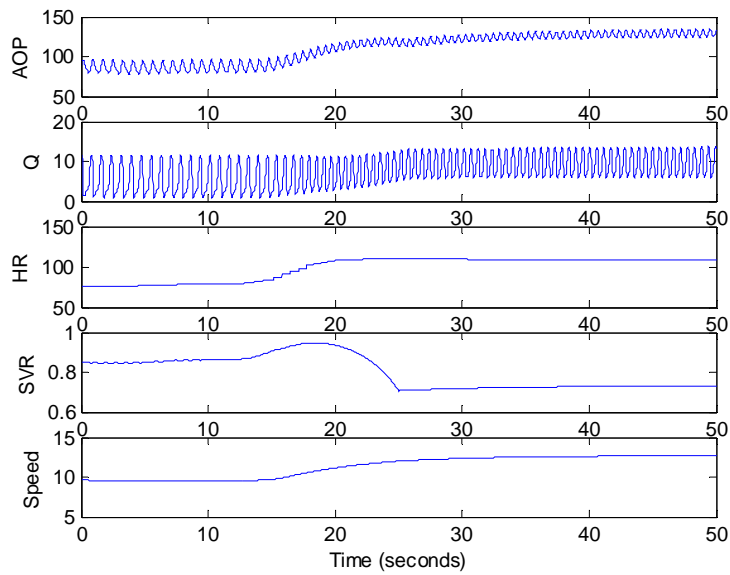


Figure 6.27. $K1 > 0.004$, $K2 < 0.004$. noise free (rest to exercise 2)

$K1 = 0.008$, $K2 = 0.001$, $LVPr = 50$ mmHg,

Operating point: $H = 104$ mmHg, $CO = 9.4$ L/min, Speed = 12.7 krpm

The H branch dominates.

Tables 6.5, 6.6 list the steady state simulation results for different pairs of proportional $K1$ and $K2$. CO means the total flow in the tables (the aortic valve is closed). Figure 6.28

summarizes these simulation results. It can be concluded that keeping the relative ratio the same, the values for K1 and K2 affect the transient response from rest to exercise but not the steady states. The relative ratio of K1 to K2 will affect the actual operating point relative to the estimated operating points corresponding to H_0 and CO_0 .

Table 6.5. Simulation results with $K1=0.005$, $K2=0.005$

Exercise level	0	1	2	3
Simulation results (O1,O2)	Rest	(0.17,0.02) R13=2.1	(0.26, 0.2) R13=1.6	(0.31, 0.6) R13=1.4
Pump Speed (rpm)	9566	10,996	12,354	13,280
MAP (mmHg)	87	104	125	140
HR (bpm)	77	89	109	136
CO (L/min)	5.2	7.5	9.1	10.5
SVR (mmHg/ml/s)	0.85	0.75	0.73	0.71

O1, O2 are offsets in outbound nervous signals in spikes/s

R13: active muscle resistance

$LVP_r=50$ mmHg

Table 6.6. Simulation results with $K1=0.003$, $K2=0.003$

Exercise level	0	1	2	3
Simulation results (O1,O2)	Rest	(0.17,0.02) R13=2.1	(0.26, 0.2) R13=1.6	(0.31, 0.6) R13=1.4
Pump Speed (rpm)	9569	11,009	12,317	13,216
MAP (mmHg)	87	104	125	139
HR (bpm)	77	89	109	136
CO (L/min)	5.3	7.3	9.3	10.7
SVR (mmHg/ml/s)	0.85	0.75	0.73	0.71

$LVP_r=50$ mmHg

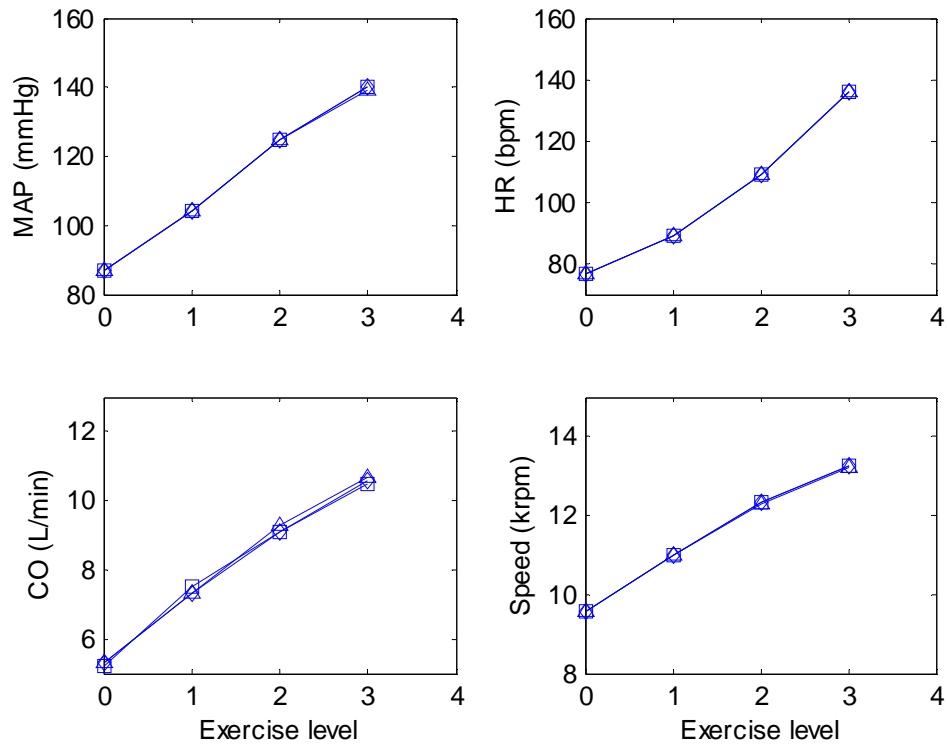
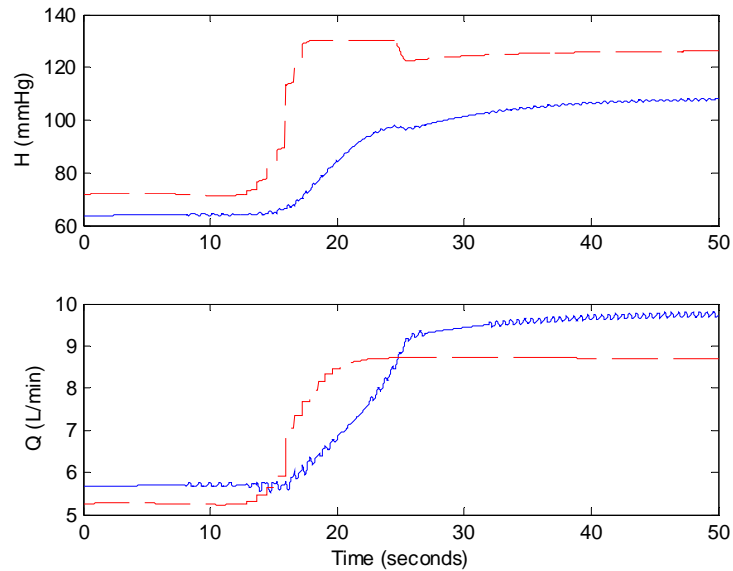
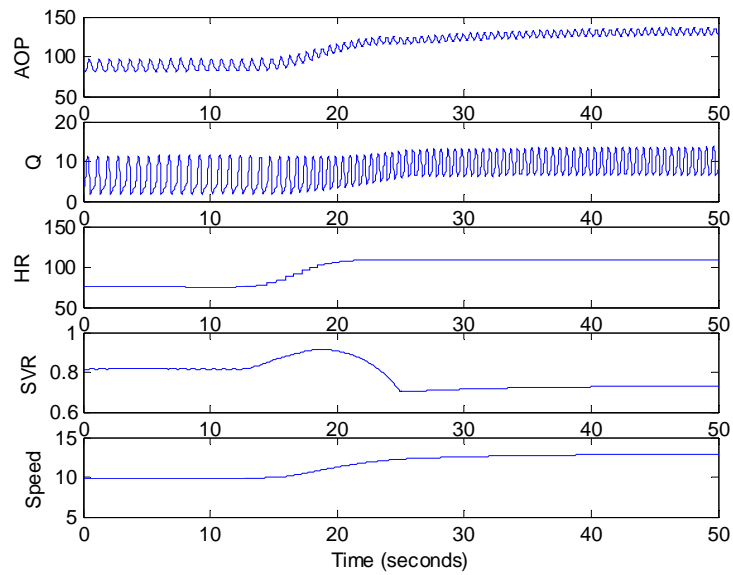


Figure 6.28. Simulation results with different K1 and K2.

Diamond: K1=0.005, K2=0.005; Square: K1=0.004, K2=0.004; Triangle: K1=0.003, K2=0.003.

6.4.2 LVPr

This preset parameter affects the estimated reference value H_0 . Specifically, the smaller LVPr implies larger H_0 according to (6.6). In this way it will have effect on the estimated operating point for H branch and consequently the actual operating point. Figure 6.29 gives an example of a smaller LVPr with the other parameters kept the same. $K1 = 0.004$, $K2 = 0.004$, $LVPr = 30$ mmHg. The smaller LVPr increases the difference between the estimated operating points for H branch and for CO branch. The resulting steady errors for both the H branch and CO branch are increased.



Operating point: $H = 108\text{mmHg}$, $CO = 9.7\text{ L/min}$, $\text{Speed} = 12.9\text{ krpm}$
 Steady Errors: $H-H_0=108-126=-18\text{mmHg}$, $CO-CO_0=9.7-8.7=1.0\text{L/min}$

Figure 6.29. $LVP_r < 50\text{ mmHg}$

Tables 6.7 and 6.8 list the simulation results for the controller responses to multiple levels of exercise with different values of LVP_r . Figure 6.30 summarizes these results. It can be seen

that there are some increases in blood pressure and pump flow with the decrease in *LVP_r* but the changes are not significant.

Table 6.7. Simulation results with *LVP_r* = 40 mmHg

Exercise level	0	1	2	3
Simulation results (O1,O2)	Rest	(0.17,0.02) R13=2.1	(0.26, 0.2) R13=1.6	(0.31, 0.6) R13=1.4
Pump Speed (rpm)	9,723	11,228	12,613	13,517
MAP (mmHg)	87	107	129	144
HR (bpm)	76	89	109	136
CO (L/min)	5.5	7.6	9.6	11.0
SVR (mmHg/ml/s)	0.83	0.75	0.73	0.71

Table 6.8. Simulation results with *LVP_r* = 30 mmHg

Exercise level	0	1	2	3
Simulation results (O1,O2)	Rest	(0.17,0.02) R13=2.1	(0.26, 0.2) R13=1.6	(0.31, 0.6) R13=1.4
Pump Speed (rpm)	9,874	11,467	12,865	13,763
MAP (mmHg)	88	110	132	147
HR (bpm)	75	88	109	136
CO (L/min)	5.8	8.0	9.7	11.1
SVR (mmHg/ml/s)	0.81	0.75	0.73	0.71

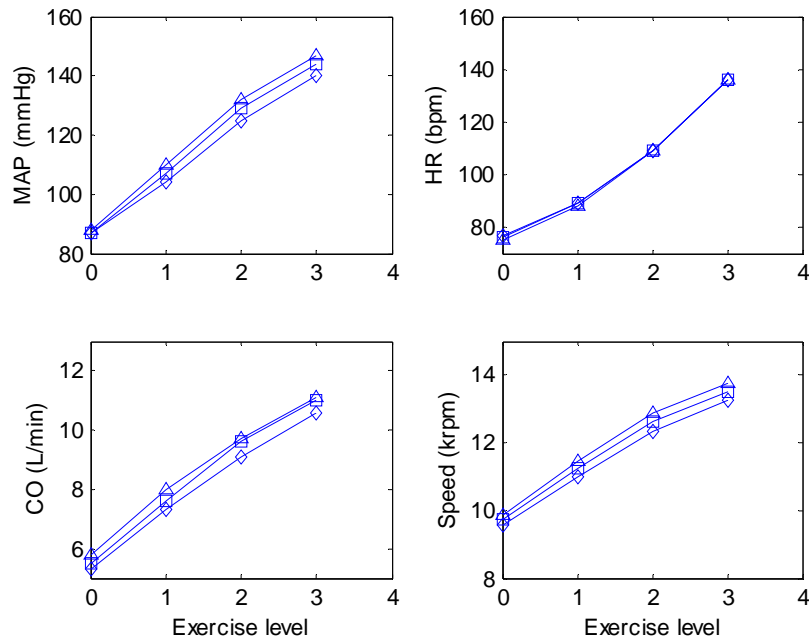


Figure 6.30. Simulation results with different LVP_r . $K1=0.004$, $K2=0.004$.

Diamond: $LVP_r = 50\text{mmHg}$; Square: $LVP_r = 40\text{mmHg}$; Triangle: $LVP_r = 30\text{mmHg}$.

6.4.3 SV_r

The value of SV_r has effect on both the H and CO branches according to (6.4), (6.5), and (6.6). A smaller SV_r will result in less estimated reference H_0 and CO_0 . Figure 6.31 gives an example for a smaller SV_r with the other parameters kept the same. In this simulation, $K1 = 0.004$, $K2 = 0.004$, $LVP_r = 50 \text{ mmHg}$,

$$SV_r = \begin{cases} 65\text{ml} & HR \leq 85\text{bpm} \\ 75\text{ml} & HR > 85\text{bpm} \end{cases} \quad (6.13)$$

Table 6.9 lists the simulation results. The resultant operating speed is lower but the steady errors do not changed greatly. Similarly, for larger SV_r ,

$$SV_r = \begin{cases} 75\text{ml} & HR \leq 85\text{bpm} \\ 85\text{ml} & HR > 85\text{bpm} \end{cases} \quad (6.14)$$

the resultant operating speed is higher. The simulation results are listed in Table 6.10. Figure 6.32 summarizes the simulation results with different SV_r values.

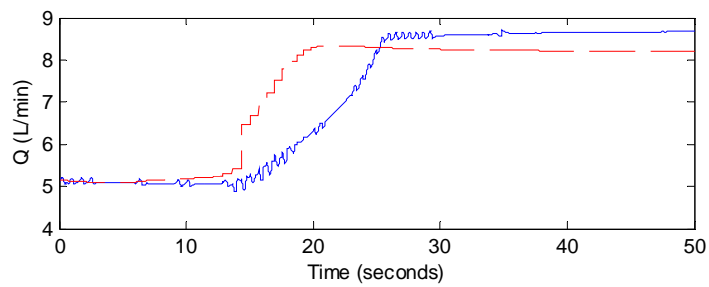
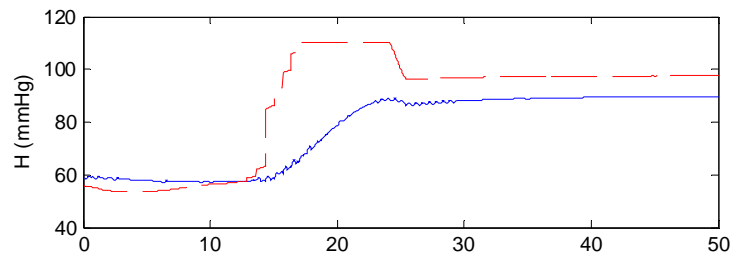
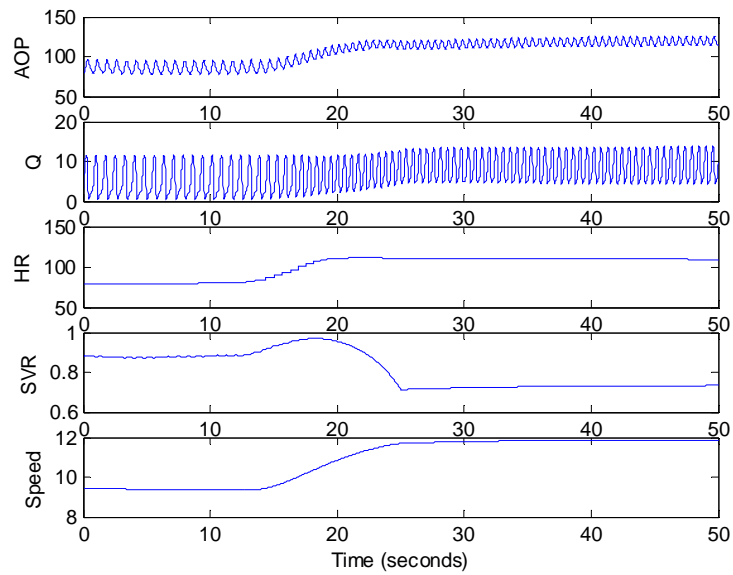


Figure 6.31. Smaller SVr.

Operating point: $H = 90\text{mmHg}$, $CO = 8.7\text{ L/min}$, $\text{Speed} = 11.9\text{ krpm}$

Steady Errors: $H - H_0 = 90 - 97 = -7\text{mmHg}$, $CO - CO_0 = 8.7 - 8.2 = 0.5\text{L/min}$

Table 6.9. Simulation results with smaller SVr

Exercise level	0	1	2	3
Simulation results (O1,O2)	Rest	(0.17,0.02) R13=2.1	(0.26, 0.2) R13=1.6	(0.31, 0.6) R13=1.4
Pump Speed (rpm)	9,348	10,648	11,864	12,981
MAP (mmHg)	86	101	119	136
HR (bpm)	80	91	109	136
CO (L/min)	5.2	7.1	8.7	10.4
SVR (mmHg/ml/s)	0.88	0.76	0.73	0.71

Table 6.10. Simulation results with larger SVr

Exercise level	0	1	2	3
Simulation results (O1,O2)	Rest	(0.17,0.02) R13=2.1	(0.26, 0.2) R13=1.6	(0.31, 0.6) R13=1.4
Pump Speed (rpm)	9,775	11,356	12,688	13,549
MAP (mmHg)	88	108	129	143
HR (bpm)	76	88	109	136
CO (L/min)	5.5	7.8	9.5	10.8
SVR (mmHg/ml/s)	0.83	0.75	0.73	0.71

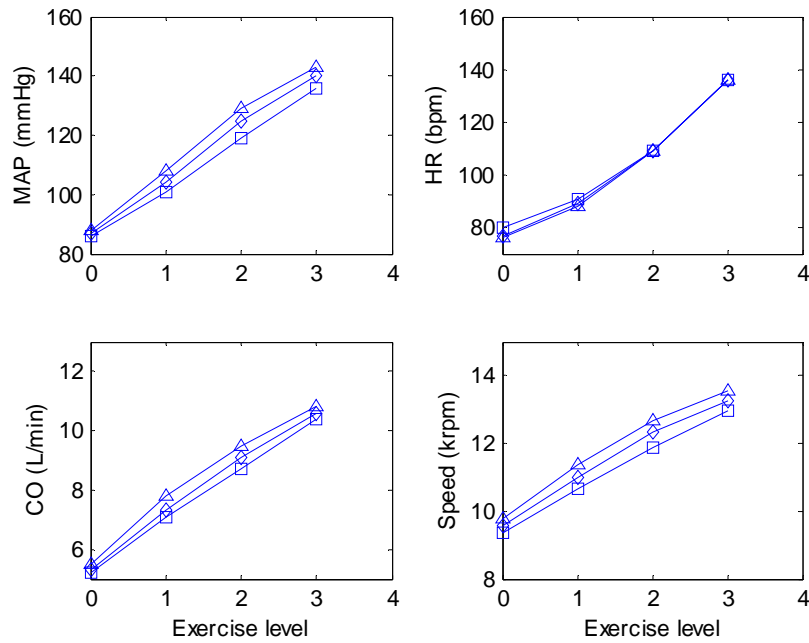


Figure 6.32. Simulation results with different SVr.

$$\text{Diamond: } SV_r = \begin{cases} 70ml & HR \leq 85bpm \\ 80ml & HR > 85bpm \end{cases}; \text{ Square: } SV_r = \begin{cases} 65ml & HR \leq 85bpm \\ 75ml & HR > 85bpm \end{cases};$$

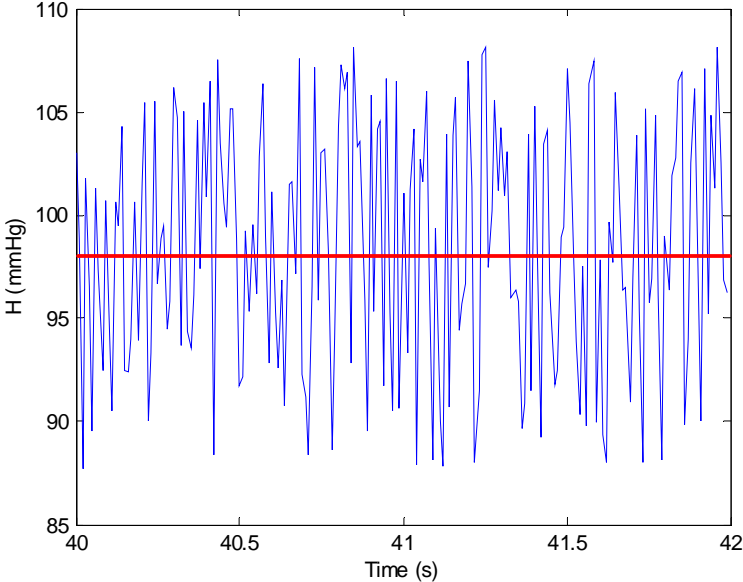
$$\text{Triangle: } SV_r = \begin{cases} 75ml & HR \leq 85bpm \\ 85ml & HR > 85bpm \end{cases}$$

6.4.4 Noise

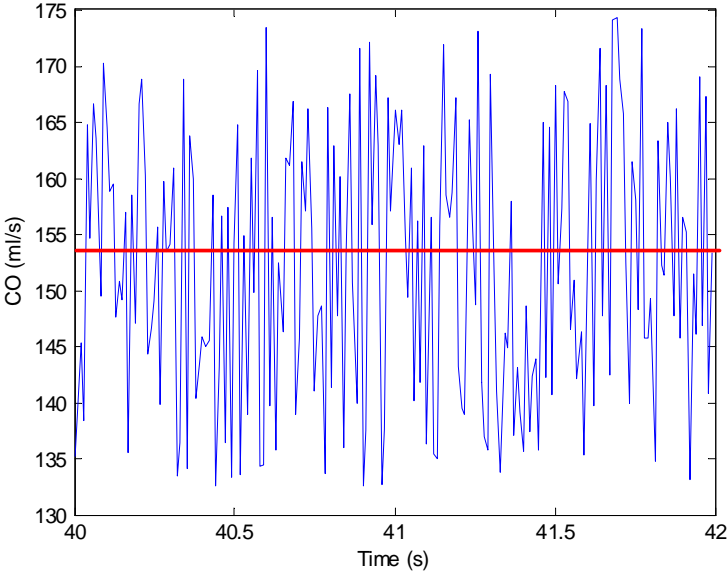
For the application of the controllers, the measurement noise or uncertainty will present in the inputs of the controllers. Therefore it is necessary to test the robustness to the noise added to the controller inputs. Since the features of the hemodynamic variables measurement noise are not clear, two types of noises are simulated in this subsection: the uniformly distributed noise and the normally distributed noise. The noises are added to the HR, SVR, H, and CO in the diagram of Figure 6.7.

1) Uniformly distributed noise

The noise feature is shown in Figure 6.33 and the responses of the controller to different levels and combinations of noise are shown in Figure 6.34 through 6.39.

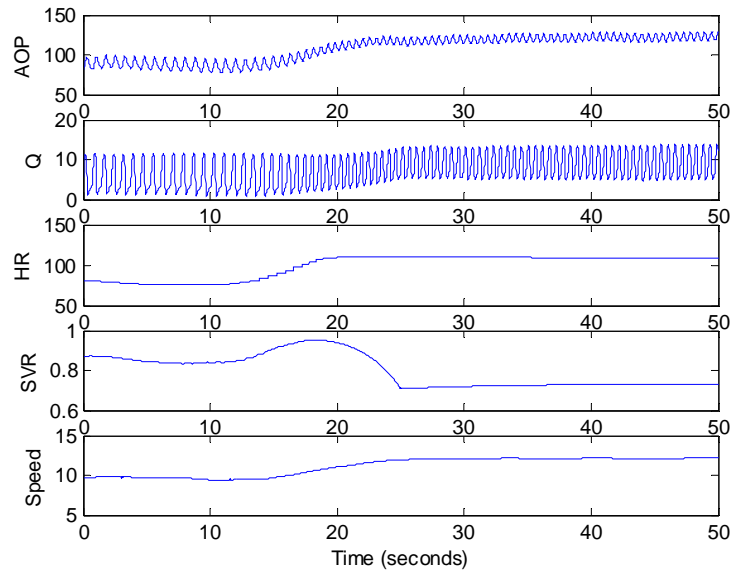


a. Measured H: 98 mmHg; Noise: [-10, 10] mmHg uniformly distributed

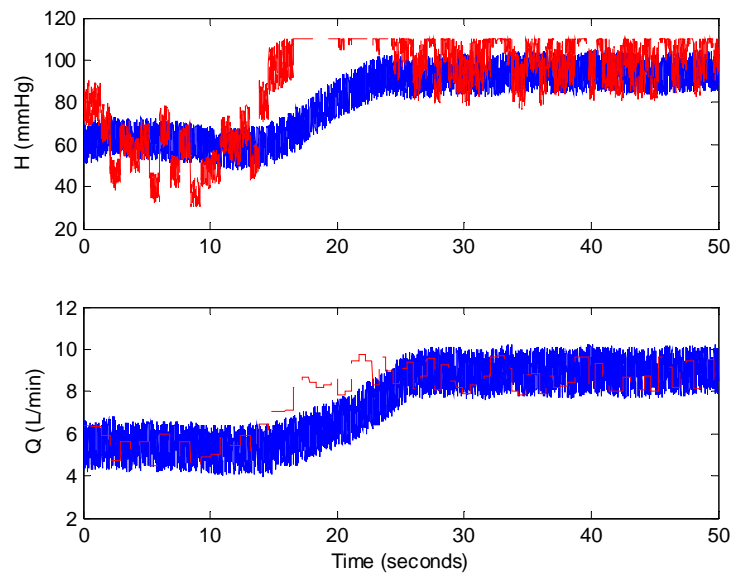


b. Measured CO: 154 ml/s; Noise: [-20, 20] ml/s uniformly distributed

Figure 6.33. Noise features



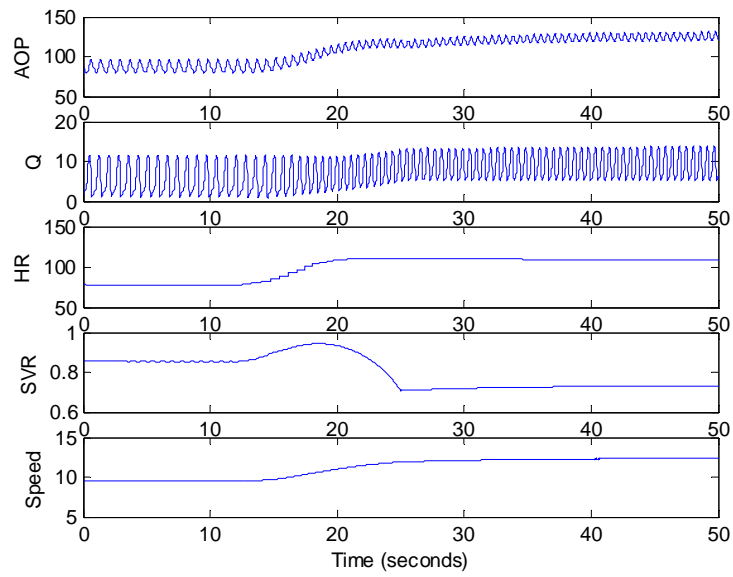
a. Response of the controller to exercise



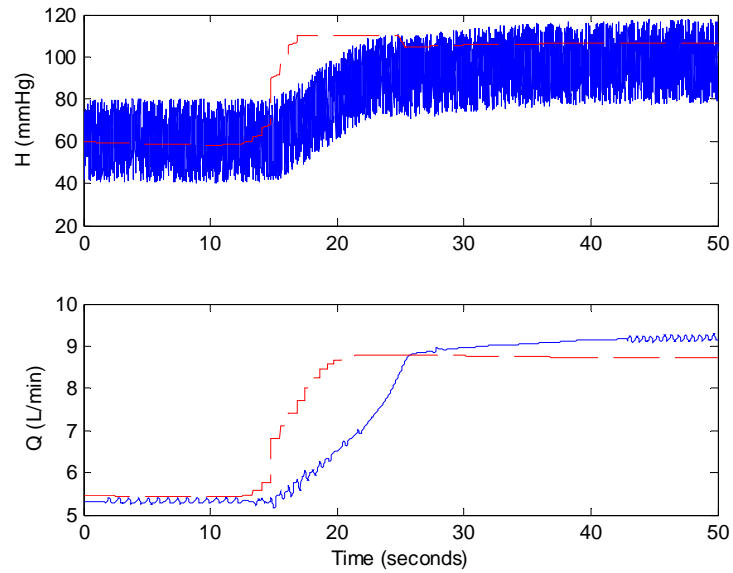
b. Measured operating point

Figure 6.34. Low level of noises for HR, SVR, H and CO

Operating point: $H = 102$ mmHg, $CO = 9.1$ L/min, $Speed = 12.2$ krpm
 SNR_{CO} : 23 dB, SNR_H : 26 dB, SNR_{SVR} : 26 dB, SNR_{HR} : 25 dB.

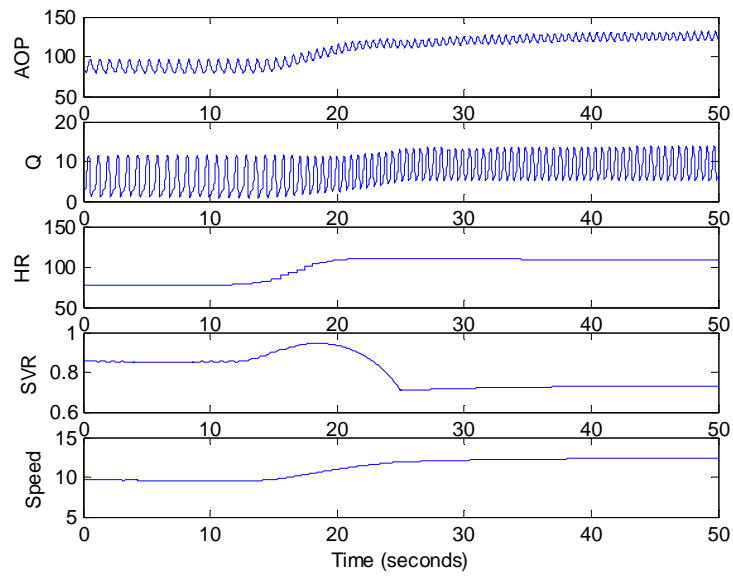


a. Response of the controller to exercise

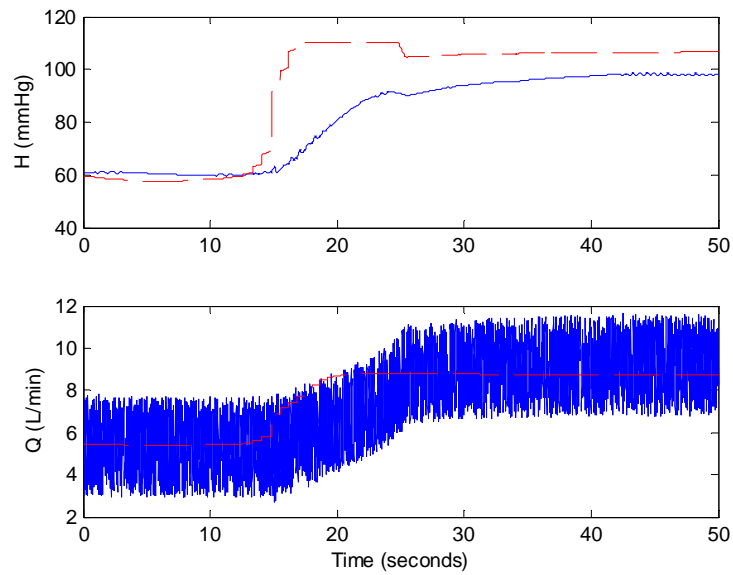


b. Measured operating point

Figure 6.35. High level of noise for H only
 SNR_H: 14 dB (S/N: 98/[-40,40] in mmHg)

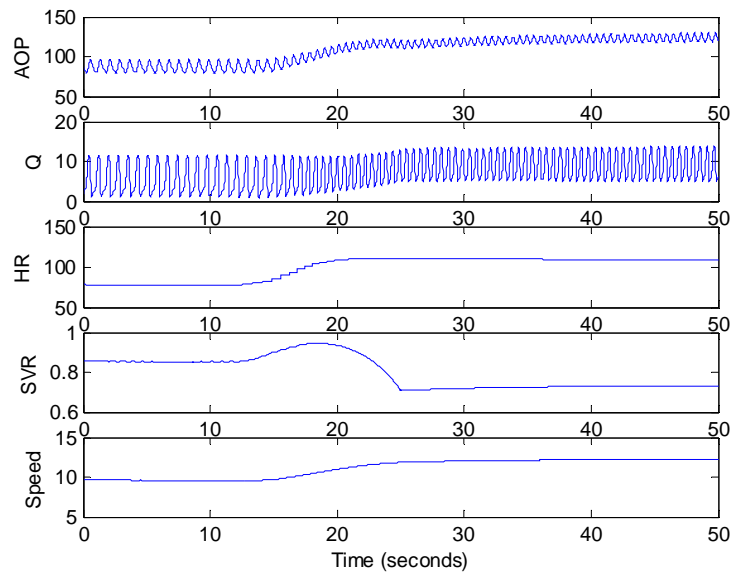


a. Response of the controller to exercise

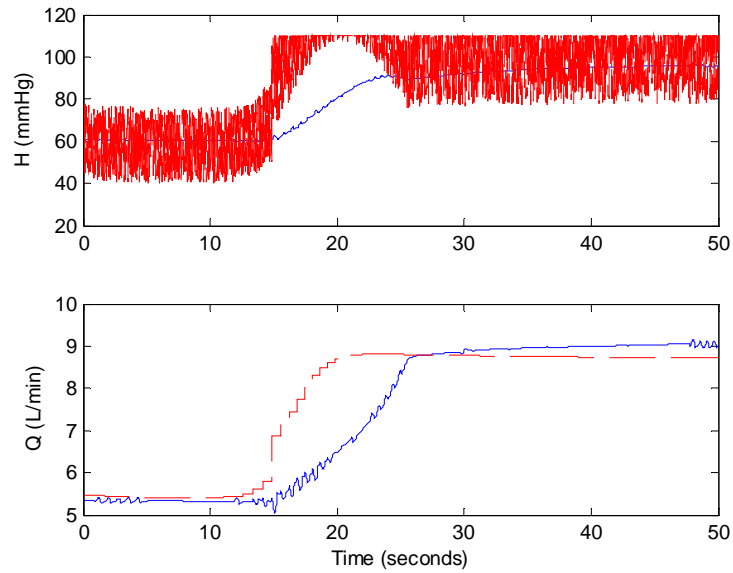


b. Measured operating point

Figure 6.36. High level of noise for CO only
 SNR_CO: 11 dB (S/N: 154/[-80,80] in ml/s)

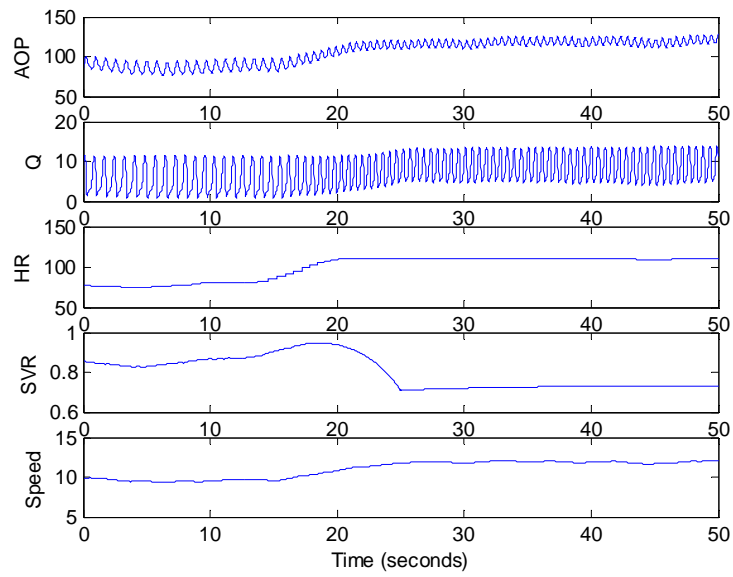


a. Response of the controller to exercise

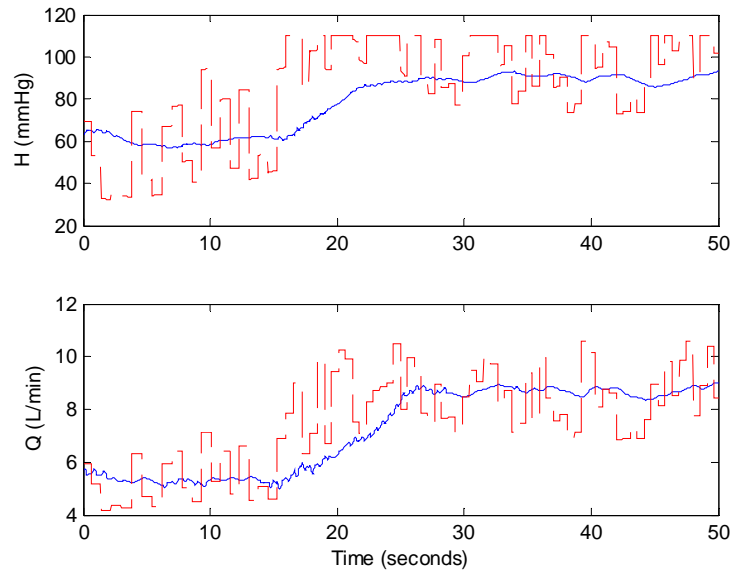


b. Measured operating point

Figure 6.37. High level noise for SVR only
 SNR_SVR: 14 dB (S/N: 0.73/[-0.4,0.4] in mmHg/ml/s)

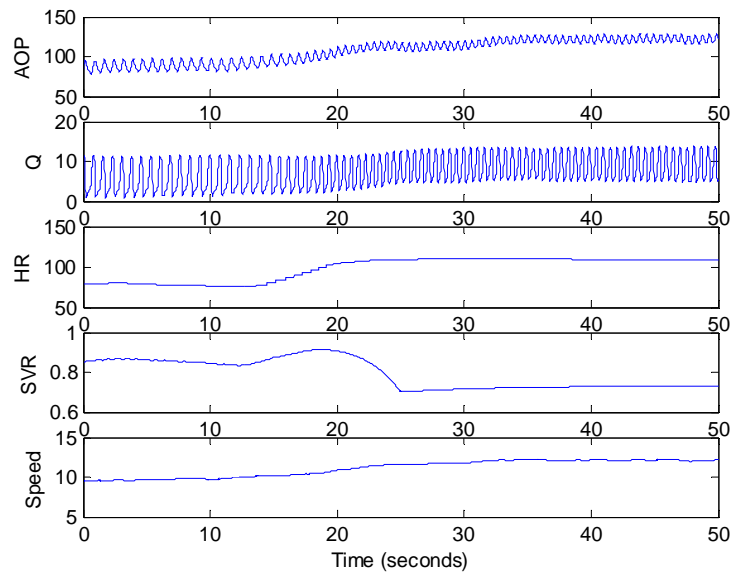


a. Response of the controller to exercise

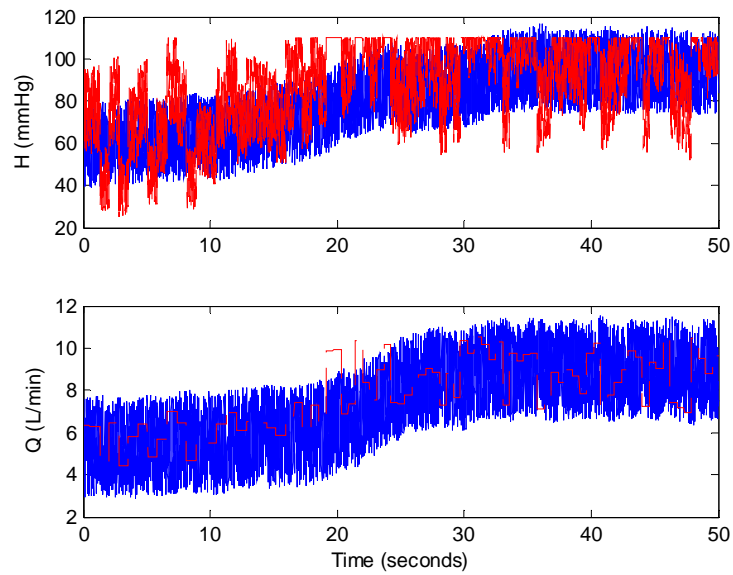


b. Measured operating point

Figure 6.38. High level of noise for HR only
 SNR_{HR}: 14 dB (S/N: 1.8/[-0.8, 0.8] in 1/s)



a. Response of the controller to exercise



b. Measured operating point

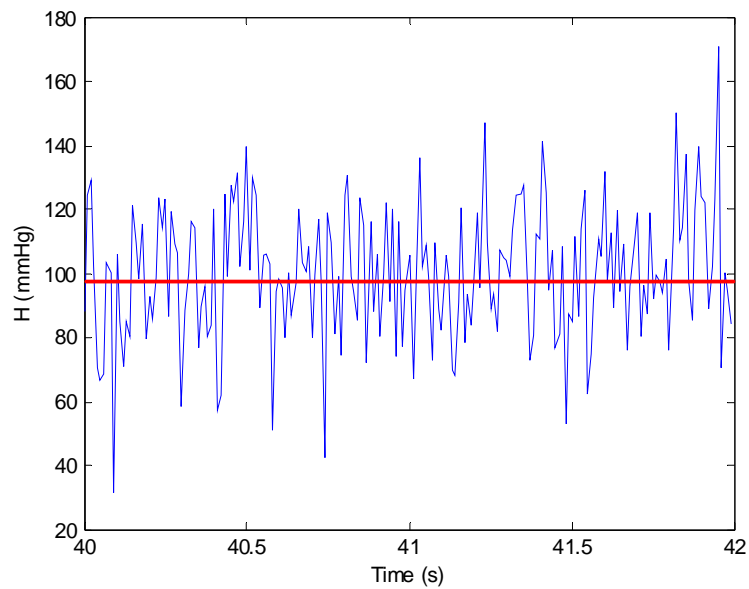
Figure 6.39. High level of noise for HR, SVR, H and CO
 SNR_CO: 15 dB, SNR_H: 17dB, SNR_SVR: 17 dB, SNR_HR: 17 dB

The following is a summary of uniformly distributed noise effect (only one of them presents at a time):

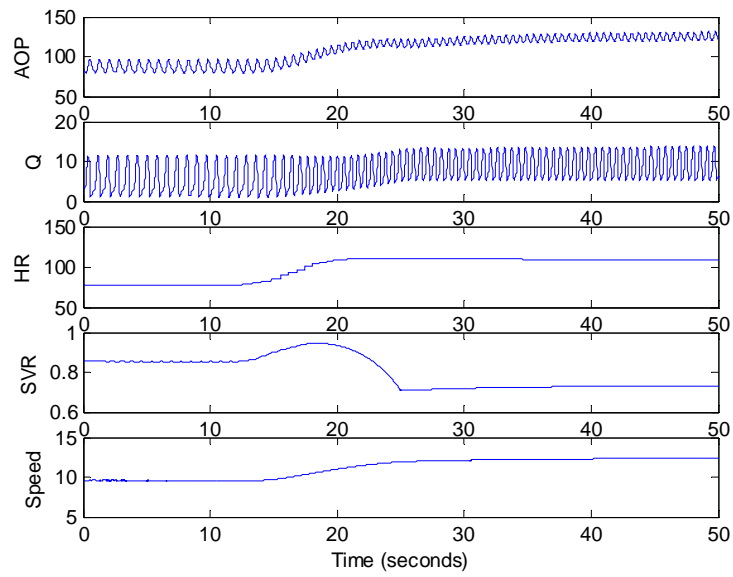
- $SNR_H = 0$ dB, works
- $SNR_{CO} = 0$ dB, works
- $SNR_{SVR} = 0$ dB, works
- $SNR_{HR} < 5$ dB, does not work

2) Normally distributed noise

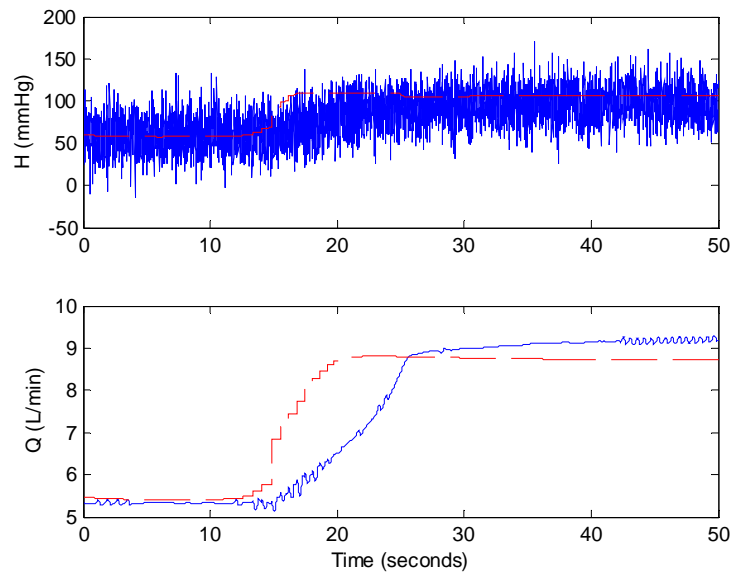
Similarly, different levels of normally distributed noises are added to the variables. The noise feature is shown in Figure 6.40 and the responses of the controller to different levels and combinations of noise are shown in Figure 6.41 through 6.44.



a. Noise feature for H

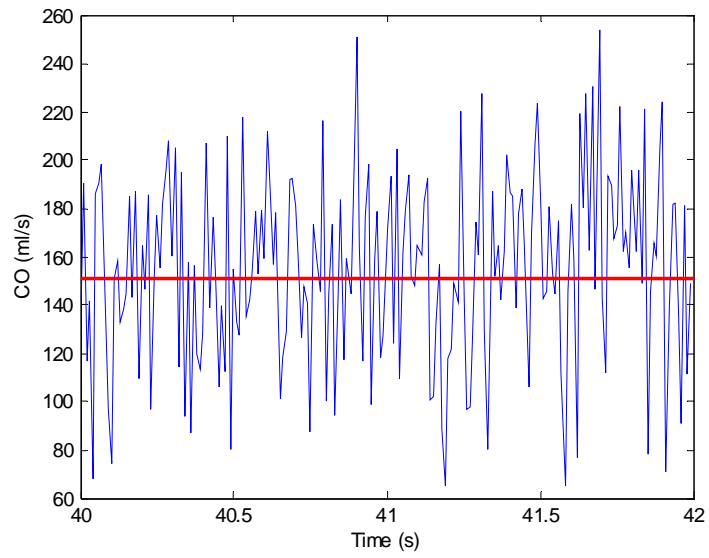


b. Response of the controller to exercise

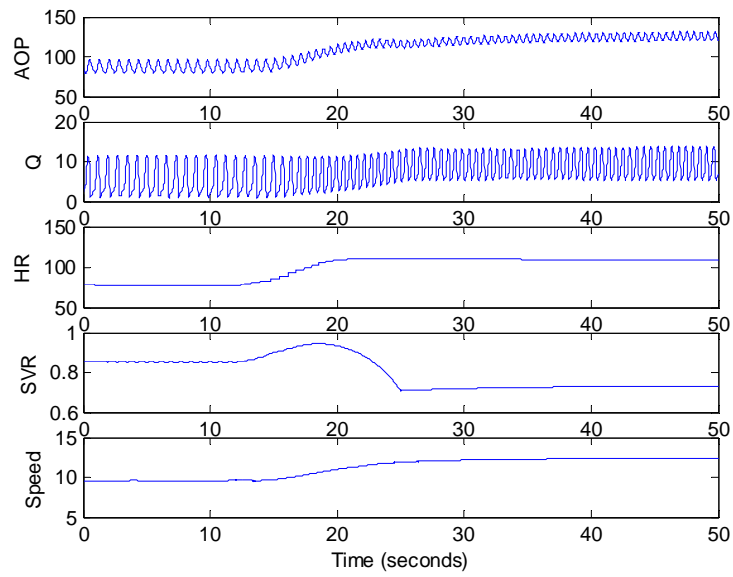


c. Measured operating point

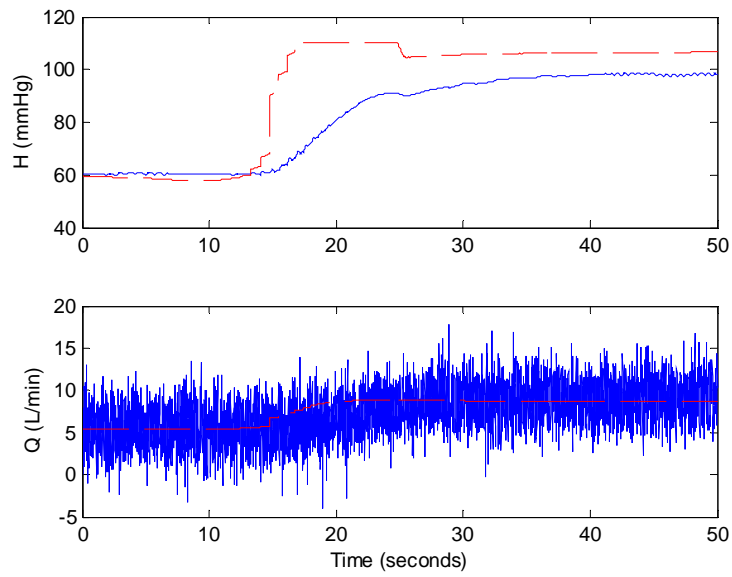
Figure 6.40. Noise for H only
 SNR_H: 13 dB (S: 98 mmHg, N: (0,20))



a. Noise feature for CO

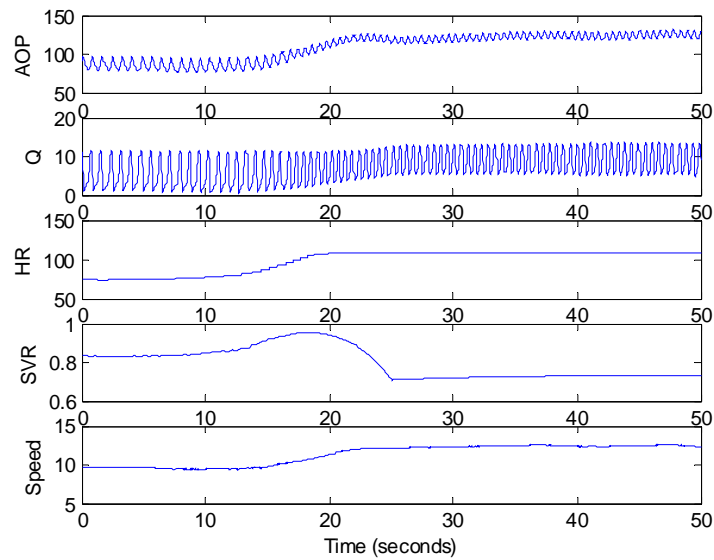


b. Response of the controller to exercise

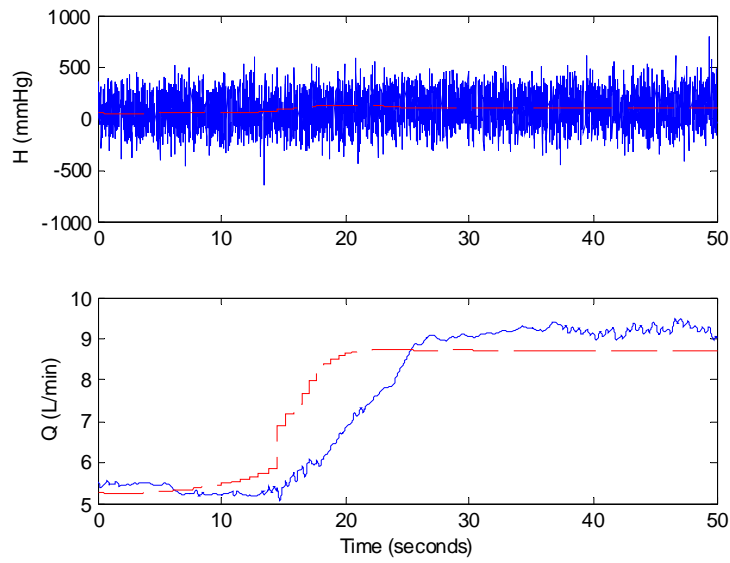


c. Measured operating point

Figure 6.41. Noise for CO only
 SNR_CO: 12 dB (S: 154 ml/s, N:(0,40))

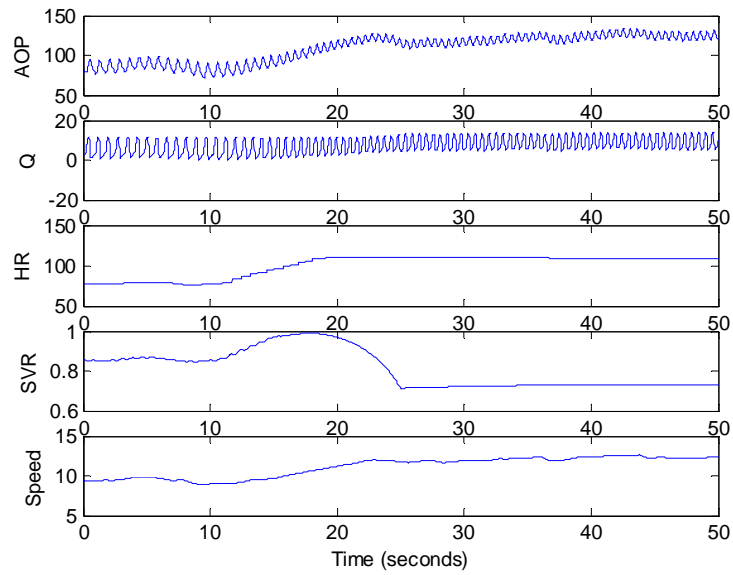


a. Response of the controller to exercise

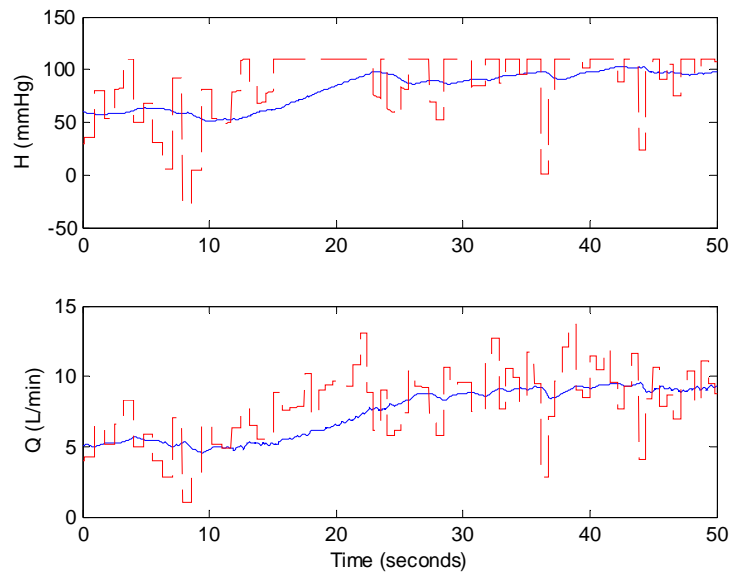


c. Measured operating point

Figure 6.42. Noise for SVR only
 SNR_H: -5 dB (S: 98 mmHg, N: (0,160))

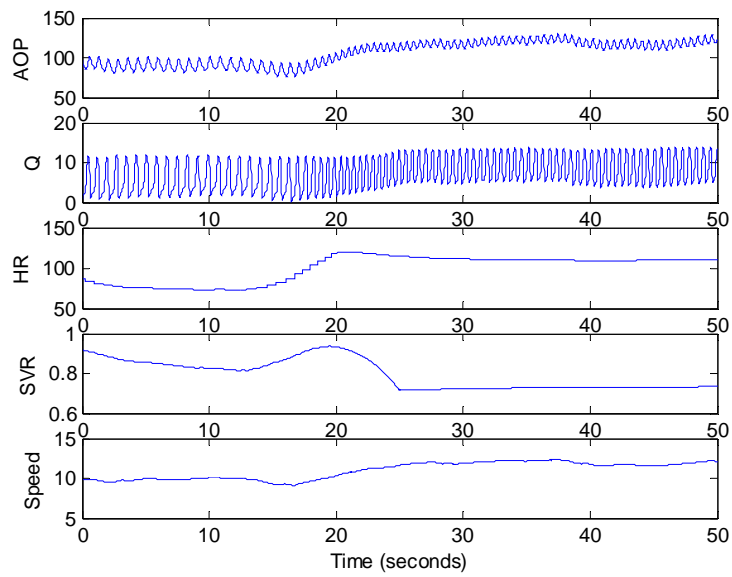


a. Response of the controller to exercise

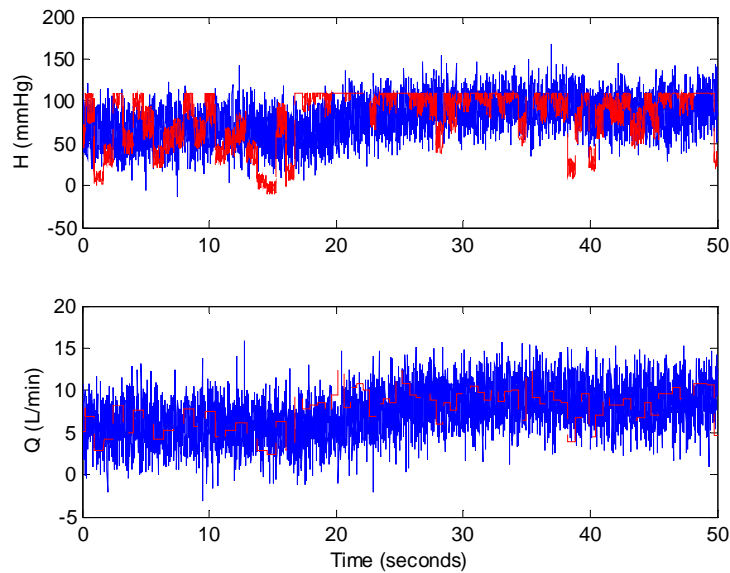


b. Measured operating point

Figure 6.43. Noise for HR only
 SNR_HR: 12 dB (S: 1.8 1/s, N: (0, 0.4))



a. Response of the controller to exercise



b. Measured operating point

Figure 6.44. Noise for all variables

SNR_CO: 12 dB, SNR_H: 13 dB, SNR_SVR: 12 dB, SNR_HR: 12 dB

The following is a summary of normally distributed noise effect (only one of them presents at a time):

- SNR_H = 0, works
- SNR_CO = 0, works
- SNR_SVR = 0, works
- SNR_HR < 10 dB, does not work

6.5 CONCLUSION

A controller based on the heart rate and systemic vascular resistance is developed and examined by comparing to other control methods such as constant speed, constant pump head and heart rate related pump speed methods in the literature. The proposed controller is implemented in the combined model of the pump and the failing cardiovascular system with built-in baroreflex. The proposed controller is responsive to change in physiological state. The proposed controller can

provide more blood flow than the constant speed and constant pump head methods and avoid the excessive mean arterial pressure generated by the heart rate related pump speed method. From rest to exercise, the controlled arterial pressure and cardiac output increase. The controller performance does not vary greatly due to changes in preset parameters $LVPr$, SVr , $K1$, and $K2$. The simulation results show the controller is also robust to the noise imposed on the variables.

7.0 CONCLUSION AND FUTURE WORK

The development of a control algorithm for an LVAD supporting a patient with heart failure is a challenging engineering problem. In this dissertation, we investigated the control algorithm for improving the rotary pump performance for patients with heart failure. An LVAD controller based on the heart rate and the systemic vascular resistance is proposed. The investigations include improving the cardiovascular system model and the pump controller that will respond to the instantaneous physiological change of the body.

In this dissertation, the baroreflex model is coupled to a cardiovascular system model and the interaction between the pump and the cardiovascular system with built-in baroreflex is simulated. The cardiovascular system model is a circuit analog model by using resistances, inductors, capacitors and diodes in which some parameter values can be varied by baroreflex. A healthy and a failing cardiovascular system models with built-in baroreflex have been developed by using the data in the literature as reference. The pathophysiological changes in the failing cardiovascular system and the baroreflex have been mapped into the model and different types of clinical heart failure can be simulated by certain combinations of parameters such as dilated and hypertrophic heart failure. An empirical rotary pump model is coupled to the failing cardiovascular system model with built-in baroreflex. These models are capable of reproducing the real data in the literature, such as exercise experimental data for the healthy people and patients with heart failure. The combined model provides a realistic simulation of the interaction between the pump and the native cardiovascular system. The P-V loops and hemodynamic variable changes with increasing pump speed are consistent with clinical observations. More useful changes in hemodynamics can be simulated and exploited in this model for the LVAD control purpose, such as heart rate and systemic vascular resistance. This model can also be used to test the performance of a pump controller before the costly and time consuming animal experiments.

A physiological control algorithm was developed which incorporates the heart rate and the systemic vascular resistance as inputs. The changes in these hemodynamic variables are related to the baroreflex and local vessel dilation during exercise and are observed in exercise experiments. The changes in heart rate and the systemic vascular resistance are two important indicators of the exercise intensity. By including this information as control input, the controller relates the pump speed to these changes and can improve the pump support for the patients with changing physiological state. This algorithm is tested on the combined model of the pump and the native cardiovascular system with built-in baroreflex. The performance of this controller was compared to that of other pump control methods, such as the constant speed, constant pump head and heart rate related pump speed methods. For comparison, the parameters for the constant speed and constant pump head methods are chosen to match the hemodynamics at rest; the parameters for heart rate related pump speed method are chosen to match the hemodynamics at rest and exercise level 1. The simulation results show that the proposed controller: (1) is responsive to exercise intensity; and (2) can generate more pump flow than the constant speed and the constant pump head methods and the heart rate related pump speed method. The simulation results with noise also show that the controller is robust to noises imposed on the measured hemodynamic variables. The noises tested here are uniformly distributed and normally distributed since the noise characteristics are not clear for the hemodynamics measurement.

There are some assumptions in the development of the controller, such as the measurability of blood pressure and blood flow, the closure of the aortic valve due to decreased left ventricular contractility. If these variables can not be measured in real life due to the difficulty or complexity, the estimations of them should be made by using pump current and/or pump voltage. As to the closure of the aortic valve, there are two possible scenarios: (1) we expect to have heart recovery by using partial support from the pump and (2) the heart muscle may recover the contractility after a period of full pump support and can open the aortic valve by itself. For both scenarios, we need to know the ratio of the pump flow to the aortic flow and adjust the values for the controller parameters SV_r and LVP_r .

So far, the work has been done on the model simulation only. In the simulation, the heart rate and systemic vascular resistance are controlled by the baroreflex and are assumed to be available. In real life, there may be some complexity with the measurement of these variables. Especially, for the case of the heart rate, it is possible that there is an irregular cardiac rhythm or

missing beats. Thus preprocessing or measurement conditioning needs to be considered for the application of this controller. As to the selection of the pump speed update gains in the controller, some more complicated algorithm based on a certain objective may be considered to enhance the performance of the controller response to exercise. The future work includes further verification of this control method by using mock loop (with baroreflex) and animal experiment. Also, to avoid the adverse phenomenon such as suction, a suction detector should be incorporated into the controller as a safeguard. This control algorithm can also be incorporated as a part of a sophisticated intelligent controller in the future.

BIBLIOGRAPHY

- [1] Magner JJ and Royston D, “Heart failure”, *British Journal of Anaesthesia*, 93(1): 74-85, 2004.
- [2] Costanzo MR, Augustine S, Bourge R, et al., “Selection and treatment of candidates for heart transplantation. A statement of health professionals from the Committee on Heart Failure and Cardiac Transplantation of the Council on Clinical Cardiology”, *American Heart Association. Circulation* 92:3593–12, 1995.
- [3] Hunt SA, Frazier OH, “Mechanical circulatory support and cardiac transplantation”, *Circulation* 97:2079 –90, 1998.
- [4] Choi S, “Modeling and control of left ventricular assist system”, Ph.D. dissertation, University of Pittsburgh, 1998.
- [5] Boston JR, Simaan MA, Antaki JF, Yu Y, “Control issues in rotary heart assist devices”, *Proceedings of the American Control Conference*, 2000, Volume: 5, Pages: 3473 – 3477, Jun 28-30, 2000.
- [6] Liu D, Boston JR, Simaan MA, Antaki JF, “Multi-objective optimal control of a heart assist device”, *Proceedings of the 39th IEEE Conference on Decision and Control*, 2000, Volume: 5, Pages: 4857 – 4858, Dec 12-15, 2000.
- [7] Wu Y, Allaire P, and Tao G, “An adaptive speed/flow controller for a continuous flow left ventricular assist device”, *Proceedings of the American Control Conference*, 2003. Volume: 2, Pages: 1171-1176, Jun 4-6, 2003.
- [8] Wu Y, Allaire P, Tao G, Wood H, Olsen D, and Tribble C, “An advanced physiological controller design for a left ventricular assist device to prevent left ventricular collapse”, *Artificial Organs* 27(10):926–930, 2003.
- [9] Kim HC, Khanwilkar PS, Bearnson GB, and Olsen DB, “Development of a microcontroller-based automatic control system for the electrohydraulic total artificial heart”, *IEEE Trans Biomed Eng*, vol. 44, (1): 77-89, 1997.
- [10] Yu Y, “Minimally invasive estimation of cardiovascular parameters”, Ph.D. dissertation, University of Pittsburgh, 1998.

- [11] Sun Y, "Modeling the dynamic interaction between left ventricle and intra- aortic balloon pump", *Am J Physiol* 261(4 Pt 2):H1300-11, 1991.
- [12] Vollkron M, Schima H, Huber L, Wieselthaler G, "Interaction of the cardiovascular system with an implanted rotary assist device: Simulation study with a refined computer model", *Artif Organs* 26(4):349-59, 2002.
- [13] Stergiopoulos N, Meister JJ, Westerhof N, "Determinants of stroke volume and systolic and diastolic aortic pressure", *Am J Physiol* 270(6 Pt 2):H2050-9, 1996.
- [14] Westerhof N, "Analog studies of human systemic arterial hemodynamics", Philadelphia, PA: University of Pennsylvania; 1968.
- [15] Stergiopoulos N, Westerhof BE, Westerhof N, "Total arterial inertance as the fourth element of the windkessel model", *Am J Physiol* 276:H81-H8, 1999.
- [16] Taylor MG, "An approach to an analysis of the arterial pulse wave. I. Oscillations in an attenuating line", *Phys Med Biol* 1(3):258-69, 1957.
- [17] Fogliardi R, Burattini R, Campbell KB, "Identification and physiological relevance of an exponentially tapered tube model of canine descending aortic circulation", *Med Eng Phys* 19(3):201-11, 1997.
- [18] Burattini R, Gnudi G, "Computer identification of models for the arterial tree input impedance: Comparison between two new simple models and first experimental results", *Med Biol Eng Comput* 20(2):134-44, 1982.
- [19] Xu L, Fu M, "Computer modeling of interactions of an electric motor, circulatory system, and rotary blood pump", *Asaio J* 46(5):604-11, 2000.
- [20] Lu K, Clark JW, Ghorbel Jr. FH, Ware DL, and Bidani A, "A human cardiopulmonary system model applied to the analysis of the Valsalva maneuver", *Am J Physiol Heart Circ Physiol* 281: H2661–H2679, 2001.
- [21] Ursino M, "A mathematical model of the carotid baroregulation in pulsating conditions", *IEEE Transactions on Biomedical Engineering*, 46(4): 382-392, 1999.
- [22] Zhou J, Armstrong GP, Medvedev AL, Smith WA, Golding LA, Thomas JD, " Numeric modeling of the cardiovascular system with a left ventricular assist device", *Asaio J* 45(1):83-9, 1999.
- [23] Antaki JF, Choi S, Amin DV, Boston JR, Yu YC, Kerrigan JP, Konishi H, Litwak P, Borovetz HS, and Griffith BP, "In search of chronic speed control for rotary pumps," In proceedings: the Waseda International Congress of Modeling and Simulation Technology for Artificial Organs, Tokyo, Japan, 1996.
- [24] Antaki JF, Choi S, Boston JR, Butler KC, and Thomas DC, "Speed control system for implanted blood pumps", US Patent 5,888,242: Nimbus, Inc., 1999.

- [25] Antaki JF, Choi S, Boston JR, Butler KC, Thomas DC, and Amin DV, “Speed control system for implanted blood pumps”, US Patent 6,066,086: Nimbus, Inc, 2000.
- [26] Konishi H, Antaki JF, Amin DV, Boston JR, Kerrigan JP, Mandarino WA, Litwak P, Yamazaki K, Macha M, Butler KC, Borovetz HS, and Kormos RL, “Controller for an axial flow blood pump”, *Artificial Organs*, vol. 20,(6): 618-20, 1996.
- [27] Yu YC, Boston JR, Simaan MA, and Antaki JF, “Minimally invasive estimation of systemic vascular parameters”, *Ann Biomedical Eng*, vol. 29,(7): 595-606, 2001.
- [28] Kitamura T, Matsushima Y, Tokuyama T, Kono S, Nishimura K, Komeda M, Yanai M, Kijima T, and Nojiri C, “Physical model-based indirect measurements of blood pressure and flow using a centrifugal pump”, *Artificial Organs*, vol. 24,(8): 589-93, 2000.
- [29] Oshikawa M, Araki K, Nakamura K, Anai H, and Onitsuka T, “Detection of total assist and sucking points based on the pulsatility of a continuous flow artificial heart: in vivo evaluation”, *Asaio J*, vol. 44,(5): M704-7, 1998.
- [30] Waters T, Allaire P, Tao G, Adams M, Bearnson G, Wei N, Hilton E, Baloh M, Olsen D, and Khanwilkar P, “Motor feedback physiological control for a continuous flow ventricular assist device”, *Artificial Organs*, vol. 23,(6): 480-6, 1999.
- [31] Giridharan GA and Skliar M, “Physiological control of blood pumps without implantable sensors”, *Proceedings of the American Control Conference*, 2003. Volume: 1, Pages: 471-476, Jun 4-6, 2003.
- [32] Oshikawa M, Araki K, Nakamura K, Anai H, and Onitsuka T, “Detection of total assist and sucking points based on the pulsatility of a continuous flow artificial heart: in vivo evaluation”, *Asaio J*, vol. 44, (5): M704-7, 1998.
- [33] Baloa L, “Certainty-weighted system for the detection of suction in ventricular assist devices”, Ph. D. dissertation, 2001.
- [34] Boston JR, Antaki JF, Simaan MA, “Hierarchical control of heart-assist devices”, *Robotics & Automation Magazine*, IEEE, Volume: 10, Pages: 54-64, Issue: 1, March 2003.
- [35] Antaki JF, Boston JR, and Simaan MA, “Control of heart assist devices”, *Proceedings of the 42nd IEEE Conference on Decision and Control*, Volume: 4, Pages: 4084-4089, Dec 9-12, 2003.
- [36] Chen S, Antaki JF, Simaan MA, and Boston JR, “Physiological control of left ventricular assist devices based on gradient of flow”, *Proceedings of the American Control Conference*, pp. 3829-3834, June 8-10, 2005, Portland, OR.
- [37] Giridharan GA, and Skliar M, “Control strategy for maintaining physiological perfusion with rotary blood pumps”, *Artificial Organs* 27(7):639–648, 2003.

- [38] Giridharan GA, and Skliar M, “Nonlinear controller for ventricular assist devices”, *Artificial Organs* 26(11):980–984, 2002.
- [39] Giridharan GA, and Skliar M, Olsen DB, and Pantalos GM, “Modeling and control of a brushless DC axial flow ventricular assist device”, *Asaio J*, vol. 48, (3): 272-89, 2002.
- [40] Waters T, Allaire P, Tao G, Adams M, Bearson G, Wei N, Hilton E, Baloh M, Olsen D, and Khanwilkar P, “Motor feedback physiological control for a continuous flow ventricular assist device”, *Artificial Organs*, vol. 23, (6): 480-6, 1999.
- [41] Nakamura M, Masuzawa T, Tatsumi E, Taenaka Y, Nakamura T, Zhang B, Nakatani T, Takano H, and Ohno T, “The development of a control method for a total artificial heart using mixed venous oxygen saturation”, *Artificial Organs*, vol. 23, (3): 235-41, 1999.
- [42] Parnis SM, Conger JL, Fuqua JM Jr., Jarvik RK, Inman RW, Tamez D, Macris MP, Moore S, Jacobs G, Sweeney MJ, and Frazier OH, “Progress in the development of a transcutaneously powered axial flow blood pump ventricular assist system”, *Asaio J*, vol. 43,(5): M576-80, 1997.
- [43] Chen S, Ferreira A, Antaki JF, Simaan MA, and Boston JR, “A Mathematic Model of a Cardiovascular System Regulated by the Baroreflex”, *Proc. of the 2006 American Control Conference*, June, 2006.
- [44] Ferreira A, Chen S, Simaan MA, Antaki JF, and Boston JR, “A nonlinear state-space model of a combined cardiovascular system and rotary pump”, *44th IEEE Conference on Decision and Control and European Control Conference ECC 2005 (CDC-ECC'05)*, pp. 897 – 902, December 12-15, 2005, Seville, Spain.
- [45] Breitenstein DS, “Cardiovascular modeling: The mathematical expression of blood circulation”, *MS Thesis*, University of Pittsburgh, 1993.
- [46] Yu Y, Boston JR, Simaan MA, and Antaki JF, “Estimation of systemic vascular bed parameters for artificial heart control”, *IEEE Transactions on Automatic Control*, Vol 43, No. 6: 765-778, June, 1998.
- [47] Suga H and Sagawa K, “Instantaneous pressure-volume relationships and their ratio in the excised, supported canine left ventricle”, *Circ Res*, vol. 35, no. 1, pp.117-126, 1974.
- [48] Ursino M, “Interaction between carotid baroregulation and the pulsating heart: a mathematical model”, *Am. J. Physiol.* 275 (Heart Circ. Physiol. 44): H1733–H1747, 1998.
- [49] Ursino M and Magosso E, “Acute cardiovascular response to isocapnic hypoxia I. A mathematical model”, *Am. J. Physiol. - Heart* 279:149-165, 2000.
- [50] Magosso E, Cavalcanti S and Ursino M, “Theoretical analysis of rest and exercise in patients with total cavopulmonary connection hemodynamics”, *Am. J. Physiol. - Heart* 282:1018-1034, 2002.

- [51] www.critcon.com/ccipublic/products/products.php3
- [52] Pawelczyk JA, Hanel B, Pawelczyk RA, Warberg J, and Secher NH, “Leg vasoconstriction during dynamical exercise with reduced cardiac output”, *J Appl Physiol* 73: 1838–1846, 1992.
- [53] Powers SK and Howley ET, *Exercise Physiology: theory and application to fitness and performance*, 4th edition, McGraw-Hill, 2001.
- [54] Sullivan MJ, Knight JD, Higginbotham MB, and Cobb FR, “Relation between central and peripheral hemodynamics during exercise in patients with chronic heart failure”, *Circulation* 80:769-781, 1989.
- [55] Klabunde RE, *Cardiovascular physiology concepts*, Lippincott Williams & Wilkins, 2004. (<http://www.cvphysiology.com/Heart%20Failure>)
- [56] http://www.merck.com/media/mmhe2/figures/fg025_1.gif
- [57] Zucker IH, Wang W, and BrCmdle M, “Baroreflex abnormalities in congestive heart failure”, *News Physiol Sci* 8: 87-90, 1993.
- [58] Sopher SM, Smith ML, Eckberg DL, Frithsch JM and Dibner-Dunlap ME, “Autonomic pathophysiology in heart failure: carotid baroreceptor-cardiac reflexes”, *Am J Physiol.* 259(3 Pt 2):H689-96, 1990.
- [59] DiBona GF and Sawin LL, “Reflex regulation of renal nerve activity in cardiac failure”, *Am. J. Physiol.* 266 (Regulatory Integrative Comp. Physiol. 35): R27-R39, 1994.
- [60] Carlos Eduardo Negrão, Maria Janieire de Nazaré Nunes Alves, “Pathophysiology of heart failure-role of peripheral circulatory mechanisms on effort tolerance”, 1st virtual congress of cardiology.
- [61] Persson PB, “Modulation of cardiovascular control mechanisms and their interaction”, *Physiological Reviews*, Vol. 76, No. 1, January 1996.
- [62] Wang W, Chen JS, and Zucker IH, “Carotid sinus baroreceptor reflex in dogs with experimental heart failure”, *Circ. Res.* 68:1294-1301, 1991.
- [63] Katz SD, Schwarz M, Yuen J, Lejemtel TH, “Coronary and peripheral blood flow: Impaired acetylcholine-mediated vasodilation in patients with congestive heart failure: Role of endothelium-derived vasodilating and vasoconstricting factors”, *Circulation.* 88(1):55-61, July 1993.
- [64] Mortara A, La Rovere MT, et al, “Arterial baroreflex modulation of heart rate in chronic heart failure”, *Circulation.* 96:3450-3458, 1997.
- [65] Thames MD, Kinugawa T, Smith ML, and Dibner-Dunlap ME, “Abnormalities of baroreflex control in heart failure”, *J Am Coll Cardiol* 22 : 56A–60A, 1993.

- [66] Lanfranchi PA and Somers VK, “Arterial baroreflex and cardiovascular variability: interactions and implications”, *Am J Physiol Regul Integr Comp Physiol*, 283:815-826, 2002.
- [67] Frazier OH, et al., “Clinical experience with an implantable, intracardiac, continuous flow circulatory support device: physiologic implications and their relationship to patient selection”, *Ann Thorac Surg* 77:133–42, 2004.
- [68] Klotz S, “Left ventricular pressure and volume unloading during pulsatile versus nonpulsatile left ventricular assist device support”, *Ann Thorac Surg* 77:143–50, 2004.
- [69] Bank AJ, et al., “Effects of left ventricular assist devices on outcomes in patients undergoing heart transplantation”, *Ann Thorac Surg* 69:1369 –75, 2000.
- [70] Popovic´ ZB, Khot UN, Novaro GM, Casas F, Greenberg NL, Garcia MJ, Francis GS, and Thomas JD, “Effects of sodium nitroprusside in aortic stenosis associated with severe heart failure: pressure-volume loop analysis using a numerical model”, *Am. J. Physiol Heart Circ. Physiol.* 288: H416–H423, 2005.
- [71] Pak PH, et al., “Marked discordance between dynamic and passive diastolic pressure-volume relations in idiopathic hypertrophic cardiomyopathy”, *Circulation*, 94:52-60, 1996.
- [72] Butler K. C., Dow J. J., Litwak P., Kormos R. L., Borovetz H. S., “Development of the Nimbus/University of Pittsburgh innovative ventricular assist system”, *Ann Thorac Surg*, 68(2):790-4, Aug 1999.
- [73] Schima H., Honigschnabel J., Trubel W., Thoma H., “Computer Simulation of the Circulatory System During Support with a Rotary Blood Pump”, *Trans Am Soc Artif Intern Org*, 36(3):M252-4, 1990.
- [74] Tohru Sakamoto, “Evaluation of native left ventricular function during mechanical circulatory support: theoretical basis and clinical limitations”, *Ann Thorac Cardiovasc Surg* 8: 1–6, 2002.
- [75] Mancini DM, et al., “Low incidence of myocardial recovery after left ventricular assist device implantation in patients with chronic heart failure”, *Circulation*, 98:2383-2389, 1998.
- [76] Takehide Akimoto, et al., “Rotary pump flow spontaneously increases during exercise under constant pump speed: results of chronic study”, *Artificial organs*, 23(8): 797-801, 1999.